Oxygen reduction reaction mechanism on glassy carbon in aprotic organic solvents

Marc Zimmermann

UNIVERSITÉ GRENOBLE ALPES

THÈSE

Pour obtenir le grade de

DOCTEUR DE L'UNIVERSITÉ GRENOBLE ALPES

Spécialité : **Matériaux, Mécanique, Génie Civil, Electrochimie**

Arrêté ministériel : 7 août 2006

Présentée par

Marc ZIMMERMANN

Thèse dirigée par **Marian CHATENET** et
codirigée par **Frédéric MAILLARD**

préparée au sein du **Laboratoire d'Electrochimie et de Physicochimie des Matériaux et Interfaces (LEPMI)**
dans **l'École Doctorale IMEP²**

Oxygen Reduction Reaction Mechanism on Glassy Carbon in Aprotic Organic Solvents

Thèse soutenue publiquement le **21 Juillet 2015**,
devant le jury composé de :

Monsieur Lorenzo STIEVANO
Professeur, Université Montpellier II, Président du Jury

Madame Meriem ANOUTI
Professeur, Université François-Rabelais Tours, Rapporteur

Monsieur Hubert GASTEIGER
Professeur, Technische Universität München, Rapporteur

Monsieur Marian CHATENET
Professeur, Grenoble-INP, Directeur de Thèse

Monsieur Frédéric MAILLARD
Chargé de Recherche, CNRS-LEPMI, Co-Directeur de Thèse

Monsieur David AYME-PERROT
Chef de Projet, Hutchinson-Centre de Recherche, Co-Encadrant de Thèse

Acknowledgments

I would like to thank my supervisors Marian Chatenet and Frederic Maillard at the LEPMI for giving me all their support in order to carry out this work in the best conditions. I also want to thank Hutchinson for funding this work, and especially David Ayme-Perrot for entrusting me this project. I am really grateful to my 3 supervisors for their mentoring and all the very fruitful discussions we had, but also for encouraging and giving me the freedom to always try to apply my ideas. I am very grateful to all the people I had the chance to collaborate with during the course of this work, would it be on designing new experiments or fixing up stuff in the laboratory, teaching me particular concepts or trying to understand me teaching those, writing papers for publications or filling those for the administration, having general scientific or casual life conversations. I cannot emphasize enough how it has been both a pleasure and a further motivation to work in such an enriching environment. Finally, I want to thank the jury for having accepted to judge this work and for the very fruitful discussion we had during the defense.

Il me serait difficile de résumer à une page l'intégralité des remerciements que j'aimerais faire à toutes les personnes qui m'ont accompagné, de près ou de plus loin, pendant ces 4 ans. De manière générale, je tiens à remercier mes amis et collègues pour tous ces moments qui m'ont amenés jusqu'ici, en particulier tous ceux que je n'ai pas pu remercier en personne. De même, il serait insensé de vouloir résumer tous les moments qui ont constitué cette aventure. Aussi, je vais simplement en profiter pour écrire quelques mots qui m'évoquent des périodes de cette thèse.

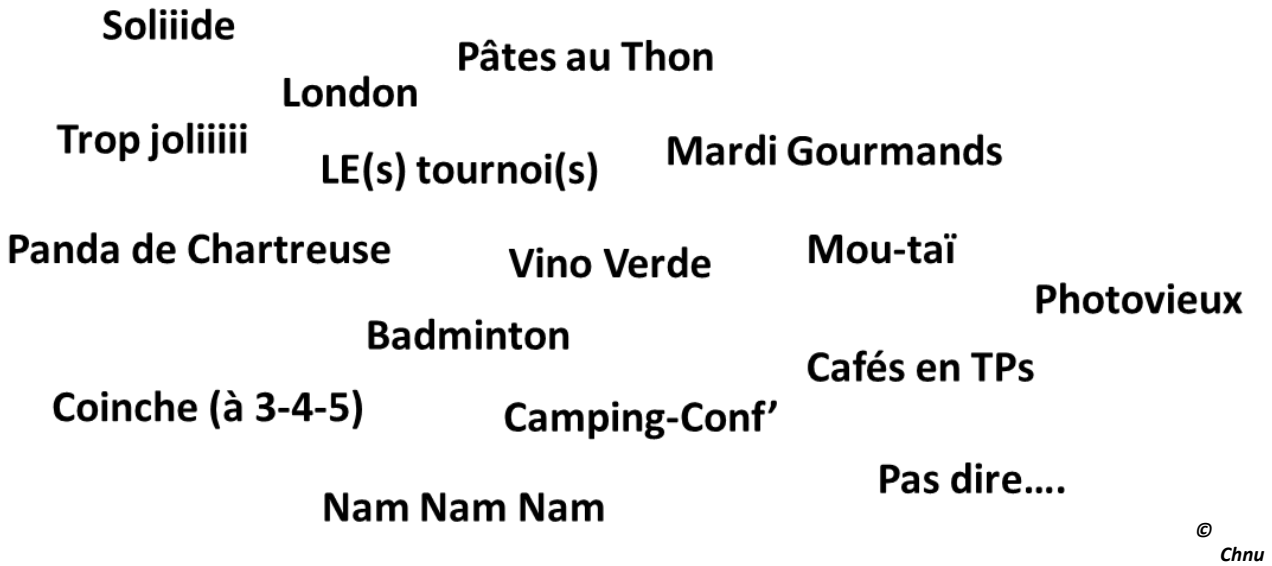

Et merci enfin à ma famille qui n'a jamais cessé de me soutenir.

General Introduction

'' England and all civilized nations stand in deadly peril of not having enough to eat.[...] The fixation of atmospheric nitrogen is one of the great discoveries awaiting the genius of chemists"

William Crookes
*Chemical News, 128, 125, **1898***
Haber-Bosch process to fix ammonia was proved 10 years later

The fast global economical development witnessed on the planet since the mid XXth century is leading to a world full of promises, but it is also generating a relatively new challenge: it is essentially based on the consumption of increasing amounts of energy, and this energy is currently essentially produced from limited (and usually fossil) reserves. From this simple statement two ways to pursue our economical development emerge: either we use new sources of energy with less limited reserves or we considerably improve the efficiency at which we are using energy; most probably, we shall do both. In each case, energy storage plays a significant role (notably because the daily energy peak production does essentially not match the daily peak consumption) and is thus directly related to the challenge mentioned above. Electrochemical energy storage technologies could be suitable for numerous applications, and technologies based on oxygen as a positive electrode active material (oxidant) would be highly interesting considering the availability of the resource. Among those technologies, the use of highly-available metals as negative electrode would make particularly suitable candidates for a massive deployment, all the more knowing that the high energy density of the resulting batteries would make them adapted to mobile applications.

In the present thesis, we will focus on one of these promising technologies: non-aqueous alkali metal oxygen batteries (MOB). The research on these technologies has been initially motivated by the discovery, twenty years ago, of the rechargeability of a lithium-oxygen battery involving an aprotic electrolyte. Such a battery could offer, in theory, one of the highest energy density available, comparable to that of oil. However, it appeared more recently that the effects of parasitic reactions were considerably underestimated, and that the actual working principle of the battery was poorly understood. In particular, the mechanisms of oxygen reduction (and evolution) in aprotic media in presence of alkali metal cations remain unclear. A considerable amount of work has been done worldwide during the 5 last years in order to better understand these mechanisms as well as the phenomena occurring during the cycling of the MOB. By doing so, many limitations of the technology have been clearly identified, and solutions to overcome them have been proposed.

Thus, a first objective of the present work is to offer a particular critical point of view on this very recent and prolific research (Chapter I), with special emphasis on the oxygen reduction reaction (Chapter II). It will be noted that the improvement of the system significantly depends on a better fundamental understanding of the influence of alkali metal cations on the oxygen reduction mechanism. From theoretical considerations (Chapter III) and electrochemical characterizations, it will be shown that the impact of the different cations can be accounted for by a unique mechanism, based on their charge-density (Chapter V). Furthermore, the influence of the solvent on the mechanism will be correlated to specific solvation parameters (detailed in Chapter IV and VI), which can be measured independently for each solvent. Therefore, these parameters could be used to account for the behavior of electrolytes, but also in a predictive manner, as to rationalize the design of electrolytes for MOB (Chapter VI). Finally, a kinetic model of the mechanism, involving solubility equilibrium, will be proposed (Chapter VII). This model will serve as a mean to confirm several qualitative hypotheses, but also to estimate thermodynamic constants associated to the non-aqueous oxygen reduction mechanism in the presence of alkali metal cations.

Table Of Contents

General Introduction ..... - 5 -

Chapter I. Toward Electrochemical Energy Storage Devices for the Future Electrical Grid. 11

1. Development and energy consumption ..... - 13 -
2. Energy storage and the future of the electrical grid ..... - 15 -
3. The current technologies ..... - 17 -
4. Aprotic metal-air ..... - 19 -

Chapter II. Oxygen Electrochemistry in the Absence of Water 39

1. Reactivity of superoxide and peroxide, and interaction with alkali metal cations ..... - 41 -
2. Oxygen reduction in presence of tetraalkylammonium cations ..... - 42 -
3. Oxygen reduction in presence of alkali metal cations ..... - 45 -
4. The role of water ..... - 49 -

Chapter III. General Considerations, Method Development and Experimental Details . - 57 -

1. Solvation effects ..... - 59 -
2. Ion-pairs formation ..... - 66 -
3. Method development ..... - 67 -
4. Experimental details. ..... - 69 -

Chapter IV. Oxygen Reduction to Superoxide in Presence of Tetraalkylammonium Cations ..... - 73 -

1. ORR in DMSO in presence of tetrabutylammonium (TBA^+) and tetraethylammonium (TEA^+) ..... - 76 -
2. Influence of the solvent on the ORR in presence of TBA^+ ..... - 79 -
3. Calculation of physicochemical parameters of interest ..... - 83 -

Chapter V. Oxygen Reduction Reaction Mechanism in DMSO in Presence of Alkali Metal Cations ..... - 87 -

1. General overview of the ORR/OER in presence of alkali metal cations ..... - 89 -
2. First reduction process ..... - 90 -
3. Second reduction process ..... - 96 -

Chapter VI. Extension of the Oxygen Reduction Reaction Mechanism to Other Aprotic Solvents ..... - 107 -

1. ORR in Acn and Acn-DMSO mixtures ..... - 110 -
2. ORR in DMA and DMA-DMSO mixtures ..... - 114 -
3. Effect of the solvent on the ORR: solvation of M^+ and $O2^{\bullet-}$ ..... - 117 -
4. Proposition of parameters to predict the behavior of solvents and solvent mixtures ..... - 123 -

5. Extrapolation of solvent and mixtures parameters ..... - 125 -

6. Proposition of a solvent structure-related parameter to predict $\mathbf{O2}^{\bullet-}$ solvation: hydrogen bond donicity ..... - 130 -

Chapter VII. Kinetic Modelling of the Oxygen Reduction Reaction Mechanism ..... - 135 -

1. Kinetic equations, linear system formulation and resolution[1-2] ..... - 137 -

2. Study of the impact of ion-pairs formation on the resulting voltammograms ..... - 140 -

3. Modelling of the precipitation of MO_2 ..... - 150 -

General Conclusion ..... - 159 -

Glossary

NaS : Sodium Sulfur Battery

VRB: Vanadium Redox-flow Battery

MAB: Metal-Air Battery

MOB: Metal-Oxygen Battery

LiOB: Lithium-Oxygen Battery

NaOB: Sodium-Oxygen Battery

KOB: Potassium-Oxygen Battery

HSAB : Hard and Soft Acids and Bases

AN : Acceptor Number

DN : Donor Number

MCB : Metal Cation Basisity

DMSO : Dimethylsulfoxide

Acn : Acetonitrile

DMA : N,N-dimethylacetamide

EN : Ethylene Diamine

DMF : N,N-dimethylformamide

DME : 1,2-dimethoxyethane

NMP : N-methyl-2-pyrrolidone

Py : Pyridine

TAA^+ : Tetraalkylammonium cation

TBA^+ : Tetrabutylammonium cation

TEA^+ : Tetraethylammonium cation

RRDE : Rotating Ring-Disk Electrode

Chapter I. Toward Electrochemical Energy Storage Devices for the Future Electrical Grid

"*The future influences the present just as much as the past*"

(attributed to) Friedrich Nietzsch

1. Development and energy consumption

"Culture evolves as the amount of energy harnessed per capita per year increases, or as the efficiency or economy of the means of controlling energy is increased, or both". This citation from anthropologist Leslie Alvin White[1] denotes the close correlation between cultural development, in the broadest definition, and the energy effectively used by mankind throughout History. In order for the human's culture to keep progressing, there has been a need to consume more energy and to use the energy available more efficiently[2].

Using the USA recent history as an example, one can see that, until the middle of the XIXth century, the daily primary energy consumption per capita[1, 3] had increased rather steadily, reaching approximately 5 10^4 kcal per day per capita (Figure I.1a). It has then been multiplied by almost 5 in one century, following the industrial revolution. In the same period, the total energy consumed was multiplied by *ca*. 40, owing to the population growth. This increase can be correlated with the simultaneous improvements in the well-being of the citizens, measured by the human development index (HDI)[4] (Figure I.1b).

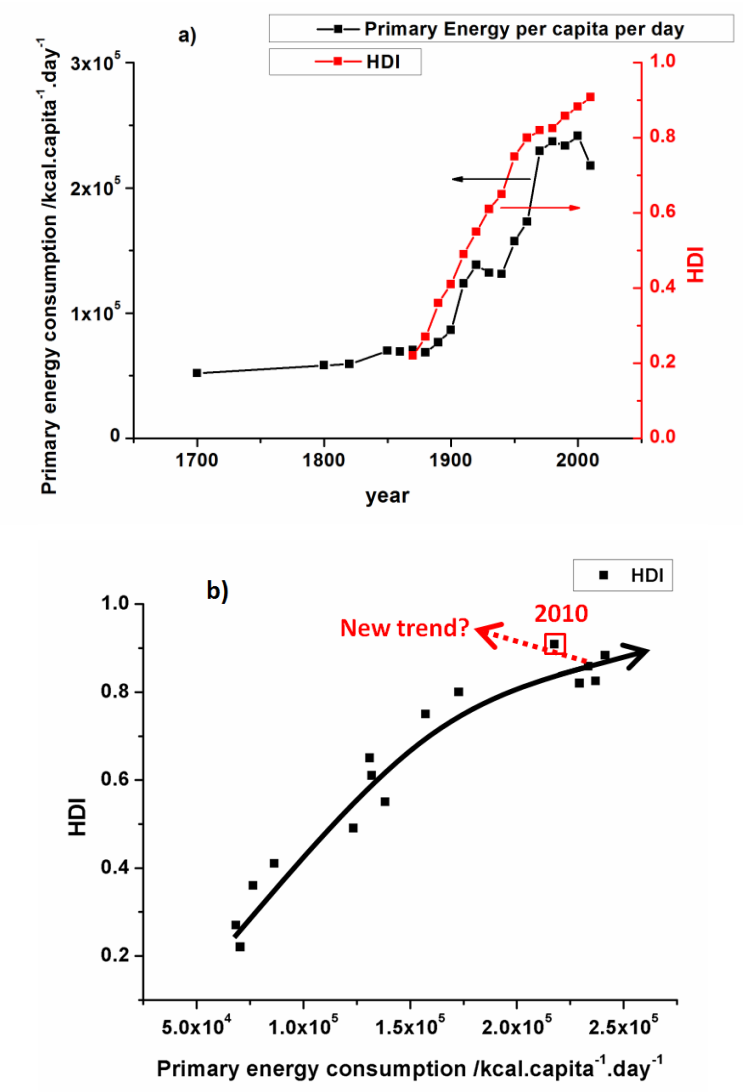

Figure I.1. a) Evolution of the primary energy consumption per capita per day[1, 3] and HDI[4] in the USA since 1700; b) Correlation of the HDI with the primary energy consumed and emergence of a possible new trend.

Considering that the world population would top around 10 billion individuals, similar energy consumption per capita worldwide would represent a total consumption of 4 ZJ per year. As a comparison, 2008 world's energy consumption was 0.5 ZJ[5], and roughly one third of it came from oil. This figure shall be compared to the present proven oil resources (that could provide only 8 ZJ overall) and the total estimated remaining oil resources, including potentially unrecoverable (representing a mere 60 ZJ). This calculation, which is obviously not a forecast of any real situation[i], demonstrates that pursuing our cultural development by further increasing our energy consumption per capita, is already not a sustainable option anymore if we keep relying mainly on non-renewable

[i] Detailed energy forecasts for the next 20/30 years can be found in technical reports[6] and more discussion oriented publications[7-8]

energy sources. Therefore, improving the efficiency at which we are using the energy resources, through technological breakthrough, optimization of our infrastructure and diversification of the sources, seems more than ever our best option (if not the only one, actually).

As an optimistic note, the current trend in developed countries seems to be a decrease in the energy consumed per capita; in parallel, the gross domestic product (GDP) per capita and HDI are still improving, therefore denoting an increase in the efficiency at which energy is used, together with a decrease of its consumption (see the possible "new trend" arrow in Figure I.1b).

2. Energy storage and the future of the electrical grid

Electric power generation accounted for 40 % of the total primary energy consumption in the USA in 2010[9] (Figure I.2). This proportion is still increasing, and will continue to do so with the expected partial electrification of the transportation (transportation represented 27 % of the primary energy consumption in 2010 in the USA). At present, the efficiency of the electrical system is rather low: around two thirds of the energy is lost before reaching the end-users. Developing smart(er) grids would allow a higher overall energy efficiency to the end-users, as well as the integration of a growing number of intermittent power sources; of course, (electrical) energy storage plays an essential role in this expected progress[10-11]. To that goal, there is a great diversity of needs, from high energy facilities for bulk services like time-shifting, to fast-response facilities for ancillary services like daily power regulation. As such, the market for energy storage on the grid is expected to grow significantly over the next decades.

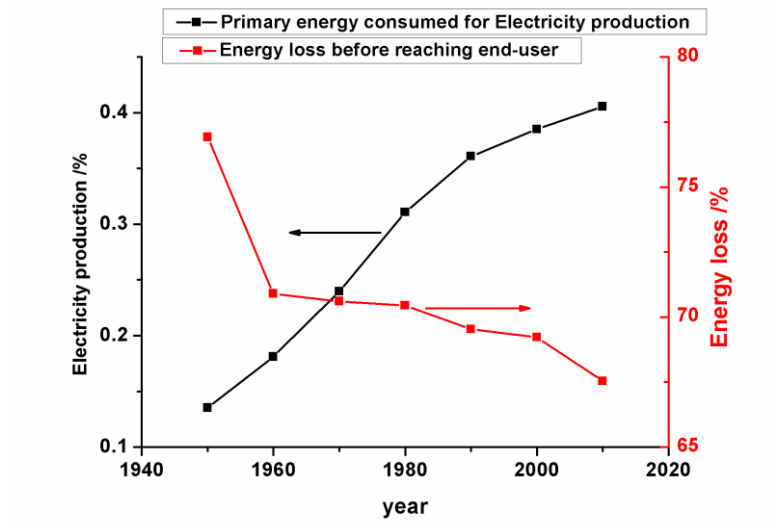

Figure I.2. Primary energy consumed for electricity production (black) and percentage of energy lost before reaching end-users (red) in the US[9].

At the moment, although most of the energy storage is based on pumped hydroelectricity (97 % of the estimated 145 GW installed worldwide), half of the projects for new installations are concerning electrochemical-based technologies[12]. One of the main advantages of the latter technologies is their adaptability to most of the situations, since they are easily scalable and do not require specific locations, though at a generally higher cost per kWh stored. They are particularly suitable for micro-grids or virtual power plants[13].

One of the main challenges regarding a long-term widespread use of a particular technology in electrical grids is the availability of its components/base materials. For example, although vanadium redox flow batteries is the most mature flow battery and its environmental impact being one of the lowest (without considering the extraction of vanadium), the reserves of vanadium available are incompatible with a massive use (Table I.1). Furthermore, vanadium accounts for one third of the cost of the system, the price of this resource being highly volatile, and the discrete localization of the extraction sites (mainly in South Africa, China and Russia) is incompatible with its safe supply[13]. A similar reasoning, to a lower extent, explains the growing interest for sodium-based batteries: the resources of sodium as a replacement to lithium can be considered as infinite, even though the latter allows higher energy densities and easier handling.

Table I.1. Comparison of different energy storage technologies; LCOE: levelized cost of energy, WDE: world daily electricity production. Levelized costs are presented as means for comparison; they might not reflect the actual cost of a real unit. The resource availability for electrochemical storage technologies is an estimation of the energy that would be provided by the use of all the reserves of the less available active material of the system, compared to the world daily electricity production (WDE).

Technology	LCOE[14-15] ($ MWh^{-1})	Round-trip efficiency (%)	Resources availability[16]
Pumped Hydro.	150-210	75-80	Geographic limitation
Compressed Air	120-200	50-70	Geographic limitation
NaS	260-290	75-85	>> 100 WDE
VRB	400-800	75-90	< WDE
Zinc-Bromine	200-900	60-75	> 10 WDE
Zinc-Air	150-200	<50	> 10 WDE
Lead-Acid	300-600	70-85	1 WDE
Li-ion	100-300	>85	< 10 WDE

3. The current technologies

Several technologies can be considered for smart grid applications. Here, the two main systems currently used and projected to be used in the short-term will be detailed.

Sodium-sulfur (NaS):

Developed by the Japanese companies TEPCO and NGK since the mid-1980s, the sodium-sulfur high-temperature battery system is commercially exploited since 2002, essentially for electricity load-leveling applications. It is based on the formation of sodium polysulfides from sulfur and sodium during discharge (Figure I.3). The core material that allowed the development of this technology is the β-alumina solid electrolyte, which provides a high ionic conductivity for sodium ions at high temperatures, comparable to that of aqueous electrolytes. Its use however render mandatory operation at temperature above 300°C, both because the ionic conductivity is insufficient at lower temperature and to enhance the wetting of the electrolyte by the molten sodium, in order to decrease the resistance at the interface and by extension the overall cell resistance[17].

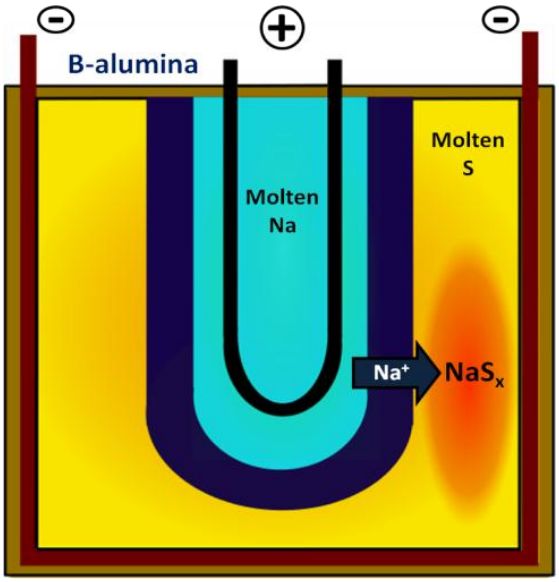

Negative electrode: liquid sodium

$$Na = Na^+ + e^-$$

Positive electrode: liquid sulfur and porous carbon

$$x\,S + Na^+ + e^- = NaS_x$$

Figure I.3. Working principle of the NaS battery.

NaS batteries offer many advantages:

- Coulombic efficiency of nearly 100 %;
- No self-discharge;
- High cyclability (4500 cycles at 90 % depth of discharge);

- Long calendar life (15 years estimated);
- Recyclability of 98 % of the components.

When also considering the high availability and low production costs of the active materials and electrolyte composing the system, the NaS battery is recognized as one of the best candidates for integration of wind power plants in electrical grids. However, the global energy efficiency of the system can be significantly limited due to its operating temperature. Indeed, although in continuous cycling operation the thermal losses are in part compensated by Joule effects, in stand-by conditions, the operation temperature can only be maintained by external heating, which can represent 0.5 to 1 % of the nominal capacity of the battery per hour[15]. The system can nevertheless be "frozen" at ambient temperature for extended stop, but will require 24 to 48 hours to be fully operational afterwards. Therefore, NaS systems are not suitable for occasional usage applications, and their energy efficiency depends on the duration of the inactivity/idling periods they are submitted to.

Since reactive molten sodium is used at high temperature, together with the formation of highly corrosive sodium sulfides during discharge, there might also be concerns regarding the battery safety in operation, and the energy storage facilities might be limited both in size and geographic locations.

At present, the research on the NaS technology mainly focuses on the lowering of the working temperature, *e.g.* by enhancing the wetting of the beta-alumina and its conductivity at lower temperatures, or by replacing it by another Na^+-conducting solid electrolyte[18].

Vanadium redox flow battery (VRB):

The main intrinsic advantage of redox flow batteries is the ability to adjust energy and power ratings independently, since energy is related to the amount of electrolyte externally stored, while power is related to the number and size of the cells used. Using the same electrolyte for all cells also prevents over or under-charging of a single cell, since the state of discharge is related to the concentration of the active species in the electrolyte. Thus, this technology is easily scalable and particularly suitable for evolutive projects[13, 19-21].

VRB were first patented by the Australian University of New South Wales (UNSW) in 1986, and are currently implemented in several 10s to 100s kW units. During discharge (Figure I.4), V(V) is reduced at the positive electrode while V(II) is oxidized at the negative, and protons are exchanged through a proton exchange membrane similar to that of a proton exchange membrane fuel cell (PEMFC). Since the anolyte and catholyte are composed of the same chemical elements, though at

different oxidation degrees, the impact of leakage or membrane failure on the system is limited. VRB also offer very high cyclability (>10,000 cycles, more than 13,000 having been demonstrated on a 20 kW unit[15]). The lifetime of the system is essentially limited by the membrane, which can be replaced after 8-10 years to extend the operating time to possibly more than 20 years. Another intrinsic advantage of the technology is that vanadium can be mostly recovered after use.

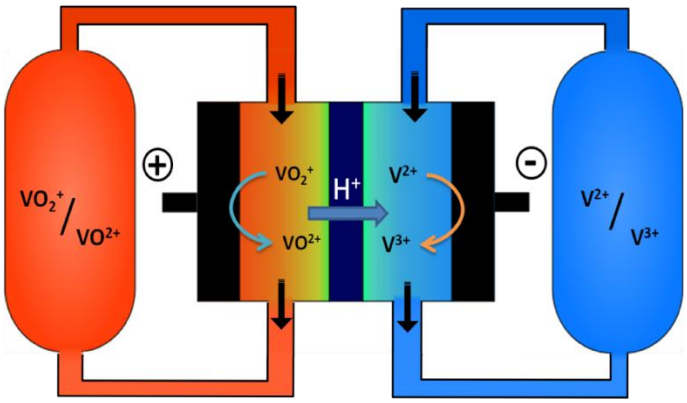

Negative electrode:

$$V^{2+} = V^{3+} + e^-$$

Positive electrode:

$$2\,H^+ + VO_2^+ + e^- = VO^{2+} + H_2O$$

Figure I.4. Working principle of the vanadium redox-flow battery.

Apart from the above-mentioned issues regarding the overall cost and vanadium resources, the system suffers from its low energy density. As the concentration in vanadium is limited to 2 M in sulfuric acid, the energy density of the electrolyte is of 25 Wh L^{-1}. A 1 MWh unit would therefore require more than 40 m^3 concentrated sulfuric acid electrolyte storage, and occupy *ca*. 100 m^2 space (compared to 5 m^2 of NaS batteries for similar energy storage), which would not make it suitable for every location/application[15].

The main research on the technology currently aims to improve the energy density of the system, either by allowing higher concentrations of vanadium or using other chemistries for one of the two electrodes (*e.g.* the vanadium/halides batteries), achieve higher round-trip efficiencies, or replace the membrane to reduce the system costs or improve its efficiency.

4. Aprotic metal-air

Systems based on the association between oxygen and highly abundant, low oxidation potential, and low molar mass alkali metals can be regarded amongst the best candidates for electrochemical energy storage on the long term. Depending on the nature of the electrolyte

(aqueous *vs.* aprotic), the chemistry and the properties of these systems are completely different. Here, we will focus on non-aqueous alkali metal-oxygen batteries.

General description of a non-aqueous alkali metal-air battery (AAB):

In its most simple embodiment, the AAB system can be described by Figure I.5. During discharge, solid alkali metal oxides, in the broadest definition, MO_x, are precipitated on the porous positive electrode, from the oxidation of the metal and the reduction of the oxygen. The possible reaction products are described in Table I.2. At current knowledge, whatever the metal used, a superoxide species MO_2 is formed as an intermediate or main discharge product. The mechanisms of the reactions at stake will be discussed in the following chapter; here we will consider the general mechanism proposed in Figure I.5 as admitted. The electrolyte can either be liquid, made of an aprotic organic solvent or an ionic liquid, or solid, and is generally concentrated in alkali metal cations[22-26].

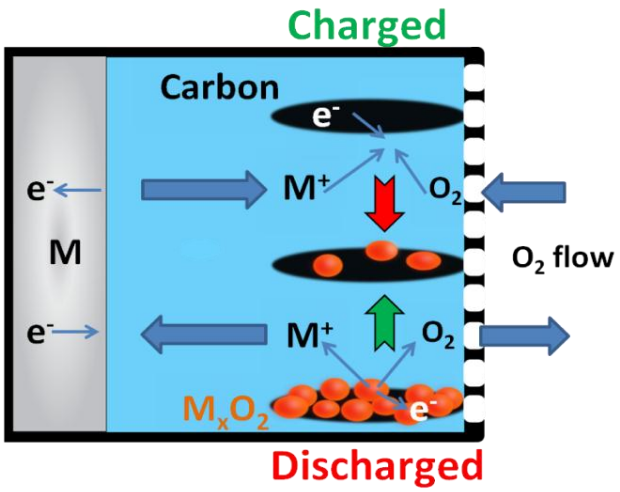

Negative electrode: solid alkali metal

$$M = M^+ + e^-$$

Positive electrode: porous air electrode

$$x\,M^+ + O_2 + x\,e^- = M_xO_2$$

Figure I.5. Working principle of the non-aqueous alkali metal-air battery.

Table I.2. Expected products and maximal theoretical energy density achievable for several non-aqueous alkali metal-air batteries.

Alkali metal	Main discharge product	Maximal energy density ($Wh\ kg^{-1}_{discharge\ product}$)
Li^+	Li_2O_2	3400
Na^+	NaO_2	1100
	Na_2O_2	1500
K^+	KO_2	950

A theoretical maximal energy density for those systems can be estimated from the weight of the main discharge product formed (Table I.2). The practical energy density is rather difficult to predict since it depends a lot on the design of the whole system, the electrolyte used or the balancing of the electrodes (the negative would be expected to be slightly overloaded). However, even if considering a factor of 3 to 4, the AAB energy density value would still be higher than that anticipated for the lithium-ion technology (at present limited to *ca*. 250 Wh kg^{-1}), and one of the highest achievable for any battery[27].

Ideally, the oxygen used would directly be harvested from ambient air. Since any of the MO_x precipitated during discharge are reactive toward water and carbon dioxide, air purification seems necessary[28]. Furthermore, there might be concerns regarding the interactions between nitrogen and alkali metals. Although dehydration through a membrane has already been demonstrated[29], selectivity to sole oxygen molecules seems much more complicated. Therefore, most of the works on non-aqueous alkali metal-air batteries are actually done using pure oxygen as an oxidant, and here we will use the term of non-aqueous alkali metal oxygen batteries (AOB).

Alkali metal negative electrodes:

The practical use of an alkali metal negative electrode, especially lithium, in a secondary battery has been long considered: reversible lithium deposition in propylene carbonate was demonstrated in 1958, for example[30]. Prototypes using titanium disulfide as positive intercalation electrode and lithium metal as negative, with a liquid electrolyte, were commercialized by Exxon in the late 1970s[31]. However, the formation of dendrites during cycling, causing short-cuts and explosions, hindered their effective use. Several solutions were proposed to allow smoother lithium deposition, such the use of additives in the electrolyte[32], but a graphite negative has been finally used as an alternative, which is the basis of the now world-wide lithium-ion technology (Sony

1991[28]). Replacing the liquid electrolyte by a polymer electrolyte is another way to limit the formation of dendrites, and is currently used in the lithium metal polymer technology of Batscap, which now equips Bolloré's Blue Car[12].

In the case of AOB, the use of a metal negative electrode might be even more complicated. Indeed, the studies already done on lithium cyclability have been performed in oxygen-free environment. In the presence of oxygen, the structure of the solid electrolyte interphase and the effect of additives would likely be different. Moreover, the formation of soluble intermediates on the positive electrode, or soluble degradation products, either on the positive or on the negative electrode, could lead to complex shuttling effects. Such effects have been demonstrated in lithium-sulfur batteries[33], and considered in some studies on lithium-oxygen batteries[34]. In the case of even more reactive sodium and potassium metals, a protection of the negative electrode by a solid electrolyte might be mandatory.

Thus, if an un-protected alkali metal negative electrode is to be used in an AOB, then, not only the phenomena related to the positive and negative electrodes have to be studied and understood, but also the indirect interactions between both of them. However, here, as in most of the literature, we will focus on the phenomena relative to the positive electrode.

Lithium oxygen battery (LiOB):

Since the first publication on an aprotic lithium oxygen battery in 1996[35], the interest on the technology has grown fast, owing to its very high theoretical energy density, which is making it a potential candidate for the replacement of lithium-ion batteries. Indeed, LiOB is one of the rare systems to meet the costs, energy density and resources availability objectives for electrical vehicles (in principles).

The beginning of the research on the subject was essentially focused on enhancing the discharge capacity and rate capability for primary batteries, by varying the structure of the electrode[36-37], composition of the electrolyte[38-39], or by improving the cell design[40]. The limited cyclability and the high recharge overvoltage were attributed to pore-blocking by insulating discharge products[37, 41], either Li_2O_2 or Li_2O, as an analogy to lithium thionyl-chloride batteries[42]. Catalysts, such as MnO_2[43] or Au-Pd[44] had proven to enhance the cyclability and limit the overvoltage, at least at the beginning of the recharge[45], but the mechanisms associated to their effects is still under debate.

In the early studies, the vast majority of the electrolytes were based on carbonates solvents (*e.g.* propylene carbonate, PC, or ethylene carbonate, EC), as they were classically used in lithium-

ion batteries. However, these solvents are generally prone to nucleophile attack by superoxide anion[46-47] and are unstable toward Li_2O_2[48]. Thus, the main products actually formed were not LiO_x but lithium carbonates or formates, mainly resulting from the decomposition of the solvent[49]. This has lead to an intense effort on the understanding of the degradation mechanisms occurring during operation of the system, and finding stable electrolytes.

These studies are in general using one or more of the following 5 major methods:

- Computational studies[50-52]: particular types of reactions (nucleophilic substitution, H abstraction) are postulated. Solvents can then be pre-sorted as being prone or not to the particular reactivity. Although this methodology can help to limit the number of solvent to be experimentally tested, it does not provide a definite answer to the question: subtle effects might be missed (specific interactions or solvation effects) and thus potential candidates might be erroneously rejected;
- Pure chemical studies[53-54]: electrolytes and materials are put in contact with the reactive product, generally KO_2 or Li_2O_2, and the formation of degradation products is monitored over (or after) a given reaction time, by infrared spectroscopy (IR) or nuclear magnetic resonance (NMR), for example. These methods are less complex to screen stable materials than electrochemical cycling of batteries. However, the latter tests are still necessary to conclude, since the degradation is usually more pronounced under potential control, and can lead to completely different phenomena than in open-circuit conditions. Thus, chemical studies are an efficient way to make a pre-selection of candidates, but also as an assessment of the actual stability of the materials over the long term (*e.g.* for calendar life assessment); they can however not substitute tests in real operating conditions..
- Electrochemical model studies[55-56]: electrode and/or electrolyte materials are tested using a 3-electrode cell with a model working electrode, and a very large excess of electrolyte. For example, the reversibility of the oxygen reduction in presence of tetraalkylammonium cations, thus the stability of superoxide in a particular solvent, can be readily assessed from cyclic voltammetries on a smooth glassy carbon surface[57]. Coupling with *in situ* physical characterization, such as Fourier transform infra-red spectroscopy (FTIR)[58], Raman spectroscopy, or mass spectrometry (DEMS: differential electrochemical mass spectrometry), can help to understand the degradation mechanisms. The main limitation of these techniques is the use of an excess of electrolyte, which also provides an excess of impurities and facilitates solubilization of the decomposition/reaction products. Thus, they are suitable to perform a first screening of electrolyte and electrode materials, and to

isolate and understand particular phenomena, but cannot substitute tests in real operating conditions.

- *Ex situ* characterizations after battery cycling[59-62]: the positive electrode and the electrolyte are analyzed at different depths of discharge or recharge, or after several cycles. Since LiO_x are reactive toward ambient air, particular attention has to be given during transfers and characterization. Also, since LiO_2 can disproportionate to Li_2O_2 over time[63], and that this reaction rate might depend on the solvent or the oxygen pressure, subtle effects might be missed.
- *In situ* characterizations during battery cycling[64-66]: the positive electrode is analyzed without disassembling the battery, which provides the advantage of avoiding contaminations and offers real-time measurements, but at the cost of a generally lower precision, a much more complex experimental design and (sometimes) far-from-real operating conditions.

Of the *in situ* characterizations, one technique was proven particularly efficient: the monitoring in nearly real time of the gases consumed and formed during discharge and charge of the battery by mass spectrometry[59, 67]. Using this technique, the amount of electrons passed through the positive electrode per molecule of O_2 consumed or evolved can be evaluated in the course of the charge and discharge. Furthermore, the evolution of gases formed by the electrode/electrolyte oxidation or decomposition products, such as H_2 and mainly CO_2, can be monitored, and isotope-labeling allows identifying the origin of these gases[68].

From these studies, it appears that most of the classical solvents are not suitable for LiOB. Some of the most stable solvents identified are ethers, particularly dimethoxyethane (DME), nitriles (acetonitrile: Acn), acetamides (dimethylacetamide: DMA), or sulfoxides (dimethylsulfoxide: DMSO), although there are also evidences for minor degradations in presence of any of these. Not only are the solvents unstable, but also the electrode materials in the aggressive environment of an operating LiOB. In particular, carbon is decomposed in contact with Li_2O_2, to form a lithium carbonates layer, and polyvinylidene fluoride (PVDF), used as a binder in some systems, is unstable toward superoxide. It has also been observed that the presence of catalysts, such as platinum and gold, was actually promoting side reactions[69], which were the reason for apparent enhancement of the capacity and cyclability of the systems. Figure I.6 schematizes the main durability issues in LiOB.

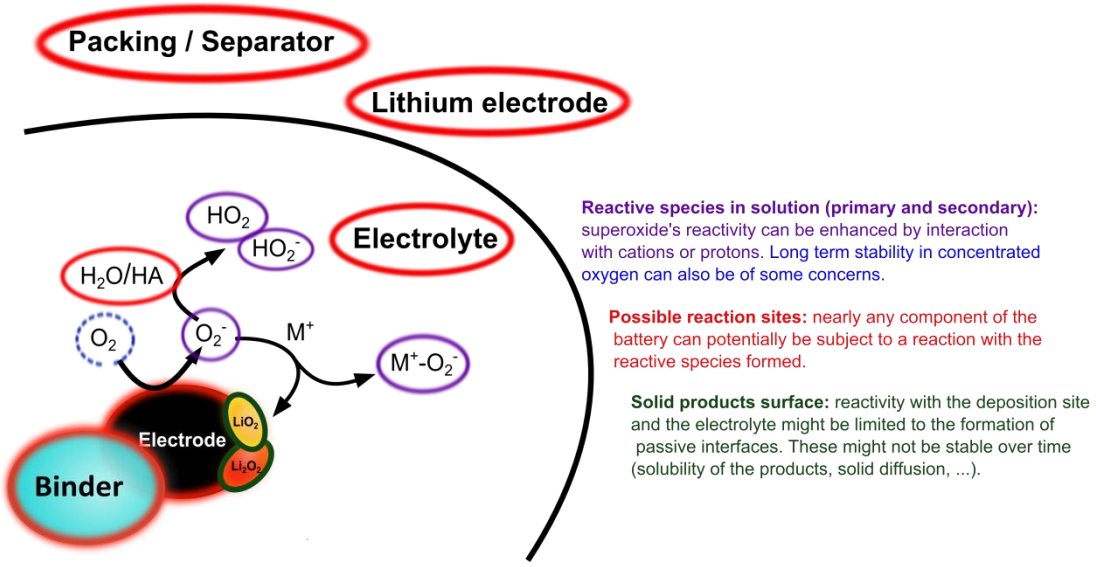

Figure I.6. Reactivity issues in LiOB

Indeed, the presence of impurities, from the electrolyte, leakages during the experiment, or degradation products formed during cycling, has a complex effect on the battery behavior.

CO_2, for example, enhances the discharge capacity[70], but also displays adverse effects. Li_2O_2 is known to react with CO_2 quickly and efficiently[71]: it is used in air purifying systems. Li_2CO_3, formed by reaction (I.1), is not likely to be more soluble than Li_2O_2, is even less conducting, and less dense.

$$Li_2O_2 + CO_2 \longrightarrow Li_2CO_3 + \frac{1}{2}O_2 \qquad (I.1)$$

Thus, in terms of a passivation and pore-blocking by a non-conductive solid product, the situation is expected to be worse in the presence of CO_2. There are however two possible explanations for the enhancement of the capacity of LiOB in the presence of CO_2:

- the formation of Li_2CO_3 is involving 4 electrons per oxygen molecule, thus the capacity per unit of volume is higher;
- the limitation of the capacity is not (only) due to pore blocking and oxygen mass-transport difficulties, but mainly to the formation of an insulating Li_2O_2 film on the electrode surface, and thus to the decrease of the surface area available; in that case, the reaction (I.1) will generates cracks in this film, liberating part of the surface.

This last proposition is related to a debate that remains partially unresolved when writing these lines[ii]: what is the actual form of the Li_2O_2 deposit? With an electrolyte based on stable

[ii] Considering the number of high quality publications and groups working on the subject, the arguments presented here are based on very recent results at the moment of the writing and might lead to outdated conclusions at the moment of the reading. Presently, a serious update of the bibliography is needed every 6 months in average.

solvents, *e.g.* DME, the most usually observed form of deposit was either large crystalline toroids (100-500 nm)[72] or a compact film of several nanometers thickness[24]. The first explanation proposed for this discrepancy is that the crystals size is essentially depending on the discharge rate[73]: higher rates would limit diffusion of the intermediates in solution or at the electrode surface, and therefore favor smaller crystals or even amorphous films.

A more recent and likely explanation has ascribed the formation of toroids mainly to the presence of water, which would, in short, better solubilize the reaction intermediates[74-75]. The complex role of water will be developed in the following chapter. Nevertheless, from a practical point of view, it is interesting to notice that:

- water can be present as an impurity, and thus not considered as an active material;
- it is consumed during discharge;
- it is not (or only partially) reproduced during charge;
- Li_2O_2 remains the main discharge product[75].

Thus, by performing only battery cycling and *ex situ* physical characterization afterwards, the actual working principle would have been missed. Furthermore, similarly to the case of carbonates-based solvents, optimization would have been done on potentially non-viable systems, since it produces much more chemical non-reversibility than expected. The very important effect of impurities also raises the question of comparability between different studies where many parameters can vary, without being even noticed.

Thus, the first analysis that should be done when working on new electrolytes, electrode materials, or additives for LiOB, is an assessment of the stability of the compounds. Since usually an excess of electrolyte is used in laboratory cells, as compared to practical prototype where the electrolyte proportion is kept as low as possible, the side reactions can actually enhance the apparent capacity and cyclability of the system[76], and even lead to apparently perfectly-working systems.

Even when using more stable electrode and electrolyte materials, the cyclability of LiOB is limited and the charging overpotentials remain above reasonable limits, thereby impeding the battery round-trip efficiency. This behavior is mainly accounted for by the formation of poorly conductive Li_2O_2 particles[56], which require high overpotentials to be completely oxidized, together with the formation of insulating degradation products[68]. These conclusions should be valid whatever the actual morphology of the products or the presence of impurities. Interestingly, this behavior can lead to a snowball effect (Figure I.7):

- high overpotentials during charge are leading to the degradation(s) of the electrolyte and/or electrode;

- the degradation products are reacting with the discharge products, apparently enhancing the discharge capacity of the subsequent cycle;
- the charging overpotentials are becoming higher due to the presence of more insulating compounds, leading to even more degradations.

Again, if the electrolyte is in excess, this snowball effect may be blurred and can lead to an apparent 100 % coulombic efficiency, even though the chemical reversibility is much lower, which emphasizes the importance of full cell (or at least half cell) experiments in the presence of "practical" amounts of electrolytes.

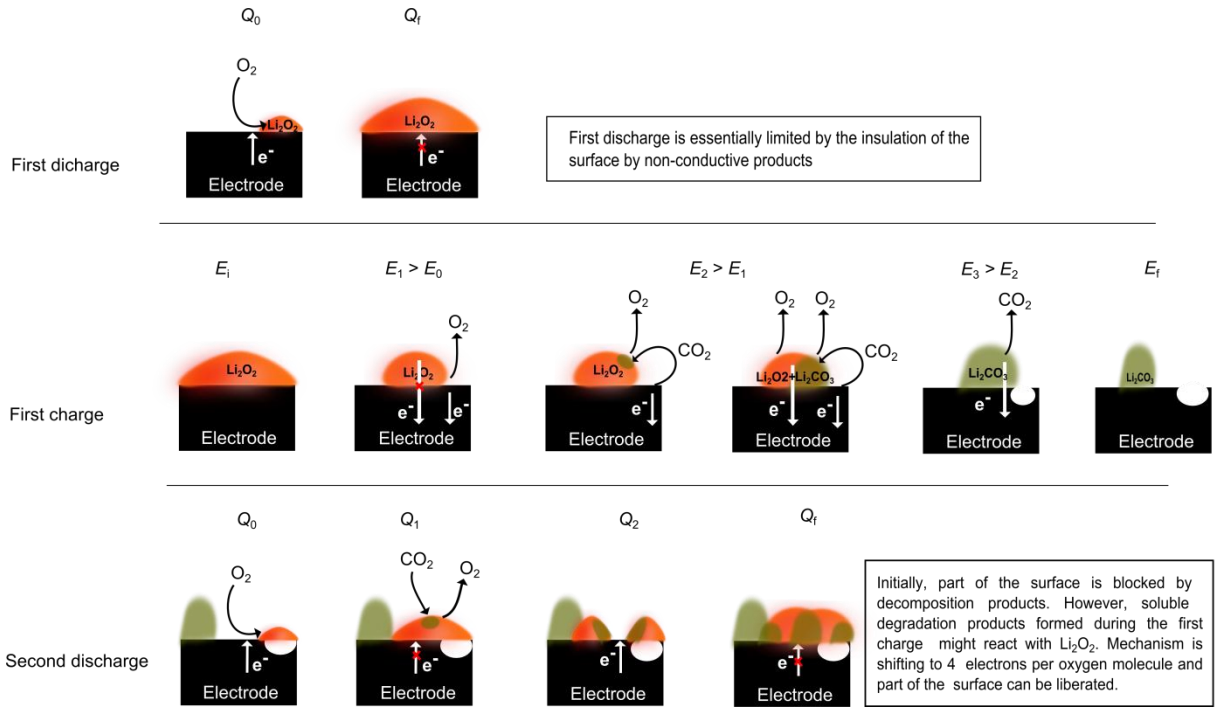

Figure I.7. Illustration of the snowball effect. For clarity, only CO_2 formation from the decomposition of the carbon electrode has been taken into account. The same reasoning can be applied to other degradations (electrolyte, binder, current collector).

In order to overcome this limitation, the use of redox mediators (also named redox shuttle or solution-phase catalysts) has been proposed, and patented in 2011[77]. This idea is based on the concept that, at a certain overpotential during charge, a fraction of the surface is freed from the insulating compounds formed during the discharge, and therefore becomes available to oxidize the mediator in solution (figure I.8.a). This oxidized mediator can diffuse to the Li_2O_2 particles which could not be oxidized at that overpotential directly by electron transfer from the electrode, and "chemically" react with it to produce the reduced mediator (its original state) and O_2[78]. In practice, the mediator has to sustain the same conditions as any other additives for LiOB: the number of potential candidates that can successfully undergo such stability test is dramatically limited. Besides,

even if candidate species are isolated, other important practical aspects have yet to be discussed, such as the amount of mediator effectively necessary or its potential interactions with the negative electrode, which could lead to shuttling effects similar to those of lithium-sulfur batteries[33] and lower the system coulombic efficiency and rechargeability.

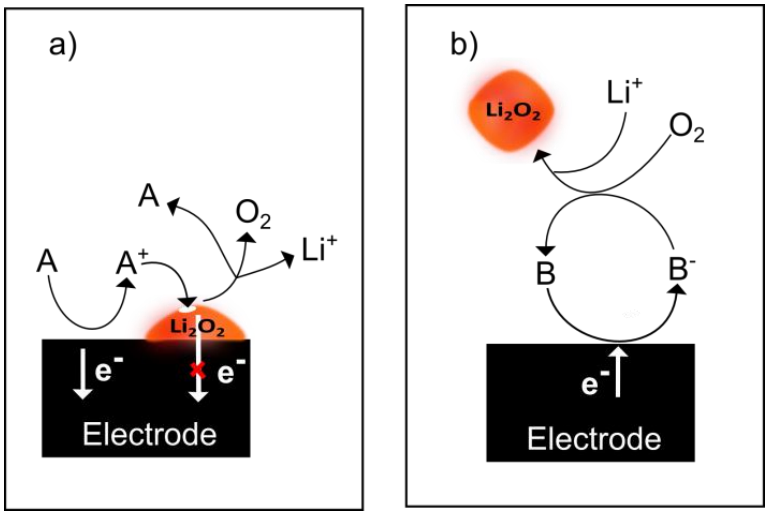

Figure I.8. Working principle of redox shuttle in LiOB during charge (a) and discharge (b)

The redox mediator concept has also been applied to the discharge (figure I.8.b); in that case, the mediator is firstly reduced at the electrode surface and then reduces the oxygen in solution in the course of its re-oxidation into its original state. Applying this strategy avoids the formation of an insulating film directly on the electrode surface, but definitely renders mandatory to use an oxidation mediator to oxidize the Li_2O_2 precipitate (present away from the electrode surface) into O_2. In a favored scenario, a bifunctional mediator would be found[79].

Another possibility that is currently explored to heighten the cyclability of LiOB, is to limit the formation of the passive film, notably by enhancing the solubility of the reactions intermediates, mainly LiO_2. This can be done either directly by using a solvent with a strong solvation of either the lithium cation or the superoxide anion, or by using additives[74]. Again, and particularly for that latter case, the stability of the additives toward the discharge products has to be checked, as their reactivity might have the same behavior as the solubilization of the reaction products (at least during the discharge).

Sodium and potassium oxygen (NaOB and KOB):

In parallel to the research on LiOB, the working principle of a very similar system using a sodium negative electrode instead of lithium has been first published in 2012[80]. Studies with potassium followed 6 months later[26].

As far as the positive electrode is concerned, the main difference between the various MOB is the final product formed upon discharge. In the case of the KOB, KO_2 seems to be the only KO_x product obtained after discharge. Since it is more conductive than Li_2O_2[81], possibly more soluble in the solvents used and is directly formed by the one-electron reduction of oxygen, the overpotentials required for its re-oxidation into O_2 are much more limited. For NaOB, NaO_2 has generally been observed as the main discharge product[82], with one exception, where Na_2O_2 has been characterized[83]. At ambient temperature, NaO_2 disproportionation is thermodynamically favored[84], and Na_2O_2 would thus be expected, even in low amounts. This reaction might be kinetically limited, possibly even more in the presence of a solvent. The same reasoning as for KOB explains the low overpotential observed during charging of the system.

In principle, those systems will suffer from the same limitations as LiOB, with however, a few major differences[85]:

- if the solubility of the superoxide anion, and thus its lifetime in the electrolyte, is higher, then it will have more time to react with the battery constitutive materials;
- since the discharge products are remaining under the form of solid superoxide, their reactivity over the long term with the electrode and the electrolyte has to be assessed. It might be higher than that of Li_2O_2;
- since the charging overpotentials are lower than for LiOB, the degradations during charge might be limited.

Conclusion

From the analysis of the working principle and the limitations of the MOB, it appears that a very interesting property of these systems is the production of solid, relatively stable and highly energetically-dense products MO_x, from widely available compounds. Thus in the optic of massive energy storage, solutions involving these products might be relevant. This opinion is further discussed in an internal classified report delivered to Hutchinson SA.

The other aspect that has been evidenced in this chapter is the importance of the understanding of the phenomena by the means of model experiments. Several techniques have been developed so far, from reproducible and optimized purely electrochemical experiments to coupled *in situ* FTIR, Raman and DEMS measurements. Those techniques allowed a better understanding of the limitations of the systems, including the snowball effect, and those results are also discussed in the internal report. They have further led to a better understanding of the oxygen

reduction mechanism itself, which is the main object of the present thesis, and the focus of the next section.

Bibliography:

1. White, L. A., *The Evolution of Culture: The Development of Civilization to the Fall of Rome*; McGraw-Hill, **1959**.
2. Kremer, M., *Quaterly Journal of Economics* **1993**, *108*, 681-716.
3. Annual Energy Review. US Energy Information Administration: **2012**. http://www.eia.gov/totalenergy/data/annual/showtext.cfm?t=ptb1601.
4. Goklany, I. M., *The Improving State of the World: Why We're Living Longer, Healthier, More Comfortable Lives on a Cleaner Planet* Cato Institute, **2007**.
5. EIA World Energy Outlook. http://www.worldenergyoutlook.org/.
6. Energy Outlook 2035. BP: **2014**. http://www.bp.com/content/dam/bp/pdf/Energy-economics/Energy-Outlook/Energy_Outlook_2035_booklet.pdf.
7. Keay, M., Energy the Long View. Oxford Institute: **2007**. http://www.oxfordenergy.org/wpcms/wp-content/uploads/2010/11/SP20-EnergyThelLongView-MalcolmKeay-2007.pdf.
8. Rühl, C.; Appleby, P.; Fennema, J.; Naumov, A.; Schaffer, M. Economic Development and the Demand for Energy: A Historical Perspective on the Next 20 Years. http://www.bp.com/content/dam/bp/pdf/statistical-review/reports_and_publications_economic_development_demand_for_energy.pdf.
9. Annual Energy Review. US Energy Information Administration: **2011**. http://www.eia.gov/totalenergy/data/annual/pdf/aer.pdf.
10. Grid Energy Storage. DOE: **2013**.
11. Parfomak, P. W., Energy Storage for Power Grids and Electric Transportation: A Technology Assessment. Congessional Research Service: **2012**.
12. Deschamps, M. Bilayer Electrolyte for a Lithium Battery, WO2006077325A2, **2006**.
13. Eckroad, S., Vanadium Redox Flow Batteries. Electric Power Research Institute: **2007**.
14. Electricity Storage Handbook. DOE/EPRI: **2013**.
15. Delille, G. M. A. Contribution Du Stockage À La Gestion Avancée Des Systèmes Électriques, Approches Organisationnelles Et Technico-Économiques Dans Les Réseaux De Distribution. PhD. Ecole Centrale de Lille, **2010**.
16. Wadia, C.; Albertus, P.; Srinivasan, V., Resource Constraints on the Battery Energy Storage Potential for Grid and Transportation Applications. *Journal of Power Sources* **2011**, *196*, 1593-1598.
17. Viswanathan, L.; Virkar, A. V., Wetting Characteristics of Sodium on B”-Alumina and on Nasicon. *Journal of Material Science* **1982**, *17*, 753-759.

18. Lu, X.; Xia, G.; Lemmon, J. P.; Yang, Z., Advanced Materials for Sodium-Beta Alumina Batteries: Status, Challenges and Perspectives. *Journal of Power Sources* **2010**, *195*, 2431-2442.

19. Cunha, Á.; Martins, J.; Rodrigues, N.; Brito, F. P., Vanadium Redox Flow Batteries: A Technology Review. *International Journal of Energy Research* **2015**, *39*, 889-918.

20. Kear, G.; Shah, A. A.; Walsh, F. C., Development of the All-Vanadium Redox Flow Battery for Energy Storage: A Review of Technological, Financial and Policy Aspects. *International Journal of Energy Research* **2012**, *36*, 1105-1120.

21. Shibata, T.; Kumamoto, T.; Nagaoka, Y.; Kawase, K.; Yano, K. *Redox Flow Batteries for the Stable Supply of Renewable Energy*; Sumitomo Electric: **2013**.

22. Lu, J.; Li, L.; Park, J.-B.; Sun, Y.-K.; Wu, F.; Amine, K., Aprotic and Aqueous Li–O2 Batteries. *Chemical Reviews* **2014**, *114*, 5611-5640.

23. Kraytsberg, A.; Ein-Eli, Y., Review on Li–Air Batteries—Opportunities, Limitations and Perspective. *Journal of Power Sources* **2011**, *196*, 886-893.

24. Luntz, A. C.; McCloskey, B. D., Nonaqueous Li–Air Batteries: A Status Report. *Chemical Reviews* **2014**, *114*, 11721-11750.

25. Das, S. K.; Lau, S.; Archer, L. A., Sodium-Oxygen Batteries: A New Class of Metal-Air Batteries. *Journal of Materials Chemistry A* **2014**, *2*, 12623-12629.

26. Ren, X.; Wu, Y., A Low-Overpotential Potassium–Oxygen Battery Based on Potassium Superoxide. *Journal of the American Chemical Society* **2013**, *135*, 2923-2926.

27. Linden, D. B.; Reddy, T. B., *Handbook of Batteries*, Fourth Edition ed., Mc Graw-Hill **2011**.

28. Christensen, J.; Albertus, P.; Sanchez-Carrera, R. S.; Lohmann, T.; Kozinsky, B.; Liedtke, R.; Ahmed, J.; Kojic, A., A Critical Review of Li/Air Batteries. *Journal of the Electrochemical Society* **2011**, *159*, R1-R30.

29. Zhang, J.; Xu, W.; Li, X.; Liu, W., Air Dehydration Membranes for Nonaqueous Lithium–Air Batteries. *Journal of the Electrochemical Society* **2010**, *157*, A940-A946.

30. Vincent, C. A., Lithium Batteries: A 50-Year Perspective, 1959–2009. *Solid State Ionics* **2000**, *134*, 159-167.

31. Scrosati, B.; Abraham, K. M.; Van Schalkwijk, W. A.; Jusef Hassoun, J., *Lithium Batteries: Advanced Technologies and Applications*; Wiley, **2013**.

32. Matsuda, Y.; Morita, M., Organic Additives for the Electrolytes of Rechargeable Lithium Batteries. *Journal of Power Sources* **1989**, *26*, 579-583.

33. Mikhaylik, Y. V.; Akridge, J. R., Polysulfide Shuttle Study in the Li/S Battery System. *Journal of the Electrochemical Society* **2004**, *151*, A1969-A1976.

34. Uddin, J.; Bryantsev, V. S.; Giordani, V.; Walker, W.; Chase, G. V.; Addison, D., Lithium Nitrate as Regenerable Sei Stabilizing Agent for Rechargeable Li/O2 Batteries. *The Journal of Physical Chemistry Letters* **2013**, *4*, 3760-3765.

35. Abraham, K. M.; Jiang, Z., A Polymer Electrolyte-Based Rechargeable Lithium/Oxygen Battery. *Journal of the Electrochemical Society* **1996**, *143*, 1-5.

36. Younesi, S. R.; Urbonaite, S.; Björefors, F.; Edström, K., Influence of the Cathode Porosity on the Discharge Performance of the Lithium–Oxygen Battery. *Journal of Power Sources* **2011**, *196*, 9835-9838.

37. Tran, C.; Yang, X.-Q.; Qu, D., Investigation of the Gas-Diffusion-Electrode Used as Lithium/Air Cathode in Non-Aqueous Electrolyte and the Importance of Carbon Material Porosity. *Journal of Power Sources* **2010**, *195*, 2057-2063.

38. Zhang, S. S.; Read, J., Partially Fluorinated Solvent as a Co-Solvent for the Non-Aqueous Electrolyte of Li/Air Battery. *Journal of Power Sources* **2011**, *196*, 2867-2870.

39. Xu, W.; Xiao, J.; Zhang, J.; Wang, D.; Zhang, J.-G., Optimization of Nonaqueous Electrolytes for Primary Lithium/Air Batteries Operated in Ambient Environment. *Journal of the Electrochemical Society* **2009**, *156*, A773-A779.

40. Adams, J.; Karulkar, M., Bipolar Plate Cell Design for a Lithium Air Battery. *Journal of Power Sources* **2012**, *199*, 247-255.

41. Mirzaeian, M.; Hall, P. J., Characterizing Capacity Loss of Lithium Oxygen Batteries by Impedance Spectroscopy. *Journal of Power Sources* **2010**, *195*, 6817-6824.

42. Hills, A. J.; Hampson, N. A.; Hayes, M., Passivation of Porous Carbon Cathodes in Lithium-Thionyl Chloride Cells. *Journal of Applied Electrochemistry* **1987**, *17*, 702-706.

43. Débart, A.; Paterson, A. J.; Bao, J.; Bruce, P. G., A-Mno2 Nanowires: A Catalyst for the O2 Electrode in Rechargeable Lithium Batteries. *Angewandte Chemie International Edition* **2008**, *47*, 4521-4524.

44. Lu, Y.-C.; Xu, Z.; Gasteiger, H. A.; Chen, S.; Hamad-Schifferli, K.; Shao-Horn, Y., Platinum−Gold Nanoparticles: A Highly Active Bifunctional Electrocatalyst for Rechargeable Lithium−Air Batteries. *Journal of the American Chemical Society* **2010**, *132*, 12170-12171.

45. Lu, Y.-C.; Gasteiger, H. A.; Crumlin, E.; McGuire, R.; Shao-Horn, Y., Electrocatalytic Activity Studies of Select Metal Surfaces and Implications in Li-Air Batteries. *Journal of the Electrochemical Society* **2010**, *157*, A1016-A1025.

46. Aurbach, D.; Daroux, M.; Faguy, P.; Yeager, E., The Electrochemistry of Noble Metal Electrodes in Aprotic Organic Solvents Containing Lithium Salts. *Journal of Electroanalytical Chemistry and Interfacial Electrochemistry* **1991**, *297*, 225-244.

47. Gibian, M. J.; Sawyer, D. T.; Ungermann, T.; Tangpoonpholvivat, R.; Morrison, M. M., Reactivity of Superoxide Ion with Carbonyl Compounds in Aprotic Solvents. *Journal of the American Chemical Society* **1979**, *101*, 640-644.

48. Laino, T.; Curioni, A., A New Piece in the Puzzle of Lithium/Air Batteries: Computational Study on the Chemical Stability of Propylene Carbonate in the Presence of Lithium Peroxide. *Chemistry – A European Journal* **2012**, *18*, 3510-3520.

49. Freunberger, S. A.; Chen, Y.; Peng, Z.; Griffin, J. M.; Hardwick, L. J.; Bardé, F.; Novák, P.; Bruce, P. G., Reactions in the Rechargeable Lithium–O2 Battery with Alkyl Carbonate Electrolytes. *Journal of the American Chemical Society* **2011**, *133*, 8040-8047.

50. Bryantsev, V. S.; Faglioni, F., Predicting Autoxidation Stability of Ether- and Amide-Based Electrolyte Solvents for Li–Air Batteries. *The Journal of Physical Chemistry A* **2012**, *116*, 7128-7138.

51. Bryantsev, V. S.; Giordani, V.; Walker, W.; Blanco, M.; Zecevic, S.; Sasaki, K.; Uddin, J.; Addison, D.; Chase, G. V., Predicting Solvent Stability in Aprotic Electrolyte Li–Air Batteries: Nucleophilic Substitution by the Superoxide Anion Radical (O2•–). *The Journal of Physical Chemistry A* **2011**, *115*, 12399-12409.

52. Khetan, A.; Luntz, A.; Viswanathan, V., Trade-Offs in Capacity and Rechargeability in Nonaqueous Li–O2 Batteries: Solution-Driven Growth Versus Nucleophilic Stability. *The Journal of Physical Chemistry Letters* **2015**, *6*, 1254-1259.

53. Black, R.; Oh, S. H.; Lee, J.-H.; Yim, T.; Adams, B.; Nazar, L. F., Screening for Superoxide Reactivity in Li-O2 Batteries: Effect on Li2o2/Lioh Crystallization. *Journal of the American Chemical Society* **2012**, *134*, 2902-2905.

54. Amanchukwu, C. V.; Harding, J. R.; Shao-Horn, Y.; Hammond, P. T., Understanding the Chemical Stability of Polymers for Lithium–Air Batteries. *Chemistry of Materials* **2015**, *27*, 550-561.

55. Albertus, P.; Girishkumar, G.; McCloskey, B.; Sánchez-Carrera, R. S.; Kozinsky, B.; Christensen, J.; Luntz, A. C., Identifying Capacity Limitations in the Li/Oxygen Battery Using Experiments and Modeling. *Journal of the Electrochemical Society* **2011**, *158*, A343-A351.

56. Viswanathan, V.; Thygesen, K. S.; Hummelshøj, J. S.; Nørskov, J. K.; Girishkumar, G.; McCloskey, B. D.; Luntz, A. C., Electrical Conductivity in Li2O2 and Its Role in Determining Capacity Limitations in Non-Aqueous Li-O2 Batteries. *The Journal of Chemical Physics* **2011**, *135*, 214704.

57. Bryantsev, V. S.; Uddin, J.; Giordani, V.; Walker, W.; Addison, D.; Chase, G. V., The Identification of Stable Solvents for Nonaqueous Rechargeable Li-Air Batteries. *Journal of the Electrochemical Society* **2013**, *160*, A160-A171.

58. Mozhzhukhina, N.; Méndez De Leo, L. P.; Calvo, E. J., Infrared Spectroscopy Studies on Stability of Dimethyl Sulfoxide for Application in a Li–Air Battery. *The Journal of Physical Chemistry C* **2013**, *117*, 18375-18380.

59. Chen, Y.; Freunberger, S. A.; Peng, Z.; Bardé, F.; Bruce, P. G., Li–O2 Battery with a Dimethylformamide Electrolyte. *Journal of the American Chemical Society* **2012**, *134*, 7952-7957.

60. Veith, G. M.; Nanda, J.; Delmau, L. H.; Dudney, N. J., Influence of Lithium Salts on the Discharge Chemistry of Li–Air Cells. *The Journal of Physical Chemistry Letters* **2012**, *3*, 1242-1247.

61. Xu, W.; Xu, K.; Viswanathan, V. V.; Towne, S. A.; Hardy, J. S.; Xiao, J.; Nie, Z.; Hu, D.; Wang, D.; Zhang, J.-G., Reaction Mechanisms for the Limited Reversibility of Li–O2 Chemistry in Organic Carbonate Electrolytes. *Journal of Power Sources* **2011**, *196*, 9631-9639.

62. Cecchetto, L.; Salomon, M.; Scrosati, B.; Croce, F., Study of a Li–Air Battery Having an Electrolyte Solution Formed by a Mixture of an Ether-Based Aprotic Solvent and an Ionic Liquid. *Journal of Power Sources* **2012**, *213*, 233-238.

63. Snow, R. H. *Thermodynamic Evaluation of the Possibility of Lithium Superoxide Production*; IIT Research Institute: **1965**.

64. Lu, Y.-C.; Crumlin, E. J.; Veith, G. M.; Harding, J. R.; Mutoro, E.; Baggetto, L.; Dudney, N. J.; Liu, Z.; Shao-Horn, Y., In Situ Ambient Pressure X-Ray Photoelectron Spectroscopy Studies of Lithium-Oxygen Redox Reactions. *Scientific Reports* **2012**, *2*.

65. Wen, R.; Hong, M.; Byon, H. R., In Situ Afm Imaging of Li–O2 Electrochemical Reaction on Highly Oriented Pyrolytic Graphite with Ether-Based Electrolyte. *Journal of the American Chemical Society* **2013**, *135*, 10870-10876.

66. Zhong, L.; Mitchell, R. R.; Liu, Y.; Gallant, B. M.; Thompson, C. V.; Huang, J. Y.; Mao, S. X.; Shao-Horn, Y., In Situ Transmission Electron Microscopy Observations of Electrochemical Oxidation of Li2o2. *Nano Letters* **2013**, *13*, 2209-2214.

67. McCloskey, B. D.; Bethune, D. S.; Shelby, R. M.; Girishkumar, G.; Luntz, A. C., Solvents' Critical Role in Nonaqueous Lithium–Oxygen Battery Electrochemistry. *The Journal of Physical Chemistry Letters* **2011**, *2*, 1161-1166.

68. McCloskey, B. D.; Speidel, A.; Scheffler, R.; Miller, D. C.; Viswanathan, V.; Hummelshøj, J. S.; Nørskov, J. K.; Luntz, A. C., Twin Problems of Interfacial Carbonate Formation in Nonaqueous Li–O2 Batteries. *The Journal of Physical Chemistry Letters* **2012**, *3*, 997-1001.

69. McCloskey, B. D.; Scheffler, R.; Speidel, A.; Bethune, D. S.; Shelby, R. M.; Luntz, A. C., On the Efficacy of Electrocatalysis in Nonaqueous Li–O2 Batteries. *Journal of the American Chemical Society* **2011**, *133*, 18038-18041.

70. Gowda, S. R.; Brunet, A.; Wallraff, G. M.; McCloskey, B. D., Implications of Co2 Contamination in Rechargeable Nonaqueous Li–O2 Batteries. *The Journal of Physical Chemistry Letters* **2013**, *4*, 276-279.

71. Capotosto, A.; Petrocelli, A. W. *Use of Lithium Peroxide for Atmosphere Regeneration*; U.S. Air Force: **1968**.

72. Mitchell, R. R.; Gallant, B. M.; Thompson, C. V.; Shao-Horn, Y., All-Carbon-Nanofiber Electrodes for High-Energy Rechargeable Li-O2 Batteries. *Energy & Environmental Science* **2011**, *4*, 2952-2958.

73. Horstmann, B.; Gallant, B.; Mitchell, R.; Bessler, W. G.; Shao-Horn, Y.; Bazant, M. Z., Rate-Dependent Morphology of Li2o2 Growth in Li–O2 Batteries. *The Journal of Physical Chemistry Letters* **2013**, *4*, 4217-4222.

74. Aetukuri, N. B.; McCloskey, B. D.; García, J. M.; Krupp, L. E.; Viswanathan, V.; Luntz, A. C., Solvating Additives Drive Solution-Mediated Electrochemistry and Enhance Toroid Growth in Non-Aqueous Li–O2 Batteries. *Nature Chemistry* **2015**, *7*, 50-56.

75. Schwenke, K. U.; Metzger, M.; Restle, T.; Piana, M.; Gasteiger, H. A., The Influence of Water and Protons on Li2o2 Crystal Growth in Aprotic Li-O2 Cells. *Journal of the Electrochemical Society* **2015**, *162*, A573-A584.

76. Meini, S.; Piana, M.; Tsiouvaras, N.; Garsuch, A.; Gasteiger, H. A., The Effect of Water on the Discharge Capacity of a Non-Catalyzed Carbon Cathode for Li-O2 Batteries. *Electrochemical and Solid-State Letters* **2012**, *15*, A45-A48.

77. Chase, G. V. Soluble Oxygen Evolving Catalysts for Rechargeable Metal-Air Batteries, US20120028137. **2011**.

78. Bergner, B. J.; Schürmann, A.; Peppler, K.; Garsuch, A.; Janek, J., Tempo: A Mobile Catalyst for Rechargeable Li-O2 Batteries. *Journal of the American Chemical Society* **2014**, *136*, 15054-15064.

79. Sun, D., et al., A Solution-Phase Bifunctional Catalyst for Lithium–Oxygen Batteries. *Journal of the American Chemical Society* **2014**, *136*, 8941-8946.

80. Hartmann, P.; Bender, C. L.; Vračar, M.; Dürr, A. K.; Garsuch, A.; Janek, J.; Adelhelm, P., A Rechargeable Room-Temperature Sodium Superoxide (Nao2) Battery. *Nature Materials* **2013**, *12*, 228-232.

81. Gerbig, O. Defect Chemistry in Alkali Peroxides and Superoxides. PhD. Max-Planck-Institut Stuttgart, **2014**.

82. Hartmann, P.; Bender, C. L.; Sann, J.; Durr, A. K.; Jansen, M.; Janek, J.; Adelhelm, P., A Comprehensive Study on the Cell Chemistry of the Sodium Superoxide (Nao2) Battery. *Physical Chemistry Chemical Physics* **2013**, *15*, 11661-11672.

83. Yadegari, H.; Li, Y.; Banis, M. N.; Li, X.; Wang, B.; Sun, Q.; Li, R.; Sham, T.-K.; Cui, X.; Sun, X., On Rechargeability and Reaction Kinetics of Sodium-Air Batteries. *Energy & Environmental Science* **2014**, *7*, 3747-3757.

84. Zhuravlev, Y. N.; Kravchenko, N. G.; Obolonskaya, O. S., The Electronic Structure of Alkali Metal Oxides. *Russian Journal of Physical Chemistry B* **2010**, *4*, 20-28.

85. McCloskey, B. D.; Garcia, J. M.; Luntz, A. C., Chemical and Electrochemical Differences in Nonaqueous Li–O2 and Na–O2 Batteries. *The Journal of Physical Chemistry Letters* **2014**, *5*, 1230-1235.

Chapter II. Oxygen Electrochemistry in the Absence of Water

"*Cum hoc ergo propter hoc*"
Sophism of directly attributing causation to correlation

Paradoxically, it is mostly the interest for the interactions between oxygen reduction products and protons that has motivated the early electrochemical studies of oxygen in aprotic media[1]. Indeed, superoxide is formed as an intermediate during oxygen metabolism in cells, and the understanding of its reactivity is of paramount importance to biologists. Since its stability in aqueous media is limited, aprotic solvents were used to obtain more concentrated and stable superoxide solutions. Furthermore, electrochemistry was proven a powerful analytical technique in order to understand the interactions of superoxide with other compounds, but also an efficient and simple way to generate it[2].[i]

1. Reactivity of superoxide and peroxide, and interaction with alkali metal cations

In its ground state, molecular oxygen is a bi-radical in a triplet state, with two unpaired electrons, explaining the low kinetics of its reactions with most organic molecules, which are in a singlet state[3-4]. Considering its electronic structure, molecular oxygen can undergo two successive one-electron reductions to form superoxide anion (Equation (II.1)) and peroxide dianion (Equation (II.2)). The second one-electron-reduction is only possible at significantly lower potential than the first one, and free superoxide is not considered as a good oxidant and will not disproportionate on its own[5-6].

$$O_2 + e^- = O_2^{\cdot -} \quad \text{(II.1)}$$

$$O_2^{\cdot -} + e^- = O_2^{2-} \quad \text{(II.2)}$$

As a free radical, the actual reactivity of the superoxide anion has been questioned over time[1]. Although the p*Ka* of its conjugate acid, the hydroperoxyl radical, is of 4.8 in water and of 12 in DMF, it can deprotonate water, which has a p*Ka* of 32.6 in DMF, in aprotic media. This can be explained by the fast reaction of the hydroperoxyl radical, either with itself (Equation (II.3)) or with superoxide (Equation (II.4)). Superoxide anion was also proven to be a very powerful nucleophile in non-aqueous media[7]. This anomalous nucleophilicity has been accounted for by a strong alpha-effect, and a favorable electron-transfer in the intermediate state of the reaction[ii].

$$HO_2 + HO_2 = H_2O_2 + O_2 \quad \text{(II.3)}$$

[i] A lot of information on oxygen electrochemistry and interactions with cations can be found in biochemical studies. Indeed, aerobic respiration is based on oxygen reduction, and thus nature-inspired strategies may consist of practical solutions in MOB.

[ii] Documentation on alpha-effect can be found in review[8]: experiments have demonstrated that nucleophiles with unshared pairs of electrons on an atom adjacent to the nucleophilic site have a markedly higher reactivity than expected from classical theories. The exact reason of this phenomena is unclear.

$$HO_2 + O_2^{\cdot -} = HO_2^- + O_2 \qquad \text{(II.4)}$$

It can be wondered whether the interaction with an alkali metal cation would increase or not the nucleophilicity of superoxide. The presence of such cation would mainly impact the charge localization on one of the oxygen atoms of the radical, thereby decreasing its stability. Interestingly, the terminal oxygen could be more nucleophilic than the one linked to the metal[9]. From experiments, a general increase in the reactivity with different solvent is observed after addition of a lithium salt to potassium superoxide solubilized using 18-crown-6 ether[10]. Considering that those solvents are not reactive toward lithium peroxide, and that the disproportionation of lithium superoxide into the latter has to be taken into account as a competitive reaction, a higher reactivity of the lithium superoxide can therefore be expected compared to free superoxide.

Superoxide has thus a particular behavior as an anionic nucleophile. Usually upon interaction with a cation, the nucleophile exhibits a decreased activity[11]. Therefore, the stronger the cation solvation, the higher the reactivity of the nucleophile. In the case of superoxide, a stronger cation solvation will decrease its reactivity.

On the contrary, since the reactivity of peroxide is generally linked to the weak bonding between the two oxygen atoms[12], the interaction between peroxide dianion and two alkali metal cations would lead to a decreased charge on the oxygen atoms, thereby strengthening the bond, and lowering the reactivity. This is illustrated by the comparison of the O-O stretching frequency of different alkali metal peroxides (measured by Raman spectroscopy): the higher the frequency, the shorter, and therefore the stronger, the bond[13].

Then, considering these two elements, the relative stability of the superoxide and peroxide species in presence of an alkali metal cation can be linked to the charge density of the cation: a higher charge density will stabilize the peroxide species, while promoting the disproportionation of the superoxide species. The relative thermodynamic stability of the solid alkali metal superoxide and peroxide is following the same trend[14]: at room temperature Li_2O_2 is more stable than LiO_2, KO_2 is more stable than K_2O_2.

2. Oxygen reduction in presence of tetraalkylammonium cations

Tetraalkylammonium cations (TAA^+), usually tetrabutylammonium (TBA^+) or tetraethylammonium (TEA^+), are of great interest as supporting electrolyte when studying oxygen reduction in aprotic media. They are relatively unreactive compounds, resisting to both oxidation and reduction, allowing a wide electrochemical stability window. Their single charge is centered on

the nitrogen atom, sterically hindered by the alkyl chains, and thus they interact only weakly with anions[15-16].

A typical cyclic voltammetry for oxygen reduction in presence of TAA^+ is presented in Figure II.1. The half wave potentials of the first and second reduction processes will be referred to as the first and second reduction potentials.

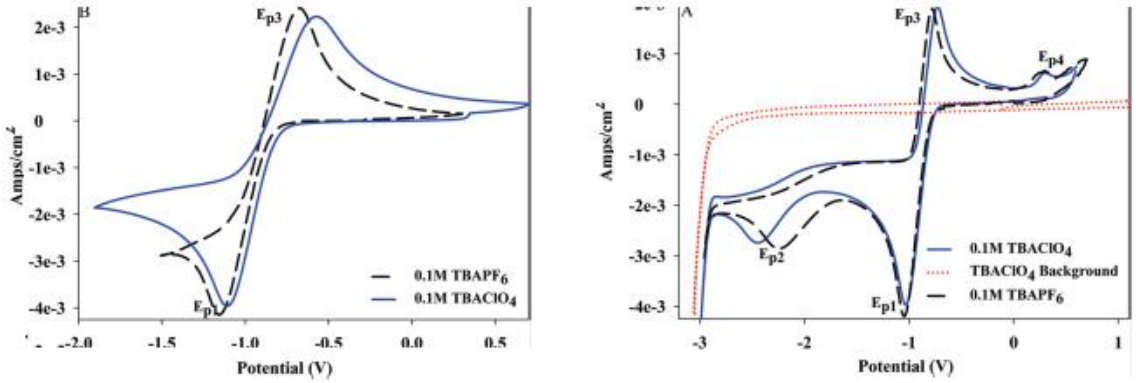

Figure II.1. Typical voltammograms of ORR, showing the first reversible reduction process (here around – 1 V) as well as the second irreversible reduction process (around – 2 V). These Voltammograms are representative of the general ORR behavior observed in aprotic solvent. For the specific conditions of the measure and reference system, see [17].

First reduction process:

It is commonly admitted that the first reduction of oxygen in aprotic solvent in presence of tetraalkylammonium cation reversibly produces superoxide anions[2]. Due to the difficulty to have a common reference system in aprotic solvent, it is complicated to make a reliable comparative review of the first oxygen reduction potential values from the literature[18-21]. The values presented here (Table II.1) were taken from selected publications where:

- an external reference system was used;
- the potential of the reference used could be reliably converted to standard calomel electrode potential, since it was the most used reference electrode in the literature;
- the ohmic drop effects are, at best, corrected, at least, limited;
- the experiments have been made at room temperature (*ca.* 20-25°C).

Table II.1. Half-peak potential of the first reduction process of oxygen in non-aqueous solvents.

Solvent	Electrolyte	Electrode	Reference	$E_{1/2}$ *vs* SCE (V)	Ref
DMSO	$TBAClO_4$	Hg drop	SCE	-0.77	[22]
	$TEAPF_6$	Hg drop	Ag/AgCl	-0.85	[23]
	$TBAClO_4$	GC	SCE	-0.75	[22]
	$TEAClO_4$	GC	Ag/AgCl (sat)	-0.77	[24]
DMA	$TEAClO_4$	GC	Ag/AgCl (sat)	-0.90	[24]
Acn	$TBAClO_4$	Hg drop	SCE	-0.82	[22]
	$TBAClO_4$	Au	SCE	-0.82	[25]
	$TBAClO_4$	GC	SCE	-0.85	[23]
	$TEAClO_4$	GC	Ag/AgCl (sat)	-0.88	[24]
DMF	$TBAClO_4$	Drop Hg	SCE	-0.87	[22]
	$TBAPF_6$	GC	SCE	-0.85	[26]
	$TBAClO_4$	GC	SCE	-0.81	[23]
	$TBAClO_4$	Pt	SCE	-0.89	[23]
	$TEAClO_4$	GC	Ag/AgCl (sat)	-0.87	[24]
Py	$TBAClO_4$	Drop Hg	SCE	-0.89	[22]
	$TEAClO_4$	GC	Ag/AgCl (sat)	-0.93	[24]
CH_2Cl_2	$TBAClO_4$	Drop Hg	SCE	-0.79	[22]
Acetone	$TBAClO_4$	Drop Hg	SCE	-0.88	[22]
	$TBAClO_4$	Au	SCE	-0.85	[25]

It is acknowledged that this selected review does not have any statistical value. However, it can nevertheless be observed that the nature of the solvent has a major impact on the reduction potential of oxygen. Neither the nature of the electrode, the length of the alkyl chain on the cation, nor the anion, seem to have an effect on the first oxygen reduction potential.

The effect of the solvent can be explained by the superoxide solvation: the better the solvation of the superoxide, the higher the first reduction potential of oxygen[15]. The thermodynamic basis at the origin of this effect will be developed in the following chapter.

In DMSO, DMF and pyridine, the cathodic/anodic peak separation on typical cyclic voltammograms is of *ca*. 100 to 200 mV, regardless of the nature of the electrode. This value, which deviates from the "classical" 60 mV expected for a 1 electron process[27], is attributed to the

conjunction of the slow charge transfer kinetics, the difference in the diffusion coefficients of oxygen and superoxide, and uncorrected or underestimated ohmic drop. In acetonitrile the difference depends on the nature of the electrode. On glassy carbon, it amounts *ca*. 100 to 150 mV, whereas on platinum, gold or mercury electrodes, the difference rises up to 500 to 700 mV. This particular effect in acetonitrile is not yet fully understood. An H-abstraction of acetonitrile is one possible explanation, considering its relatively low p*Ka* (30) in DMSO[28-29].

Second reduction process:

A second reduction wave is observed whatever the solvent, the salt or the electrode material. However, its potential is difficult to measure, due to the particular shape of the wave, and seem to depend significantly on the experimental conditions. It has been assigned to the formation of peroxide dianion[23], although physical characterizations were not supporting this statement. Its fast reaction with the solvent, the salt and the electrode, possibly mediated by impurities, particularly water traces, renders complex its identification. The existence of a second electron transfer on the superoxide (formation of peroxide dianion) is however supported by the observation of some reversibility for the process in ammonia on platinum[30]. The reason for the increased reversibility in this particular case would be a higher purity of ammonia as compared to other solvents, as well as its higher resistivity toward deprotonation (p*Ka* of 41 in DMSO), but could also be linked to the very low operation temperature (-55 °C). Reversibility for this second reduction has also been observed using ultrafast cyclic voltammetries on gold ultramicroelectrode in acetonitrile[31]; a scan rate of more than 10 kV s^{-1} was necessary, illustrating the very high reactivity of the peroxide dianion. In both cases, a separation of 1.5 to 2 V has been observed between the first and second reduction potentials.

3. Oxygen reduction in presence of alkali metal cations

"Pre-MAB" studies:

From the first publications addressing the effects of cations on ORR in aprotic solvents[32-34], it has been observed that the potential of the first reduction process was increasing slightly with increasing concentration in Li^+ (by less than 0.1 V), while it remained quite stable in presence of Na^+ and K^+. The second reduction process could not be observed in presence of Li^+, while its potential increased by approximately 1 V in presence of 0.1 M of Na^+, and by 0.7 V in presence of 0.1 M of K^+.

These increases in potential have been attributed to the interactions between alkali metal cations and $O_2^{\cdot-}$ or O_2^{2-}, in analogy with similar results for the reduction of other organic compounds in the same conditions. The first reduction process in presence of Li^+ has been attributed to the formation of LiO_2, which could not be further reduced electrochemically, but could possibly undergo chemical decomposition into Li_2O_2. The high increase in potential for the second reduction process in presence of Na^+ and K^+ has been attributed to the formation of Na_2O_2 and K_2O_2, which would be much more stable than the peroxide dianion. A general conclusion was that: the larger the charge-density of the cation, the higher the increase in potential of the reduction processes.

To my knowledge, there have not been much electrochemical studies on the impact of alkali metal cations on ORR in aprotic solvent, before the recent interest for MAB. Actually, one very interesting result comes from the study of ORR in ammonia[30]: in presence of potassium iodide, the first reduction wave on the cyclic voltammogram becomes distorted, a second reversible process is observed only at 0.4 to 0.5 V more negative potentials and no subsequent reduction process is being observed at even more negative potentials. These phenomena have been attributed to the precipitation of KO_2 on the surface of the electrode during the first reduction process. However, the potential of the second reduction in presence of K^+ is consistent with the potential of the second wave observed in similar conditions in DMSO[32]. It could then be attributed to a second reduction of oxygen, and the formation of a peroxide compound. Finally, in [35], it has been demonstrated that the first reduction process in PC was not reversible, as already discussed, but also that in presence of 5 mM of Li^+ in DME, the electrode was passivated due to the formation of solid products, which were considered as LiO_2 and Li_2O_2, the latter being formed either by chemical disproportionation of $O_2^{\cdot-}$ (or LiO_2) or the electrochemical second reduction of LiO_2.

Recent studies:

As mentioned in the previous chapter, the main discharge products observed after discharge of MOB were unambiguously Li_2O_2 and KO_2 in LiOB and KOB. For NaOB, formation of NaO_2 and Na_2O_2 has been observed in different studies, the reason for such discrepancy remains unclear[36-37]. These results are however in agreement with the thermodynamic stability of the compounds. Since oxides, M_2O, are even more thermodynamically stable, they could also have been expected as products. Nevertheless, their possible presence, even as by-products, is still unclear[38]. A comparison can also be made with the reduction of oxygen in liquid ammonia in presence of dissolved alkali metal cations. Ammonia has the property to dissociate alkali metals into the corresponding cation and

solvated electrons [39]. In these solutions, oxygen can therefore be reduced by the solvated electrons, and yield Li_2O_2, KO_2[40] and a mix of NaO_2 and Na_2O_2 [40] in presence of the respective cations[41].

By electrochemical characterizations, it has been observed that the first step of ORR in presence of Li^+ was most likely a one-electron reduction process to form either $O_2^{\cdot-}$ or LiO_2. The first direct physical characterization of this intermediate by means of surface enhanced Raman spectroscopy (SERS) on a roughened gold electrode in acetonitrile has been published in 2011[42]. Rotating ring-disk experiments, published in 2012[43], have demonstrated the formation of an intermediate in solution in DMSO, with an oxidation potential corresponding to that of superoxide species, while in acetonitrile, no soluble intermediate have been detected. From both studies, no evidence for a superoxide intermediate was found during reoxidation of the ORR products. Thus, the accepted general mechanism for ORR/OER in presence of lithium can be described by Equations (II.5-7).

$$O_2 + Li^+ + e^- = LiO_2 \quad \text{(II.5)}$$

$$LiO_2 + Li^+ + e^- = Li_2O_2 \quad \text{(II.6)}$$

$$2\,LiO_2 = Li_2O_2 + O_2 \quad \text{(II.7)}$$

This mechanism raises, however, the question of the formation of Li_2O_2, either by a second electrochemical reduction, or by chemical disproportionation, as well as the actual form of the intermediate, either solvated $O_2^{\cdot-}$, a solvated ionic pair Li^+-$O_2^{\cdot-}$, an adsorbed superoxide species $LiO_{2,ad}$ or solid LiO_2.

Donor number and HSAB:

A first general theory for the impact of both the cations and the solvent on the ORR has been proposed by Laoire and al.[44], and can be summed up as the following two points:

- If $O_2^{\cdot-}$ is considered as a weak Lewis base, then it will be more stabilized by weak Lewis acids such as tetraalkylammonium cations. If O_2^{2-} is considered as a hard Lewis base, then it will be more stabilized by hard Lewis acids, such as Li^+. Thus, the relative stability of ORR products in solution in presence of cations can be understood accordingly to Pearson's Hard and Soft Acids and Bases principle, which states, quoting the authors, "that hard acids prefer hard bases and soft bases prefer soft acids";
- A solvent of high basicity, which can be measured by its donor number (DN), will tend to solvate hard acids and will lower their acidity. Thus, in presence of Li^+, $O_2^{\cdot-}$ will be "stabilized

longer in solution" if a high DN solvent, like DMSO, is used as compared to a lower DN solvent like acetonitrile.

The exact rule of HSAB actually states that "hard acids prefer to bind to hard bases and soft acids prefer to bind to soft bases" [45], which in my opinion makes a significant difference. Indeed, the binding energy between cations and superoxide seems to be positively correlated to the charge-density of the cation: Na^+ would bind less strongly to $O_2^{\cdot-}$ than Li^+[46]. This is further supported by the shift of the Raman peak associated to the O-O bond of MO_2 to higher frequency with higher charge-density of the cation[47-48].

Even if the HSAB theory is discarded, the effect of the solvent can still be understood as a modulation of the interactions between cations and $O_2^{\cdot-}$ due to solvation effects. Indeed, the DN of a molecule is related to the formation enthalpy of a complex between this molecule and a reference Lewis acid ($SbCl_5$)[49], and is generally used as a measure of the solvent ability to solvate cations[15] (this will be discussed in the following chapter). A higher DN solvent will therefore tend to solvate cations more strongly, possibly leading to the formation of non-contact ionic pairs in solution, and limiting the interactions between cations and $O_2^{\cdot-}$. Thus, the longer lifetime of soluble superoxide species in DMSO as compared to acetonitrile can still be related to DN.

Solubility of the intermediate:

DN of the solvent has recently been correlated to the solubility of superoxide intermediates in presence of lithium cations, by electrochemical study on gold using RRDE and SERS[50]. The study led to the following conclusions:

- There is a competition between the surface and solution-oriented ORR pathways, and the orientation of the mechanism depends on the solubility of LiO_2; the solubility of LiO_2 in the solvents used is mainly dependent on the solvation of Li^+, which can be approximated by the DN of the solvent.
- The morphology of the deposit depends on the orientation of the mechanism; the solution oriented pathway leads to the formation of large crystallites, whereas several nanometer-thick compact films are formed when the process is surface oriented.

Similar conclusions have been proposed in [28], and the importance of the solvation of $O_2^{\cdot-}$ has been accounted for. Based on thermodynamic calculations, it has also been argued that solvents with the highest solubility capability for LiO_2 were also more prone to decomposition either by nucleophilic attack or proton abstraction.

The second electrochemical reduction:

A second electrochemical reduction of oxygen in presence of Li^+ is proposed in most studies[51-53]. However, the exact nature of the species being reduced is still an open question[50]. Interestingly, a second electrochemical reduction process was proposed by Laoire and al. in the initial works of the Northeastern University group, on the basis of the comparison between electrochemical analysis in presence of Li^+, Na^+ and K^+, in acetonitrile[17]. It was discarded in a subsequent study[54] of the same group using a similar approach in ionic liquids[iii]. It was then re-introduced for Li^+ in DMSO, without specifying the state of the intermediate[43]. The chemical second reduction of oxygen, due to the disproportionation of LiO_2, is generally considered as the main formation pathway for Li_2O_2, in particular in presence of high Li^+ concentrations in LiOB[52, 55].

4. The role of water

So far it has been considered in nearly all the non-aqueous ORR studies that the electrolyte used was pure enough to discard any influence of impurities. In particular, the role of water has not been considered, although an already small presence of 10 ppm water represents a concentration as high as 0.5 mM, which is only 1 order of magnitude inferior to the solubility of oxygen in most aprotic solvents. The influence of water can be considered in two different ways: either as a proton source or as a complexing agent, which could enhance the solubilization of the intermediates, without chemical reaction.

In presence of acids (HA) in solution, the following mechanism has been proposed[5] (Equations (II.8-10), with the formation of peroxide species being due to electron transfer between HO_2 and O_2.

$$O_2 + e^- = O_2^{\cdot -} \quad \text{(II.8)}$$

$$O_2^{\cdot -} + HA = HO_2^{\cdot} + A^- \quad \text{(II.9)}$$

$$O_2^{\cdot -} + HO_2 = HO_2^- + O_2 \quad \text{(II.10)}$$

Water is only weakly acidic in aprotic solvents, its p*Ka* is actually in the same order as the one of acetonitrile in DMSO. Thus, in presence of tetraalkylammonium cations and small water concentration, protonation of superoxide could be limited. In the meantime, water has a very strong

[iii] Ionic liquids can be particularly interesting for MOB; however, solvation in ionic liquids involves different phenomena as compared to classical solvents, and the reaction mechanisms in the two media cannot be directly compared that easily. Therefore, they will not be discussed in detail in the present thesis.

affinity for anions, and could therefore complex $O_2^{\cdot-}$ into $O_2^{\cdot-} - H_2O$. This reasoning is at the basis of a purely electrochemical study on water effect on the ORR in acetonitrile on glassy carbon[56], which led to the following mechanism (Equations (II.11-13)), with (II.13) being a proton-concerted electron transfer (PCET).

$$O_2 + e^- = O_2^{\cdot-} \quad \text{(II.11)}$$

$$O_2^{\cdot-} + H_2O = O_2^{\cdot-} - H_2O \quad \text{(II.12)}$$

$$O_2^{\cdot-} - H_2O + e^- = HO_2^- + OH^- \quad \text{(II.13)}$$

In presence of alkali metal cations, the situation is becoming much more complex since:

- Several complexes and equilibrium could be taken into account, with formation of ionic pairs between the cation and $O_2^{\cdot-}$ or $HO_2^{\cdot}$, possibly involving water molecules as well as intermediate solid phases of general formula MO_xH_y;
- Proton abstraction from water might be favored by the cation, which could increase the reactivity of superoxide and precipitate the hydroxide ions formed;
- The solid MO_x formed are reactive toward water.

Two effects are observed experimentally when discharging LiOB in presence of water. Firstly, with increasing water content, the morphology of the deposit is going from homogeneous compact films to large heterogeneous crystals[57-58]. This can simply be accounted for by the better solvation of $O_2^{\cdot-}$ by water, which leads to longer-life intermediates in solution and favors growth as compared to nucleation. A second observation is that the main solid discharge product characterized at the surface of the electrode still seems to be Li_2O_2[58]. This might be due to the kinetics of the Li_2O_2 formation mechanism, which is favored compared to the proton abstraction from water. The reaction between solid Li_2O_2 and water could then be slow, due to the formation of a crust of LiO_xH_y at the surface of Li_2O_2 particles. Interestingly, in presence of MnO_2, the reaction of solid Li_2O_2 pellets with water vapor is much faster than without the catalyst[59]. The good performances of this particular catalyst in LiOB[60] might be linked.

Conclusion

It appears from this study of the literature that, even though the understanding of the influence of alkali metal cations (especially Li^+) on the oxygen reduction in aprotic solvents has considerably improved over the past few years, several important details of the mechanism remain unclear. In particular, it has been shown that the use of HSAB theory as to account for the influence of the solvent could be criticized on a theoretical basis. It has also recently been questioned on an

experimental basis. Thus a re-examination of the actual relation between the DN of the solvent and its ability to allow a solution-based mechanism is needed. Furthermore, the actual process behind the second electrochemical reduction of oxygen, which has recurrently been observed experimentally, and the effect of alkali metal cations on this process are still unsolved.

The comparative analysis of the experimental results obtained in presence of different alkali metal cations has shown to be a very fruitful approach in the past to understand their actual influence on the ORR. Since alkali metals have relatively similar chemical properties, and that similarities in the ORR mechanism are observed in the literature, it would be interesting to determine if a common mechanism could be applied to understand their influence on ORR.

Three-electrode electrochemical characterizations on a model smooth glassy carbon surface allow both a very high sensitivity and to isolate the parameters of interest in the study. Since the theoretical background behind electrochemical techniques is considerable and accurate kinetic modelling of the experimental results is possible, such techniques are powerful means to elaborate and understand chemical mechanisms.

Finally, it is, in my opinion, worth noting that the understanding of the ORR mechanism in aqueous media is fine enough to allow not only the optimization of electrodes material and catalysts, but also the monitoring of their efficiency and durability, to be at least partially based on the study of voltammograms on model-electrodes[61]. If similar techniques could be applied to research on metal-oxygen batteries, considerable efficiency on the design of practical systems could be earned.

Bibliography :

1. Sawyer, D. T.; Valentine, J. S., How Super Is Superoxide? *Accounts of Chemical Research* **1981**, *14*, 393-400.

2. Sawyer, D. T., *Oxygen Chemistry*, Oxford University Press, **1991**.

3. Foote, C. S., *Active Oxygen in Chemistry*, First ed., Springer, **1995**.

4. Augusto, O.; Miyamoto, S., *Principles of Free Radical Biomedicine*, 2011; Vol. 1.

5. Andrieux, C. P.; Hapiot, P.; Saveant, J. M., Mechanism of Superoxide Ion Disproportionation in Aprotic Solvents. *Journal of the American Chemical Society* **1987**, *109*, 3768-3775.

6. Bielski, B. H. J.; Allen, A. O., Mechanism of the Disproportionation of Superoxide Radicals. *The Journal of Physical Chemistry* **1977**, *81*, 1048-1050.

7. Danen, W. C.; Warner, R. J., The Remarkable Nucleophilicity of Superoxide Anion Radical. Rate Constants for Reaction of Superoxide Ion with Aliphatic Bromides. *Tetrahedron Letters* **1977**, *18*, 989-992.

8. Fina, N. J.; Edwards, J. O., The Alpha Effect. A Review. *International Journal of Chemical Kinetics* **1973**, *5*, 1-26.

9. Uzunova, E. L.; Mikosch, H.; Nikolov, G. S., Electronic Structure of Oxide, Peroxide, and Superoxide Clusters of the 3d Elements: A Comparative Density Functional Study. *The Journal of Chemical Physics* **2008**, *128*, 094307.

10. Black, R.; Oh, S. H.; Lee, J.-H.; Yim, T.; Adams, B.; Nazar, L. F., Screening for Superoxide Reactivity in Li-O2 Batteries: Effect on Li2O2/LiOH Crystallization. *Journal of the American Chemical Society* **2012**, *134*, 2902-2905.

11. Carey, A. F.; Sundberg, J. R., *Advanced Organic Chemistry*, Fifth ed., Springer, **2007**.

12. Ho, R. Y. N.; Roelfes, G.; Feringa, B. L.; Que, L., Raman Evidence for a Weakened O−O Bond in Mononuclear Low-Spin Iron(Iii)−Hydroperoxides. *Journal of the American Chemical Society* **1999**, *121*, 264-265.

13. Gerbig, O. Defect Chemistry in Alkali Peroxides and Superoxides. PhD. Max-Planck-Institut für Festkörperforschung, **2014**.

14. Zhuravlev, Y. N.; Kravchenko, N. G.; Obolonskaya, O. S., The Electronic Structure of Alkali Metal Oxides. *Russ. Journal of Physical Chemistry B* **2010**, *4*, 20-28.

15. Izutsu, K., *Electrochemistry in Nonaqueous Solutions*; Wiley-VCH, 2002.

16. House, H. O.; Feng, E.; Peet, N. P., Comparison of Various Tetraalkylammonium Salts as Supporting Electrolytes in Organic Electrochemical Reactions. *The Journal of Organic Chemistry* **1971**, *36*, 2371-2375.

17. Laoire, C. O.; Mukerjee, S.; Abraham, K. M.; Plichta, E. J.; Hendrickson, M. A., Elucidating the Mechanism of Oxygen Reduction for Lithium-Air Battery Applications. *The Journal of Physical Chemistry C* **2009**, *113*, 20127-20134.

18. Gritzner, G.; Kůta, J., Recommendations on Reporting Electrode Potentials in Nonaqueous Solvents: Iupc Commission on Electrochemistry. *Electrochimica Acta* **1984**, *29*, 869-873.

19. Prins, R.; Korswagen, A. R.; Kortbeek, A. G. T. G., Decomposition of the Ferricenium Cation by Nucleophilic Reagents. *Journal of Organometallic Chemistry* **1972**, *39*, 335-344.

20. Diggle, J. W.; Parker, A. J., Solvation of Ions—Xx. The Ferrocene—Ferricinium Couple and Its Role in the Estimation of Free Energies of Transfer of Single Ions. *Electrochimica Acta* **1973**, *18*, 975-979.

21. Hurvois, J. P.; Moinet, C., Reactivity of Ferrocenium Cations with Molecular Oxygen in Polar Organic Solvents: Decomposition, Redox Reactions and Stabilization. *Journal of Organometallic Chemistry* **2005**, *690*, 1829-1839.

22. Peover, M. E.; White, B. S., Electrolytic Reduction of Oxygen in Aprotic Solvents: The Superoxide Ion. *Electrochimica Acta* **1966**, *11*, 1061-1067.

23. Vasudevan, D.; Wendt, H., Electroreduction of Oxygen in Aprotic Media. *Journal of Electroanalytical Chemistry* **1995**, *392*, 69-74.

24. Ohsaka, T.; Tsushima, M.; Tokuda, K., Reaction Entropies for the O2/O2− Redox Couple in Aprotic Solvents. *Bioelectrochemistry and Bioenergetics* **1993**, *31*, 289-300.

25. Mohammad, M.; Khan, A. Y.; Subhani, M. S.; Bibi, N.; Ahmad, S.; Saleemi, S., Kinetics and Electrochemical Studies on Superoxide. *Research on Chemical Intermediates* **2001**, *27*, 259-267.

26. Jain, P. S.; Lal, S., Electrolytic Reduction of Oxygen at Solid Electrodes in Aprotic Solvents-the Superoxide Ion. *Electrochimica Acta* **1982**, *27*, 759-763.

27. Bard, A. J.; Faulkner, L. R., *Electrochemical Methods*, Second ed., Wiley, **2001**.

28. Khetan, A.; Luntz, A.; Viswanathan, V., Trade-Offs in Capacity and Rechargeability in Nonaqueous Li–O2 Batteries: Solution-Driven Growth Versus Nucleophilic Stability. *The Journal of Physical Chemistry Letters* **2015**, *6*, 1254-1259.

29. Bryantsev, V. S.; Uddin, J.; Giordani, V.; Walker, W.; Addison, D.; Chase, G. V., The Identification of Stable Solvents for Nonaqueous Rechargeable Li-Air Batteries. *Journal of The Electrochemical Society* **2013**, *160*, A160-A171.

30. Uribe, F. A.; Bard, A. J., Electrochemistry in Liquid Ammonia. 5. Electroreduction of Oxygen. *Inorganic Chemistry* **1982**, *21*, 3160-3163.

31. Guo, Z.; Lin, X., Kinetic Studies of Dioxygen and Superoxide Ion in Acetonitrile at Gold Electrodes Using Ultrafast Cyclic Voltammetry. *Journal of Electroanalytical Chemistry* **2005**, *576*, 95-103.

32. Johnson, E. L.; Pool, K. H.; Hamm, R. E., Polarographic Reduction of Oxygen in Dimethylsulfoxide. *Analytical Chemistry* **1966**, *38*, 183-185.

33. Fujinaga, T.; Sakura, S., Polarographic Investigation of Dissolved Oxygen in Nonaqueous Solvent. *Bulletin of the Chemical Society of Japan* **1974**, *47*, 2781-2786.

34. Sawyer, D. T.; Chiericato, G.; Angelis, C. T.; Nanni, E. J.; Tsuchiya, T., Effects of Media and Electrode Materials on the Electrochemical Reduction of Dioxygen. *Analytical Chemistry* **1982**, *54*, 1720-1724.

35. Aurbach, D.; Daroux, M.; Faguy, P.; Yeager, E., The Electrochemistry of Noble Metal Electrodes in Aprotic Organic Solvents Containing Lithium Salts. *Journal of Electroanalytical Chemistry and Interfacial Electrochemistry* **1991**, *297*, 225-244.

36. Yadegari, H., et al., Three-Dimensional Nanostructured Air Electrode for Sodium–Oxygen Batteries: A Mechanism Study toward the Cyclability of the Cell. *Chemistry of Materials* **2015**, *27*, 3040-3047.

37. Hartmann, P.; Bender, C. L.; Sann, J.; Durr, A. K.; Jansen, M.; Janek, J.; Adelhelm, P., A Comprehensive Study on the Cell Chemistry of the Sodium Superoxide (Nao2) Battery. *Physical Chemistry Chemical Physics* **2013**, *15*, 11661-11672.

38. Gunasekara, I.; Mukerjee, S.; Plichta, E. J.; Hendrickson, M. A.; Abraham, K. M., Microelectrode Diagnostics of Lithium-Air Batteries. *Journal of The Electrochemical Society* **2014**, *161*, A381-A392.

39. Combellas, C.; Kanoufi, F.; Thiébault, A., Solutions of Solvated Electrons in Liquid Ammonia: Part 1. Chemical Properties of Magnesium Solutions. *Journal of Electroanalytical Chemistry* **2001**, *499*, 144-151.

40. Schechter, W. H.; Thompson, J. K.; Kleinberg, J., Further Studies on the Oxidation of Sodium in Liquid Ammonia. *Journal of the American Chemical Society* **1949**, *71*, 1816-1818.

41. Petrocelli, A. W., Superoxides. In *Van Nostrand's Encyclopedia of Chemistry*, John Wiley & Sons, Inc.: **2005**.

42. Peng, Z.; Freunberger, S. A.; Hardwick, L. J.; Chen, Y.; Giordani, V.; Bardé, F.; Novák, P.; Graham, D.; Tarascon, J.-M.; Bruce, P. G., Oxygen Reactions in a Non-Aqueous Li+ Electrolyte. *Angewandte Chemie International Edition* **2011**, *50*, 6351-6355.

43. Trahan, M. J.; Mukerjee, S.; Plichta, E. J.; Hendrickson, M. A.; Abraham, K. M., Studies of Li-Air Cells Utilizing Dimethyl Sulfoxide-Based Electrolyte. *Journal of The Electrochemical Society* **2013**, *160*, A259-A267.

44. Laoire, C. O.; Mukerjee, S.; Abraham, K. M.; Plichta, E. J.; Hendrickson, M. A., Influence of Nonaqueous Solvents on the Electrochemistry of Oxygen in the Rechargeable Lithium−Air Battery. *The Journal of Physical Chemistry C* **2010**, *114*, 9178-9186.

45. Pearson, R. G., Hard and Soft Acids and Bases. *Journal of the American Chemical Society* **1963**, *85*, 3533-3539.

46. Fukuzumi, S.; Ohkubo, K., Fluorescence Maxima of 10-Methylacridone−Metal Ion Salt Complexes: A Convenient and Quantitative Measure of Lewis Acidity of Metal Ion Salts. *Journal of the American Chemical Society* **2002**, *124*, 10270-10271.

47. Bates, J. B.; Brooker, M. H.; Boyd, G. E., Raman Spectra of O2- and O3- Ions in Alkali Metal Superoxides and Ozonides. *Chemical Physics Letters* **1972**, *16*, 391-395.

48. Dietzel, P. D. C.; Kremer, R. K.; Jansen, M., Superoxide Compounds of the Large Pseudo-Alkali-Metal Ions Tetramethylammonium, -Phosphonium, and -Arsonium. *Chemistry – An Asian Journal* **2007**, *2*, 66-75.

49. Laurence, C.; Gal, J.-F., *Lewis Basicity and Affinity Scales*, Wiley, **2010**.

50. Johnson, L.; Li, C.; Liu, Z.; Chen, Y.; Freunberger, S. A.; Ashok, P. C.; Praveen, B. B.; Dholakia, K.; Tarascon, J.-M.; Bruce, P. G., The Role of Lio2 Solubility in O2 Reduction in Aprotic Solvents and Its Consequences for Li–O2 Batteries. *Nat Chem* **2014**, *6*, 1091-1099.

51. Cecchetto, L.; Salomon, M.; Scrosati, B.; Croce, F., Study of a Li–Air Battery Having an Electrolyte Solution Formed by a Mixture of an Ether-Based Aprotic Solvent and an Ionic Liquid. *Journal of Power Sources* **2012**, *213*, 233-238.

52. Luntz, A. C.; McCloskey, B. D., Nonaqueous Li–Air Batteries: A Status Report. *Chemical Reviews* **2014**, *114*, 11721-11750.

53. Padbury, R.; Zhang, X., Lithium–Oxygen Batteries—Limiting Factors That Affect Performance. *Journal of Power Sources* **2011**, *196*, 4436-4444.

54. Allen, C. J.; Hwang, J.; Kautz, R.; Mukerjee, S.; Plichta, E. J.; Hendrickson, M. A.; Abraham, K. M., Oxygen Reduction Reactions in Ionic Liquids and the Formulation of a General Orr Mechanism for Li–Air Batteries. *The Journal of Physical Chemistry C* **2012**, *116*, 20755-20764.

55. Zhai, D., et al., Raman Evidence for Late Stage Disproportionation in a Li–O2 Battery. *The Journal of Physical Chemistry Letters* **2014**, *5*, 2705-2710.

56. Singh, P. S.; Evans, D. H., Study of the Electrochemical Reduction of Dioxygen in Acetonitrile in the Presence of Weak Acids. *The Journal of Physical Chemistry B* **2006**, *110*, 637-644.

57. Aetukuri, N. B.; McCloskey, B. D.; García, J. M.; Krupp, L. E.; Viswanathan, V.; Luntz, A. C., Solvating Additives Drive Solution-Mediated Electrochemistry and Enhance Toroid Growth in Non-Aqueous Li–O2 Batteries. *Nature Chemistry* **2015**, *7*, 50-56.

58. Schwenke, K. U.; Metzger, M.; Restle, T.; Piana, M.; Gasteiger, H. A., The Influence of Water and Protons on Li2o2 Crystal Growth in Aprotic Li-O2 Cells. *Journal of The Electrochemical Society* **2015**, *162*, A573-A584.

59. Capotosto, A.; Petrocelli, A. W. *Use of Lithium Peroxide for Atmosphere Regeneration*; **1968**.

60. Song, K.; Jung, J.; Heo, Y.-U.; Lee, Y. C.; Cho, K.; Kang, Y.-M., [Small Alpha]-Mno2 Nanowire Catalysts with Ultra-High Capacity and Extremely Low Overpotential in Lithium-Air Batteries through Tailored Surface Arrangement. *Physical Chemistry Chemical Physics* **2013**, *15*, 20075-20079.

61. Castanheira, L. Corrosion of High Surface Area Carbon Supports Used in Proton-Exchange Membrane Fuel Cell Electrodes. PhD. Université de Grenoble, **2014**.

Chapter III. General Considerations, Method Development and Experimental Details

"Most *chemists are familiar with chemistry in aqueous solutions. However, the common sense in aqueous solutions is not always valid in non-aqueous solutions. This is also true for electrochemical measurements.*"

Kosuke Izutsu *Electrochemistry in Non-Aqueous Solutions*, **2002**

When starting to work in aprotic solvents, one of the first striking facts is that the solvent itself becomes a parameter that can be changed to study reactions. Indeed, in protic solvents, water in particular, interactions between the proton H^+ and superoxide anions $O_2^{\cdot-}$ will be strong enough to mostly blur other solvent-related effects. Thus, pH might become the most important parameter to study. This is even more true that the reaction between H^+ and $O_2^{\cdot-}$ will lead to the formation of water, and thus its influence on the mechanisms cannot be overlooked.

1. Solvation effects

Let us consider the following reaction (III.1), a simple E mechanism with both species A and A^- in solution:

$$A + e^- = A^- \quad \text{(III.1)}$$

If reaction (III.1) is taking place in two different solvents, R and S, the following Scheme III.1 can be considered:

$$\begin{array}{ccc} A_R + e^- & = & A_R^- \\ S \,||\, R & & S \,||\, R \\ A_S + e^- & = & A_S^- \end{array}$$

Scheme III.1. Square scheme representation of the transfer of a redox reaction in two different solvents R and S.

With X_Y corresponding to the species X solvated by solvent Y. It appears from this particular square scheme that the difference in standard potential between the same E mechanism in two different solvents is directly linked to the difference in solvation of both the oxidant and the reducer. Intuitively, if A^- is solvated equally by R and S and if the solvation of A is stronger in S than in R, then $E°_R$ will be superior to $E°_S$. Conversely, if A is solvated equally by R and S and if the solvation of A^- is stronger in S than in R, then $E°_R$ will be inferior to $E°_S$.

Thermodynamic definitions[1]:

In order to discuss solvation, it is needed to introduce several useful equations. The Gibbs solvation energy of species X in solvent R, $\Delta G^o_{SV}(X,R)$, corresponds to the energetic cost of the transfer of species X from the gas phase to the solvent R (III.2):

$$X_{(g)} \longrightarrow X_R \quad \text{(III.2)}$$

If X is a salt of the form (A^+B^-), completely dissociated in R, the solvation energy of X will be the sum of the solvation energy of A^+ and B^-, according to Equation (III.3):

$$\Delta G^o_{\mathrm{SV}}(\mathrm{X},\mathrm{R}) = \Delta G^o_{\mathrm{SV}}(\mathrm{A}^+,\mathrm{R}) + \Delta G^o_{\mathrm{SV}}(\mathrm{B}^-,\mathrm{R}) \quad \text{(III.3)}$$

The Gibbs energy of transfer of X from solvent R to solvent S will be defined by Equation (III.4):

$$\Delta G^o_{\mathrm{t}}\left(\mathrm{X},\mathrm{R}\rightarrow\mathrm{S}\right) = \Delta G^o_{\mathrm{SV}}(\mathrm{X},\mathrm{S}) - \Delta G^o_{\mathrm{SV}}(\mathrm{X},\mathrm{R}) \quad \text{(III.4)}$$

If X is a neutral species or a salt completely dissociated in both solvents, then Gibbs energy of transfer of X from solvent R to solvent S can be expressed by Equation (III.5):

$$\Delta G^o_{\mathrm{t}}\left(\mathrm{X},\mathrm{R}\rightarrow\mathrm{S}\right) = RT\,\ln\left(\frac{S_{\mathrm{R}}(X)}{S_{\mathrm{S}}(X)}\right) \quad \text{(III.5)}$$

with $S_Y(X)$ the solubility of X in solvent Y. For convenience, a transfer activity coefficient γ_{t} is also introduced, and defined by Equation (III.6):

$$\log\left(\gamma_{\mathrm{t}}\left(\mathrm{X},\mathrm{R}\rightarrow\mathrm{S}\right)\right) = \frac{\Delta G^o_{\mathrm{t}}\left(\mathrm{X},\mathrm{R}\rightarrow\mathrm{S}\right)}{2.303\,RT} \quad \text{(III.6)}$$

If a reference solvent R is used to measure transfer activity coefficients of X with two other solvents S_1 and S_2, then the transfer activity coefficient becomes (Equation (III.7)):

$$\log\left(\gamma_t\left(\mathrm{X},\mathrm{S}_1\rightarrow\mathrm{S}_2\right)\right) = \log\left(\gamma_{\mathrm{t}}\left(\mathrm{X},\mathrm{R}\rightarrow\mathrm{S}_2\right)\right) - \log\left(\gamma_{\mathrm{t}}\left(\mathrm{X},\mathrm{R}\rightarrow\mathrm{S}_1\right)\right) \quad \text{(III.7)}$$

Finally, it arises that the solubility product K_{S} of X, as a salt of the form (A^+B^-), in a solvent S can be calculated from its solubility in R according to Equation (III.8):

$$\mathrm{p}K_{\mathrm{s}}(\mathrm{X},\mathrm{S}) = \mathrm{p}K_{\mathrm{s}}(\mathrm{X},\mathrm{R}) + \log\left(\gamma_{\mathrm{t}}\left(\mathrm{A}^+,\mathrm{R}\rightarrow\mathrm{S}\right)\right) + \log\left(\gamma_{\mathrm{t}}\left(\mathrm{B}^-,\mathrm{R}\rightarrow\mathrm{S}\right)\right) \quad \text{(III.8)}$$

Using the parameters introduced above, it is possible to express quantitatively the difference in standard potentials between equations (III.2a) and (III.2b) as a function of the transfer activity coefficients (Equation (III.9)):

$$E^o_{1,\mathrm{S}} - E^o_{1,\mathrm{R}} = \frac{RT}{F}\ln\left(\frac{\gamma_{\mathrm{t}}\left(\mathrm{A},\mathrm{R}\rightarrow\mathrm{S}\right)}{\gamma_{\mathrm{t}}\left(\mathrm{A}^-,\mathrm{R}\rightarrow\mathrm{S}\right)}\right) \quad \text{(III.9)}$$

Equation (III.9) can provide an estimation of the transfer activity coefficients directly from electrochemical measurements, as long as a common reference system can be found. It can also possibly be used to predict standard potentials, but this would require measuring the transfer activity coefficient of all the species involved in the reaction of interest from a reference solvent to any solvent of interest. However, if the ability for a solvent to solvate a particular species can be parameterized and correlated to a general scale, then such a prediction might become practicable.

Factors influencing solvation[1]:

Electrostatic interactions related to the permittivity of the solvent account for roughly 80 % of the total solvation energy of ions. The effect of permittivity on the electrostatic part of the solvation energy can be roughly approximated by the Born equation (III.10), with *r* the ionic radius and ε_r the relative permittivity of the solvent (Figure III.1). It is only an approximation in that case, since it does not take into account the chemical interactions with the solvent. It can be observed that, for high-permittivity solvents (above 20), a change in permittivity from one solvent to another will not influence much the solvation energy (less than 3 % of the total energy). In that case, the solvation energy will be more related to other parameters, which will be discussed below. However, for low-permittivity solvents (typically below 10), the permittivity is the most influencing factor (Figure III.1).

$$\Delta G_{\mathrm{el}} = \frac{69.4 z^2}{r}\left(1 - \frac{1}{\varepsilon_{\mathrm{r}}}\right) \qquad \text{(III.10)}$$

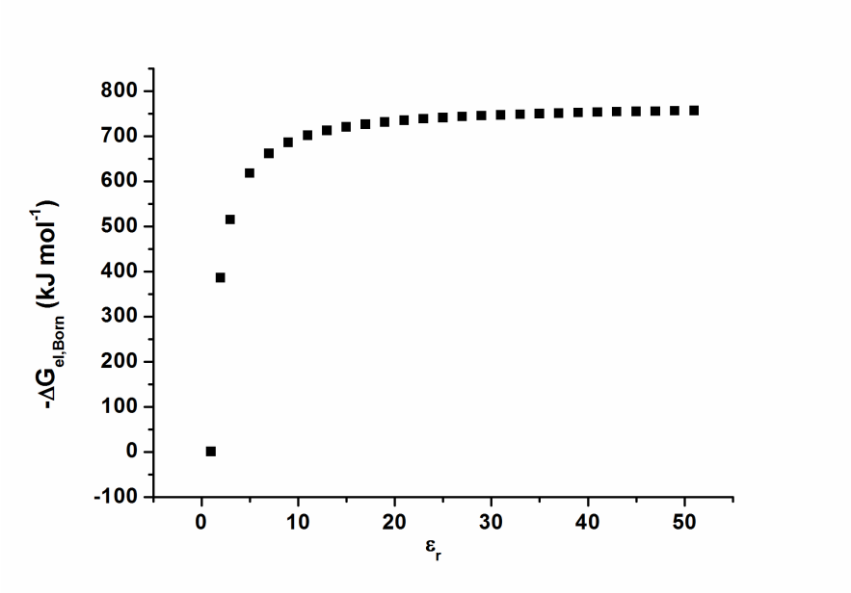

Figure III.1. Effect of the solvent permittivity on the relative electrostatic free energy of Li^+ (approximated by Born equation)

In particular, in the case of Li^+ in solution, the difference in ΔG_{el} between dimethylsulfoxide (DMSO) (ε_r = 46.7) and N,N-dimethylacetamide (DMA) (ε_r = 37.8) would be of 0.5 %, when it is of 12 % between 1,2-dimethoxyethane (ε_r = 7.2) and dimethylsulfoxide. Thus, the interpretation of a difference in solubility for a lithium salt in the two lasts solvents should be essentially based on the difference of permittivity, while other parameters will be of more importance for the two firsts.

The first of these other parameters is related to the Lewis acidity and basicity of the solvent. The interaction between a cation (anion) and a solvent is related to the capability of the latter to give (accept) electron pair. This is modulated by concepts relative to the hard and soft acids and bases principle (HSAB): in a general manner, a strongly basic (acid) solvent will bind preferentially to a strongly acidic cation (basic anion), while a softly basic (acid) solvent will bind preferentially to a softly acidic cation (basic anion). Several scales have been elaborated to parameterize the Lewis acidity and basicity of solvents, as detailed below.

The most frequently-used scale, especially in research on LiOB, is the Donor and Acceptor Numbers (DN/AN). The AN of a solvent is based on the determination of the relative ^{31}P-NMR shift of triethylphosphine oxide, a strong Lewis base, in the solvent of interest. The DN is based on the measurement of the heat of coordination with $SbCl_5$ of solvents diluted in a large excess of 1,2-dichloroethane. The use of DN as a solvent parameter has been criticized, in particular because:

- It is actually a measurement of enthalpy, and not of Gibbs energy. Enthalpy and Gibbs energy are generally not linearly related (because of the entropic term);

- Since 1,2-dichloroethane is actually used as a solvent for the measurement, it might not reflect the actual Lewis basicity as a solvent of the compound tested;
- Coordination to the large $SbCl_5$ might not reflect coordination to much smaller cations, like alkali metal cations.

Another scale is based on the Swain's theory[2]. Swain's A and B parameters represent respectively the tendency for a solvent to solvate anions and cations. The determination of these two independent parameters is based on the study of 77 chemical reactions in different conditions. In a very general manner, AN and A as well as DN and B are following the same trends, although there are exceptions. However, the A and B Swain parameters have also been criticized, in particular because they are actually strongly correlated when only non-hydrogen bond donor solvent are considered (their independency is at the basis of their physical meaning, and a mathematical condition for their determination).

In order to avoid the issues related to a measurement in solution, gas phase measurements of affinities have been proposed. The results are of great interest here, since alkali metal cations were particularly studied. Practically, the free energy associated to equation (III.11) is determined for a particular cation M^+ and several ligands R in the gas phase. Scales are called metal cation basicities (MCB). It could be wondered whether these scales could provide useful information in solution, though they provide an intrinsic measurement of the affinity of a molecule for a particular cation.

$$R + M^+ = R - M^+ \qquad \text{(III.11)}$$

A third factor which could influence the solvation of anions specifically is the capability of the solvent to provide hydrogen bonds. In particular anions with localized negative charge are prone to hydrogen bonding, and will thus be strongly solvated by hydrogen donor solvent. In general, hydrogen bond donor solvents are also relatively acid.

Finally, solvation energy can be influenced by the formation of particular structuration of the solution when solvating ions. These effects will not be considered here, since aprotic solvents are generally not structured, as opposed to water.

It should also be noted that a modification of the Born equation has been proposed, including a correcting factor to the ionic size: the polarization parameter which depends on the solvent and the sign of the charge of the ion. This parameter, taken for a particular solvent, has been shown to correlate quite well with AN (DN) when considering interactions with anions (cations).

The relevant values of the different parameters for the solvents used in this study are listed in Table III.1.

Table III.1. Parameters related to solvation for the solvents studied. *bidentate

Solvent	A[2]	B[2]	AN[3]	DN[4]	ε_r[1]	LiCB[5] (kJ mol^{-1})	NaCB[5] (kJ mol^{-1})	KCB[5] (kJ mol^{-1})
Acn	0.37	0.86	18.9	14.1	37.5	142.1	98.7	75.3
DMSO	0.34	1.08	19.3	29.8	46.7	175.1	129.7	104.6
DMA	0.27	0.97	13.6	27.8	37.8	179.1	132.8	104.4
Py	0.24	0.96	14.2	33.1	12.4	146.7	100	64.6
DMF	0.30	0.93	16	26.6	36.7	173.7	125.9	96.2
DME	0.21	0.5	10.2	20	7.2	187.9*	133.1*	86.6*
NMP	ND	ND	13.3	27.3	32.2	ND	ND	ND

Application to the ORR:

Let us consider the following two equations (III.12) and (III.12b), that are representation of the non-aqueous ORR (see chapter 1):

$$O_2 + e^- = O_2^{\cdot -} \qquad \text{(III.12)}$$

$$O_2 + n\,M^+ + n\,e^- = M_nO_{2\,(s)} \qquad \text{(III.12b)}$$

Equation (III.12) is analogue to (III.1) and thus the difference in standard potentials of the reaction between two solvents can be given by (III.9). This firstly raises the question of the transfer activity coefficient of O_2. If oxygen is considered as a neutral species, then the difference in solvation energy between two solvents is related to the difference in oxygen solubility between them, according to (III.5). Considering that the solubility of oxygen is 5 times higher in acetonitrile than in DMSO at ambient temperature and 1 bar pressure, a difference of 40 mV in the standard potentials could be expected. However, no theoretical basis to support or not this reasoning has been found in the literature. Thus, since all the solvents studied here have solubility values of oxygen in between that of acetonitrile and DMSO, the solvation of oxygen will be considered as independent from the solvent. In addition, the transfer activity coefficient of $O_2^{\cdot -}$ is also not tabulated in the literature. Thus, the standard potentials experimentally measured can only be correlated to solvents acidity scales, such as AN.

The variation of the standard potential of equation (III.13), which corresponds to the general oxidation reaction in MOB, from one solvent to another should only depend on the transfer activity coefficient of M^+ (III.13b).

$$E^o_{12b,S} - E^o_{12b,R} = \frac{RT}{nF}\ln(\gamma_t\left(O_2, R \rightarrow S\right).(\gamma_t\left(M^+, R \rightarrow S\right))^n) \quad \text{(III.13)}$$

$$E^o_{12b,S} - E^o_{12b,R} = \frac{RT}{F}\ln(\gamma_t\left(M^+, R \rightarrow S\right)) \quad \text{(III.13b)}$$

The difference in the standard potentials of the reduction of M^+ (Equation (III.14)) measured in two different solvents follows the same dependency in the transfer activity coefficient of M^+ (Equation (III.15)).

$$M^+ + e^- = M_{(s)} \quad \text{(III.14)}$$

$$E^o_{14,S} - E^o_{14,R} = \frac{RT}{F}\ln(\gamma_t\left(M^+, R \rightarrow S\right)) \quad \text{(III.15)}$$

$E_{14}^{1/2}$ values measured in different solvents using a bis(phenyl)chromium reference[1] are reported in Table III.2. At first sight, DN seems as a good approximation of solvation of alkali metal cations, but with the notable exception of Py.

Table III.2. Half-wave potentials of alkali metal cations in different solvents (V *vs* BCr/BCr$^+$)[1]

Solvent	DN	Li^+	Na^+	K^+
Acn	14.1	-1.211	-1.092	-1.09
DMF	26.6	-1.623	-1.349	-1.371
NMP	27.3	-1.697	-1.367	-1.375
DMA	27.8	-1.765	-1.38	-1.404
DMSO	29.8	-1.86	-1.37	-1.4
Py	33.1	-1.428	-1.201	-1.231

Assuming the equilibrium (III.16) and solubility product $K_{s,17}$ (Equation (III.17)), the difference in standard potentials between (Equation III.12) and (Equation III.12b) can also be expressed in terms of solubility of MO_2 for the case n = 1 (Equation III.18):

$$O_2^{\cdot -} + M^+ = MO_{2\,(s)} \quad \text{(III.16)}$$

$$K_{s,17} = (O_2^{\cdot -}).(M^+) \quad \text{(III.17)}$$

$$E^o_{12b,R} - E^o_{12,R} = -\frac{RT}{F}\ln(K_{s,17}) \quad \text{(III.18)}$$

These equations can be used to understand qualitatively the differences of half-wave / onset potential values observed for the ORR in different solvents; more quantitatively, they enable to determine the solvation energy of superoxide in those solvents, the solubility of M_nO_2 compounds (which might be difficult to measure otherwise), and to predict the behavior of other possible candidate solvents for MOB.

An interesting observation can also be made on the study of the working potential of LiOB. Usually, the charge of the battery starts around U = 3.1 - 3.2 V, whatever the solvent (as long as it is not reactive of course). This can easily be understood from (Equation III.13b) and (Equation III.15): the solvation of Li^+ has the same effect on the positive and negative electrodes potential. However, the difference between the standard potentials of (Equation III.12b) and (Equation III.12) will depend on the solvation of $O_2^{\cdot-}$. Thus, if the discharge mechanism is intermediate between a direct precipitation of Li_nO_2 and a solubilization of the intermediates, a change in the working discharge potential of the battery could be observed from one solvent to another. It can be argued that this change could also be ascribed to the more pronounced passivation of the electrode in the case of a lower solubility.

2. Ion-pairs formation

The thermodynamic reasoning developed until here was based on the assumption that the salts were completely dissociated into free ions. However, in practice, the formation of ion-pairs has to be taken into account, in particular in low-permittivity solvents. Let us consider two ionic species A^+ and B^-, which can precipitate as AB (Equation (III.19)) with a solubility product $K_{s,AB}$ defined by (III.20). The formation of the simplest ion-pairs $A^+ - B^-$ can be described by (III.21), associated to a formation constant $K_{f,AB}$ (III.22).

$$A^+ + B^- = AB_{(s)} \tag{III.19}$$

$$K_{s,AB} = (A^+)(B^-) \tag{III.20}$$

$$A^+ + B^- = A^+ - B^- \tag{III.21}$$

$$K_{f,AB} = \frac{(A^+ - B^-)}{(A^+)(B^-)} \tag{III.22}$$

It directly appears from these equations that $A^+ - B^-$ has a saturation concentration which only depends on $K_{s,AB}$ and $K_{f,AB}$ (III.23). Thus, at a fixed concentration in A^+, the total solubility of AB cannot be calculated simply by the solubility product (III.24).

$$(A^+ - B^-)_{sat} = K_{f,AB} K_{s,AB} \tag{III.23}$$

$$(\mathrm{A}^+ - \mathrm{B}^-)_{\mathrm{sat}} + (\mathrm{B}^-)_{\mathrm{sat}} = K_{\mathrm{f,AB}} K_{\mathrm{s,AB}} + \frac{K_{\mathrm{s,AB}}}{(\mathrm{A}^+)} \quad \text{(III.24)}$$

In a general manner, the solubility product and the formation constant are inversely related[6]: the higher the solubility, the lower the ion-pairs formation constant. Then, for a sparingly soluble salt, it appears that the salt is essentially solubilized as ion-pairs. Furthermore, the formation of higher aggregates such as triple ion-pairs ($\mathrm{A}^+ - \mathrm{B}^- - \mathrm{A}^+$or $\mathrm{B}^- - \mathrm{A}^+ - \mathrm{B}^-$) and quadrupoles ($(\mathrm{A}^+ - \mathrm{B}^-)_2$) should also be taken into account, which complicates considerably the mechanisms involving ion-pairs formation[7].

If only the formation of simple ion-pairs is considered, then the dependency on the concentration in A^+ of the difference in standard potentials between equations (III.25) and (III.26) can be expressed by (III.27).

$$\mathrm{B} + \mathrm{e}^- = \mathrm{B}^- \quad \text{(III.25)}$$

$$\mathrm{B} + \mathrm{A}^+ + \mathrm{e}^- = \mathrm{A}^+ - \mathrm{B}^- \quad \text{(III.26)}$$

$$\Delta E^o_{26-25} = E^O_{26} - E^O_{25} = \frac{RT}{F} \ln(1 + K_{\mathrm{f,AB}}(M^+)) \quad \text{(III.27)}$$

Finally, the structure of the ion-pairs is also dependent on the interactions between the ions and the solvent. Ions in ion-pairs are still partially solvated. This solvation can lead to several different structures, which likely have different properties. The solvent molecules R can either be unshared by the two ions, leading to the formation of solvent separated ion-pairs $\mathrm{A}^+\mathrm{RR}\,\mathrm{B}^-$, or shared, thus forming solvent shared ion pairs $\mathrm{A}^+\mathrm{R}\,\mathrm{B}^-$. Contact ion-pairs $\mathrm{A}^+\mathrm{B}^-$can also be formed. The actual structure of the ion-pairs can be determined by physical characterizations, such as UV-spectroscopy, infrared or Raman spectroscopy, or NMR for example.

In the present study, ion-pairs will be considered, as a first approximation, in their simplest form $\mathrm{A}^+ - \mathrm{B}^-$, without assumptions on their fine structure. The formation of triple ion-pairs of the form $\mathrm{A}^+ - \mathrm{B}^- - \mathrm{A}^+$ will only be accounted for in the final chapter VII as an opening for future work.

3. Method development

From the study of the bibliography in the two firsts chapters and the definitions given here, it appears that solvation effects have a great influence on the ORR in non-aqueous solvents, and that its mechanism, in particular regarding the second electrochemical reduction, is still unclear.

The first objective of this thesis is to confirm and possibly clarify the mechanism of the ORR in the presence of tetraalkylammonium salts (Chapter 4). This will fix the first parameter of the

study, which is the solvation of $O_2^{\cdot-}$, in the relative absence of interactions with cations. Since the studies in these conditions are numerous in the literature, this will actually also serve as a means to check if the experimental set-ups designed and used in the present thesis are efficient.

The second step will be to study the influence of the addition of alkali metal cations in a particular solvent: DMSO (Chapter 5). As it will be shown, DMSO is one of the best solvent for the superoxide intermediates, thus it can be a good starting point to develop a general model. Therefore, the second parameter under study in the thesis is the effect of the charge-density of the cations (Li^+, Na^+ and K^+ will particularly be evaluated).

Then, the knowledge acquired through the studies performed in DMSO will be extended to other solvents (Chapter 6). The third parameter under study will then be the influence of the solubility of the intermediates in the solvent at stake.

Finally, it will become obvious that the proposed mechanism involves many coupled phenomena, and that its modelling will become necessary to correctly understand the whole ORR process.

Therefore, chapter 7, as a conclusion of the experimental work, is focused on the development of a model which could qualitatively reproduce the phenomena, in particular the effect of passivation on cyclic voltammetries, and quantitatively propose several thermodynamic values.

4. Experimental details.

Materials and solutions

The chemical compounds were provided by Sigma-Aldrich. Anhydrous high purity grade solvents were stored as soon as received in a glove-box (MBraun) under argon atmosphere, with oxygen and water content both below 0.1 ppm, and used without further purification. Tetraethylammonium hexafluorophosphate ($TEAPF_6$) > 99%, Tetraethylammonium perchlorate ($TEAClO_4$) > 99%, Tetrabutylammonium hexafluorophosphate ($TBAPF_6$) > 99%, Tetrabutylammonium perchlorate ($TBAClO_4$) > 98%, Lithium triflate (LiTf) battery grade, sodium perchlorate ($NaClO_4$) > 98%, potassium hexafluorophosphate (KPF_6) > 99.5% and silver nitrate > 99.998%, were dried under vacuum and stored in the glove-box as soon as received.

In aprotic media, when surface-related catalytic effects are discarded, the effect of anions can be limited to a difference in the solvation of the cations. Based on the mechanism developed in the present work, this effect should be limited to slight changes in the complexation constants and solubility values. These effects would not change the trends experimentally observed and used as input to develop the mechanism, all the more that an excess of $TAAPF_6$ (either $TBAPF_6$ or $TEAPF_6$) is used as supporting electrolyte. However, the effect of the presence of a different cation with a larger charge-density would be much more important. Therefore, the choice has been made to use the salts with the fewer metallic impurities available at the moment of the experiment, instead of keeping the same anion.

Electrochemical procedures

The electrochemical experiments were performed using a VMP3 potentiostat from Bio-Logic®, in a custom-made 3 electrodes air-tight glass cell using a platinum wire as a counter-electrode. Two different $Ag/AgNO_3$ reference electrodes were used. The first with 10 mM $AgNO_3$ and 0.5 M $TEAPF_6$ in acetonitrile ($E_{ref,1}$ = -0.08 V versus the half-peak potential ($E_{1/2}$) of the ferrocenium/ferrocene redox couple in acetonitrile). The second with 10 mM $AgNO_3$ and 0.1 M $TBAClO_4$ in 1:1 acetonitrile:pyridine mixture ($E_{ref,2}$ = -0.320 V *vs.* $E_{ref,1}$). All potentials are expressed versus the first reference ($E_{ref,1}$), indicated as Ref in the following, unless otherwise stated. Some of the experiments were performed using two different references with different solvents and supporting salt concentrations. The results were not dependent on the reference, and half-peak potentials remained identical within 5 mV, ruling out any effects due to junction potential or reference shift.

Electrochemical experiments at different concentrations in cations were made using a fresh electrolyte solution and a freshly-polished glassy-carbon electrode (geometric surface area, S = 0.2

cm²) for each concentration, in order to avoid any bias due to the decomposition of the electrode and/or electrolyte, internal/external pollution over time and to confirm the repeatability of the measurements. RRDE experiments were performed inside a custom-made glove-box filled with argon, using a S = 0.125 cm² glassy carbon disk and 2.5 mm/3.5 mm inner/outer radii gold ring. The geometrical collection efficiency of this electrode is N_{geo} = 0.42.

In RRDE experiments, the potential of the ring was maintained at a potential high enough to re-oxidize species formed during reduction at the disk (Scheme III.2). No electrochemical reduction of oxygen was performed on the gold ring in order to prevent it from damages or passivation from insoluble ORR products, as it could not be easily polished after use.

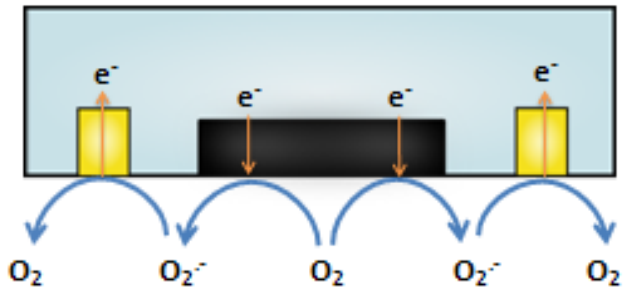

Figure III.2. RRDE measurement principle

Two major experimental difficulties had to be overcome in these electrochemical characterizations. The first one is related to the purity of the solvents used. Here, an assessment of the concentration in water could not have been done. This is acknowledged as a serious lack of the present work. However, considerable changes on the voltammograms were noticed upon the addition of 20-50 ppm water in the electrolyte at the end of the experiments. On this basis and other experimental and theoretical considerations, it has been concluded that the results and trends observed were not the consequence of a non-negligible contamination by water. The effects of water on the mechanism and in practical aprotic alkali metal-oxygen batteries will not be discussed further here.

The second important parameter is the stability and precision of the reference electrode. It has been chosen here to work with a reference electrode the least physically and chemically separated from the working electrolyte as possible. This has the advantage of considerably limiting potential junction related effects. However, it also leads to a faster contamination of the reference by the working electrolyte, as well as possible leaks of the reference electrolyte in the working electrolyte. The reference electrolyte had a volume of less than 1% of the working electrolyte, considerably limiting the possibility of a contamination of the latter due to dilution effects. Stability

of the reference electrode has been assessed by continuous cycling during the saturation in oxygen in different electrolytes. No change in the reduction peak has been observed during these experiments.

Other

Simulations were done using Scilab© software. Coding is handmade, except for matrix inversion algorithms.

Bibliography:

1. Izutsu, K., *Electrochemistry in Non-Aqueous Solutions*, First ed., Wiley, **2002**.

2. Swain, C. G.; Swain, M. S.; Powell, A. L.; Alunni, S., Solvent Effects on Chemical Reactivity. Evaluation of Anion- and Cation-Solvation Components. *Journal of the American Chemical Society* **1983**, *105*, 502-513.

3. Mayer, U.; Gutmann, V.; Gerger, W., The Acceptor Number — a Quantitative Empirical Parameter for the Electrophilic Properties of Solvents. *Monatshefte für Chemie* **1975**, *106*, 1235-1257.

4. Sandström, M.; Persson, I.; Persson, P., A Study of Solvent Electron Pair Donor Ability and Lewis Basicity Scales. *Acta Chemica Scandinavia* **1990**, *44*, 653-675.

5. Laurence, C.; Gal, J.-F., *Lewis Basicity and Affinity Scales*, Wiley, **2010**.

6. Chabanel, M., Ionic Aggregates of 1-1 Salts in Non-Aqueous Solutions: Structure, Thermodynamics and Solvation. In *Pure and Applied Chemistry*, **1990**; Vol. 62, p 35.

7. Kim, J. I.; Duschner, H., Preferential Solvation of Single Ions: The Medium Effects of the Ag+, Agcln1—N), and Cl— Ions in Mixed Acetonitrile-Water Solvents. In *Zeitschrift für Physikalische Chemie*, **1977**; Vol. 106, p 1.

Chapter IV. Oxygen Reduction to Superoxide in Presence of Tetraalkylammonium Cations

Introduction

In the theoretical treatment of the first reduction of oxygen proposed in chapter (III), it was considered that only the solvent had an influence on the solvation of the superoxide anion. However, an association of the latter with the cation of the supporting salt could also be taken into account. This leads to a more complex mechanism, which can be described by equations (IV.1-3), considering a tetraalkylammonium (TAA^+) based supporting salt and $O_2^{\cdot-} - TAA^+$ as an ionic pair. For simplicity, only one type of ion-pairs is considered here, and its actual structure is not anticipated.

$$O_2 + e^- = O_2^{\cdot-} \quad \text{(IV.1)}$$

$$O_2 + TAA^+ + e^- = O_2^{\cdot-} - TAA^+ \quad \text{(IV.2)}$$

$$O_2^{\cdot-} + TAA^+ = O_2^{\cdot-} - TAA^+ \quad \text{(IV.3)}$$

In that case, not only the affinity of the solvent for $O_2^{\cdot-}$ has to be taken into account, but also the solvation of TAA^+ and the capability of the solvent to separate or not the ion-pairs. The precipitation of the tetraalkylammonium superoxide salt could even be possible in low-permittivity solvents.

It appeared from the literature (chapter II) that a strong association between TAA^+ and $O_2^{\cdot-}$ was not likely, especially since the binding energy in alkali metal superoxides MO_2 was decreasing with a decrease in the charge-density of the cation. In order to further support this, the following reasoning is proposed. Let us consider that TAA^+ cations are interacting strongly with $O_2^{\cdot-}$, according to the Hard and Soft Acids and Bases principles (HSAB)[1]:

- In a high-permittivity solvent with a strong affinity for cations, the potential of the first reduction of oxygen should shift with a change in the length of the alkyl chain of TAA^+ cations, since their charge-density would change. If the potential is not affected by the length of the alkyl chain of TAA^+, then either TAA^+ cations have a very similar affinity for $O_2^{\cdot-}$ regardless of their ionic size, which is not likely, or the solvent has the ability to solvate TAA^+ cations enough to mitigate the effect of their ionic size (and charge-density);
- In high-permittivity solvents, with different capabilities to solvate ions, if the potential of the first reduction of oxygen is unaffected by a change in the solvent, then TAA^+ cations must have a strong affinity for $O_2^{\cdot-}$ regardless of their solvation. If the potential is shifting and if it is the solvent ability to solvate cations that has the main effect on this shift, then TAA^+ cations must have a strong affinity for $O_2^{\cdot-}$, which is modulated by their solvation. However, if it is the ability for a solvent to solvate anions that has the main effect on the shift, then it

becomes obvious that the hypothesis of highly interacting TAA^+ with $O_2^{\cdot-}$ does not hold anymore.

To evaluate the above-mentioned scenarios in this chapter, the ORR will be firstly studied in dimethylsulfoxide (DMSO), a solvent that has a high permittivity and a strong affinity for both anions and cations. Then, the potential for the first reduction of oxygen will be compared with the one obtained in 3 other high-permittivity solvents: acetonitrile (Acn), N-methyl-2-pyrrolidone (NMP), and N,N-dimethylacetamide (DMA). A solvent of lower permittivity, pyridine (Py), will also be studied, as well as solvents mixtures. These solvents have all been shown to be relatively stable toward superoxide species[2-4]. Several physicochemical values and parameters of interest will be calculated from these experimental measurements and summarized at the end of the chapter in Table IV.2.

1. ORR in DMSO in presence of tetrabutylammonium (TBA^+) and tetraethylammonium (TEA^+)

The reduction of oxygen has been performed in DMSO, using different batch of the solvent, in presence of different concentrations in tetrabutylammonium (TBA^+) and tetraethylammonium (TEA^+), with different counter-anions (hexafluorophosphate: PF_6^-, perchlorate: ClO_4^- or tetrafluoroborate: BF_4^-), on different glassy-carbon electrodes. Representative ORR/OER voltamperograms are presented on Figure IV.1. In all cases, the half-peak potential for the first reduction of oxygen remained the same within 5 mV, which is considered in the rest of the study as the margin of error of our measurements. It is thus concluded here that the half-peak potential for the first reduction of oxygen in DMSO is neither depending on the length of the alkyl chain of TAA^+ (if longer than ethyl), nor on the nature of the counter-anion and the concentration in TAA^+. However, the peak current is less reproducible, and a margin of error of 5 % has to be taken into account for this parameter. This has been attributed to the changes in ambient temperature (the cell was not thermostated, and the room temperature was *ca*. 20 $\pm$ 3°C), a lack of reproducibility of the surface state of the glassy-carbon electrode, and the dependence of the oxygen solubility and diffusion coefficient on the electrolyte composition (and temperature), all these phenomena having a larger effect on the current than on the potential of the ORR. Nevertheless, this margin of error can be considered as acceptable considering the discrepancy on the oxygen solubility and diffusion coefficient in the literature[5].

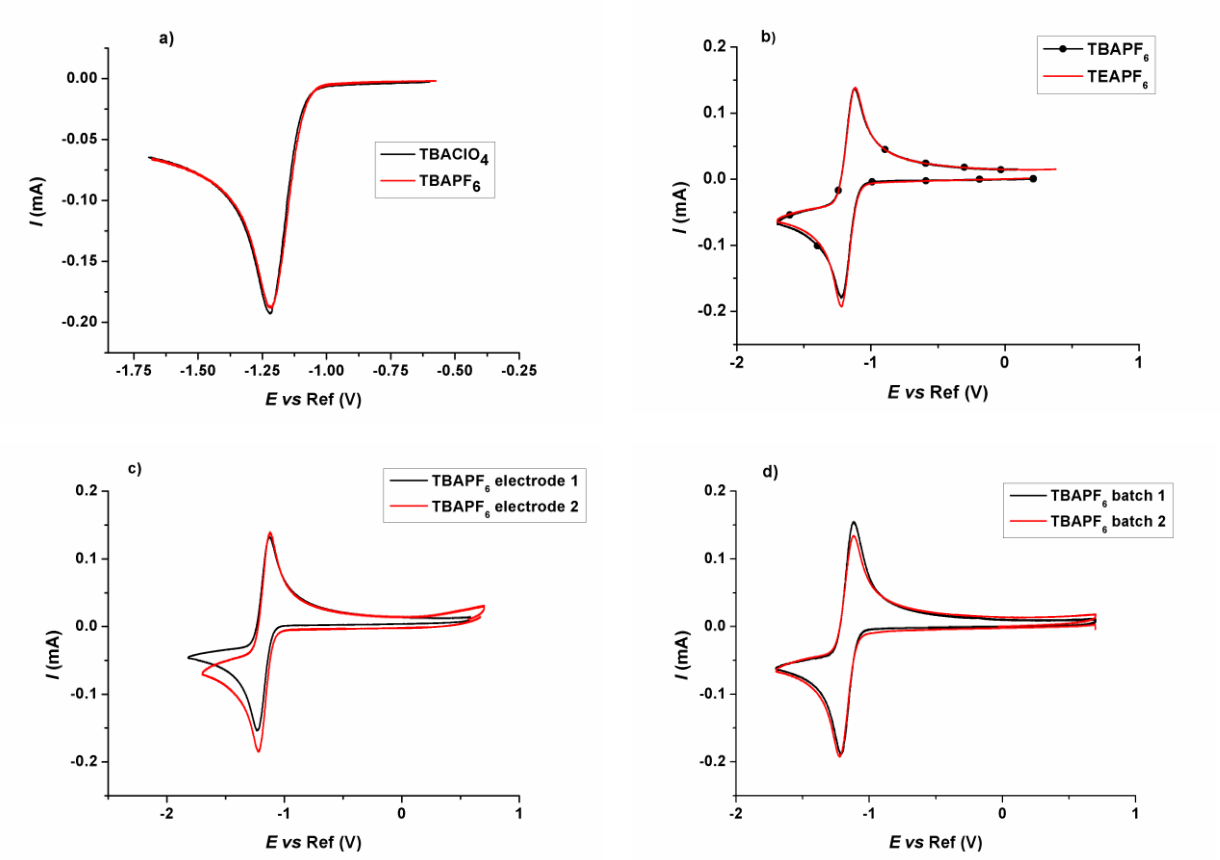

Figure IV.1. Reproducibility of ORR measurements in DMSO in presence of TAA^+ under different conditions: (a) effect of the anion (b) effect of the alkyl chain length (c) effect of the surface state of the electrode (d) effect of the batch of electrolyte (both solvent and salt) used. All the cyclic voltammetries were performed at v = 0.1 V s^{-1} in oxygen-saturated DMSO.

In order to further characterize the reaction, rotating ring-disk electrode (RRDE) measurements have been undertaken (Figure IV.2). When the potential of the ring is fixed above E_R = - 0.7 V *vs*. Ref (*i.e*. a potential just positive of the oxidation peak of the first reversible electron transfer, which shall enable the re-oxidation of any superoxide anions passing in the vicinity of the ring, the measured current is directly proportional to the reduction current measured on the disk, the latter being polarized at E_D = - 1.7 V *vs*. Ref (*i.e*. a potential just negative of the reduction peak of the first reversible electron transfer). Whatever the revolution rate, the ratio of the ring to the disk current remains constant ($\frac{I_R}{I_D} = 0.38$, Figure IV.2a), and corresponds to the collection efficiency measured with dissolved ferrocene species ($\frac{I_R}{I_D} = 0.39$), itself being close to the geometrical efficiency (N_{geo} = 0.42). In addition, the quasi-steady state disk current varies proportionally to the square-root of the revolution rate of the rotating ring-disk electrode; using the Levich equation (IV.4) and O_2 solubility and diffusion coefficient taken from References [5] and [6] (Table IV.1), a mono-

electronic transfer allows fitting the measured variations (Figure IV.2b). These results further support the already widely accepted idea that superoxide is produced reversibly by a one-electron reduction of oxygen, and that it is relatively stable in DMSO in presence of tetraalkylammonium salt.

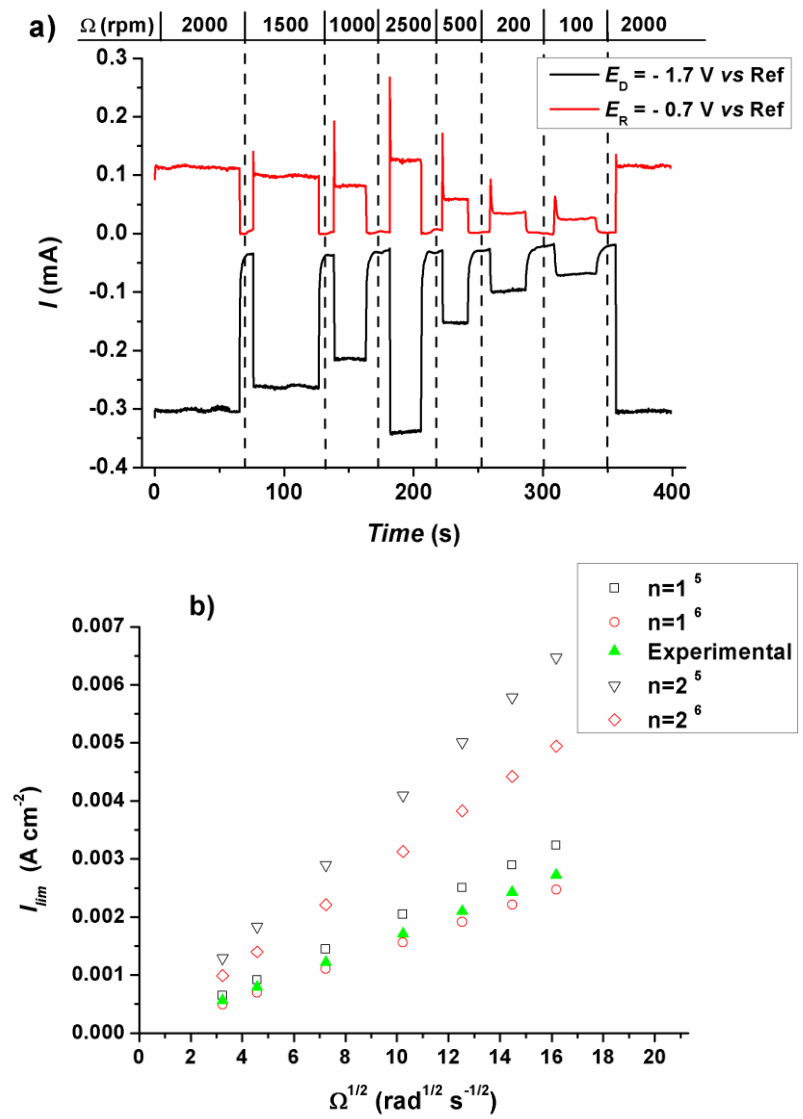

Figure IV.2. (a) Response of a RRDE in oxygen-saturated DMSO containing 150 mM $TEAPF_6$ upon variation of the revolution rate Ω of the electrode while the potential of the disk is set at E_D = - 1.7 V *vs.* Ref and the potential of the ring is set at E_R = - 0.7 V *vs.* Ref (IR uncorrected). (b) Levich plots calculated from experimental data from (a) (green) and compared to theoretical calculations using D_{O_2} and C_{O_2} values from [5] (black) and [6] (red).

$$I_{\mathrm{lim}} = 0.62nFD_{\mathrm{O}}^{2/3}\,\nu^{-1/6}C_{\mathrm{O}}\,\Omega^{1/2} \qquad \text{(IV.4)}$$

with n the number of electrons exchanged, I_{lim} the limiting current density, D_{O} the diffusion coefficient of the oxidant, C_O its bulk concentration, Ω the revolution rate of

the electrode and v the kinematic viscosity of the electrolyte solution.

Table IV.1. Oxygen mass-transport properties of DMSO-based electrolyte solutions at 0.1 M ionic strength

ν_{DMSO} (cm² s^{-1})	C_{O_2} (mM)	$10^5 D_{O_2}$ (cm² s^{-1})
0.01896 [5]	2.24 [5] 1.8 [6]	2.08 [5] 1.93 [6]

2. Influence of the solvent on the ORR in presence of TBA^+

Since the potential of the first reduction of oxygen does not depend on the length of the alkyl chain of the TAA^+ in DMSO (Figure IV.1), cyclic voltammetries have been performed in 3 other high-permittivity solvents in presence of TBA^+ (Figure IV.3a). Acetonitrile and DMSO have both a much higher affinity for anions than DMA and NMP, as measured by their acceptor number (AN) (Table III.1). DMSO, DMA and NMP should have a much higher affinity for cations than acetonitrile, as measured by their donor number (DN) (Table III.1). Given the low amount of data points, correlations hardly make sense here, but were nevertheless attempted to evaluate the possible scenarios (Figure IV.3b and c). The half-peak potential for the first reduction of oxygen is highly correlated to the AN of the 4 solvents (R^2 = 0.988), while there is no correlation with the DN of the solvents (R^2 = 0.092). Therefore it is concluded that the DN of the solvent, which reflects its general tendency to solvate cations, has no influence on the reduction potential of oxygen to superoxide in presence of TBA^+. Based on the reasoning proposed in introduction of this chapter, the idea of a low interaction between superoxide and TBA^+ is further supported by these results.

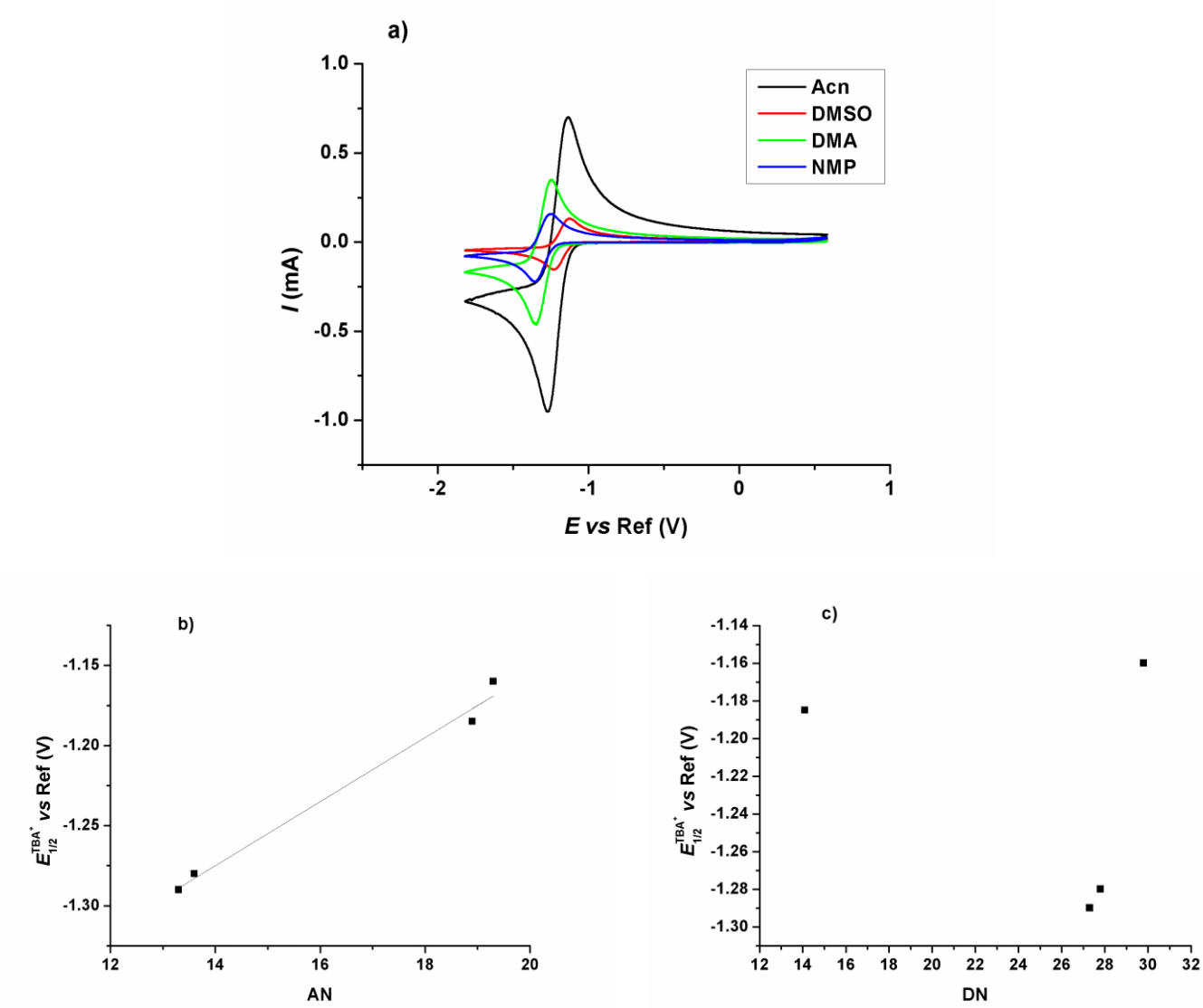

Figure IV.3. a) Cyclic voltammetries at *v* = 100 mV s^{-1} in oxygen saturated DMSO (red), Acn (black), DMA (green), NMP (blue) in presence of 200 mM $TBAClO_4$. Correlation of the half-peak potential of the first reduction process measured in presence of TBA^+ in different solvents with the AN (b) or DN (c) of the solvents.

Since the permittivity of the solvent has a high influence on ion-pairing (Chapter III) it could be interesting to study the oxygen reduction reaction in a solvent of lower permittivity (Figure IV.4). Pyridine has a much lower permittivity than the 4 previous solvents tested and an AN sensibly higher than that of DMA. Adding the half-peak potential for the first oxygen reduction process in pyridine in presence of TBA^+ to the previous correlation leads to a decrease of the correlation coefficient to R^2 = 0.938. Addition of 50 mM of TEA^+ leads to a positive shift of the half-peak potential (35 mV), while it does not in DMSO. Thus, ion-pairing of superoxide with TAA^+ has to be considered in lower permittivity solvents (this was not the case for high-permittivity solvents). Furthermore, the half-

peak potential measured in pyridine in presence of TBA^+ might be superior to the actual potential that would be measured in a non-interacting support electrolyte. A measure in presence of an even larger cation would be interesting.

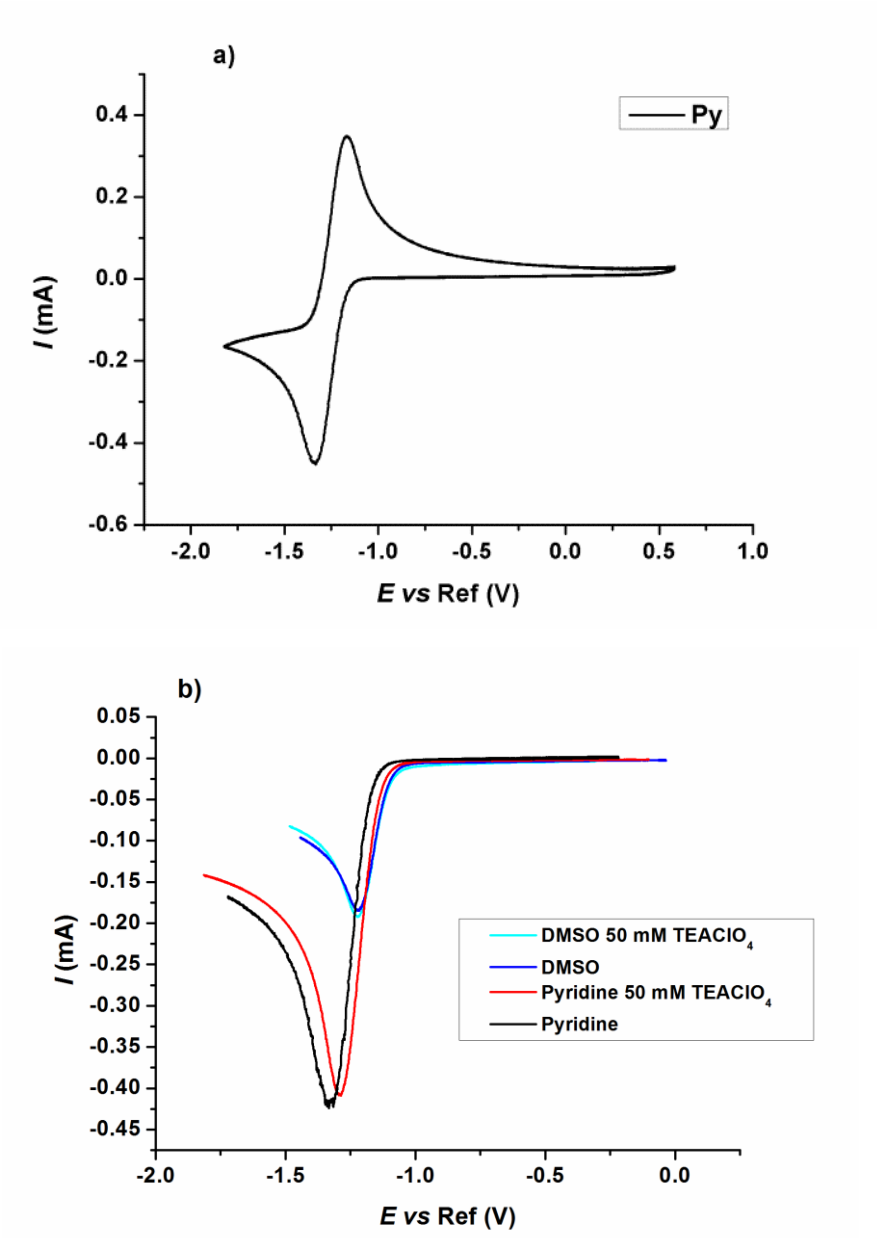

Figure IV.4. a) CV at 100 mV s^{-1} in oxygen-saturated pyridine in presence of 200 mM TBAClO4; b) CV at 100 mV s^{-1} in pyridine (red and black) and dimethylsulfoxide (dark and light-blue) with 200 mM TBAClO4 (red and light-blue) or 150 mM TBAClO4 + 50 mM TEAClO4 (black and dark-blue).

In order to design an electrolyte with tailored properties (permittivity, conductivity, solubility of specific compounds), it could be interesting to mix two (or more) solvents, as often done for Li-ion batteries[7]. It is rather complicated to predict the exact properties of such mixtures, but the permittivity of the resulting medium is expected to fall in between those of the two solvents. If an

almost linear relation is observed for solvents with comparable permittivity[8-9], a large difference in permittivity can result in non-linear effects. Still, mixing a solvent of low permittivity with increasing amounts of a solvent of higher permittivity will most-probably lead to a mixture of increasing permittivity, and this is usually at the basis of the design of electrolytes for lithium-ion batteries[7]. Considering solvation, the situation is more complex. Indeed, effects of preferential solvation are observed for salts: the solvent with the higher affinity for the cation (anion) of the salt will preferentially solvate the cation (anion)[8, 10]. Thus, it can be possible to actually have a higher solubility for a salt in a solvent mixture than in both solvents taken separately[10-11]. Again, these effects are usually non-linear, and thus the proportions to be used in the mixture to achieve a particular solubility of the salt are rather complicated to predict.

The half-peak potential for the first reduction of oxygen in an Acn-DMSO mixture is increasing with increasing content in DMSO, while remaining in between that of the two pure solvents (Figure IV.5.a). In a DMA-DMSO mixture (Figure IV.5.b), the half-peak potential is almost equal to that in pure DMSO. These two examples demonstrate the effect of preferential solvation in solvents of markedly different anion solvation capability. A similar effect is observed in Acn-Py mixture and Acn-DMA mixture (Table IV.2).

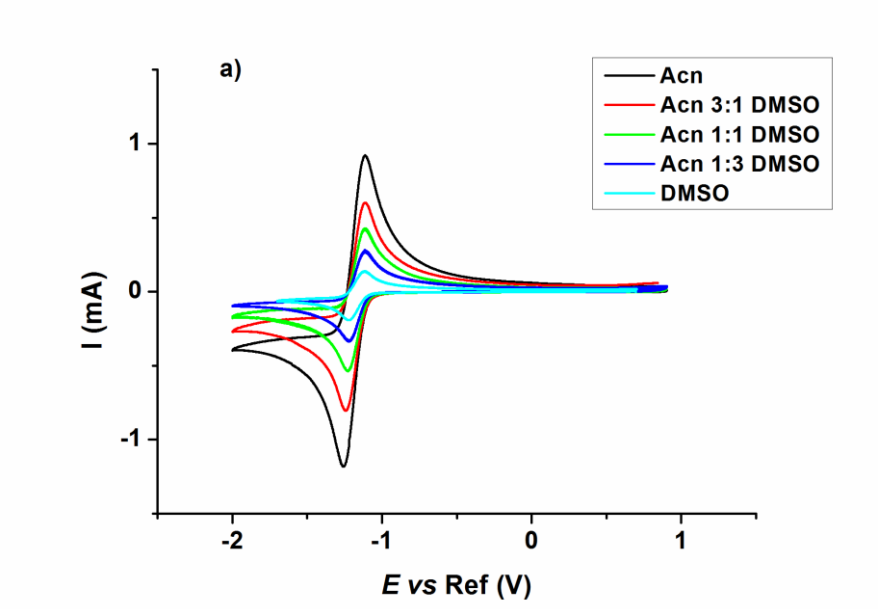

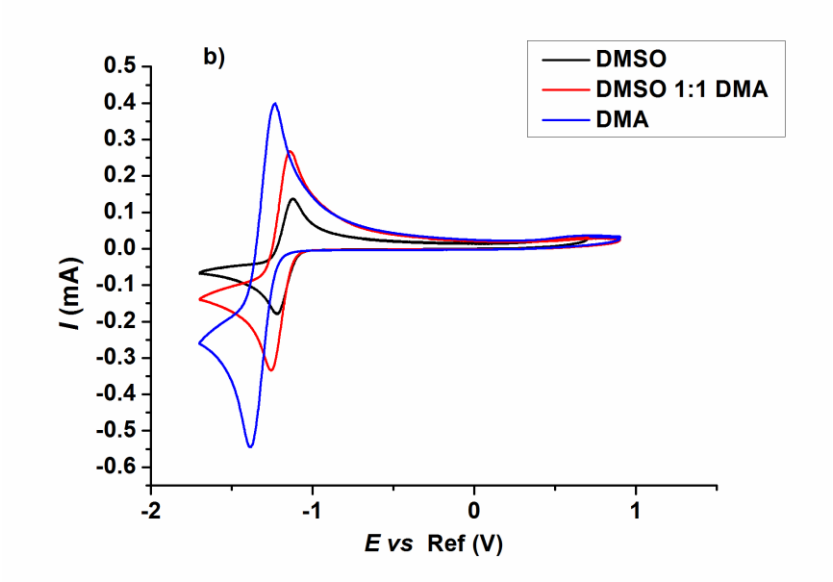

Figure IV.5. Cyclic voltammetries at v = 100 mV s^{-1} in oxygen-saturated Acn-DMSO (a) or DMA-DMSO (b) mixtures in presence of 200 mM $TBAClO_4$.

3. Calculation of physicochemical parameters of interest

From the cyclic voltammetries at different sweep rates (example for DMSO on Figure IV.6), it can be possible to calculate the oxygen mass-transport parameter $C^*_{O_2}(D_{O_2})^{1/2}$ using the Randles-Sevcik equation (IV.5). The parameter calculated in a mixture is in between those calculated in the two pure solvents (Figure IV.6 and Table IV.2).

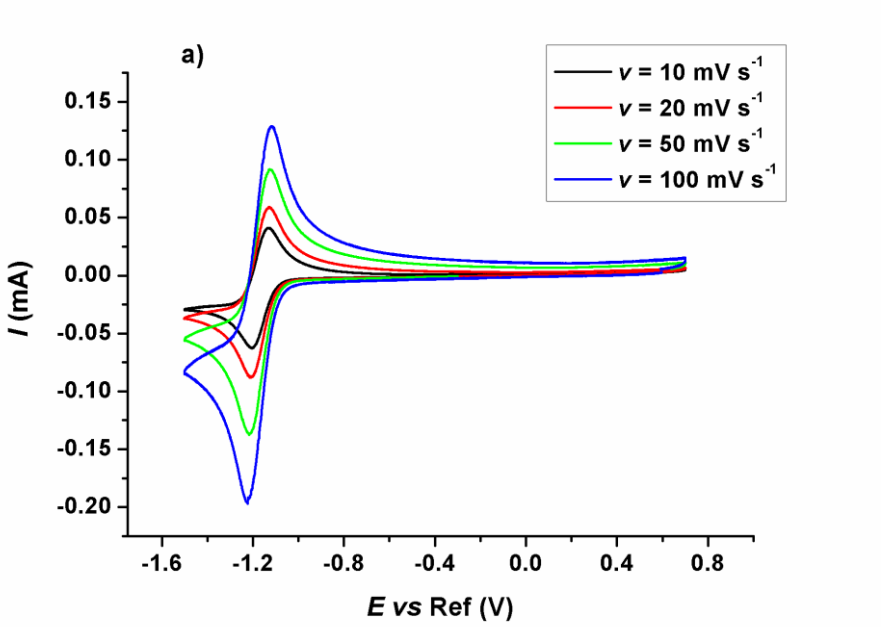

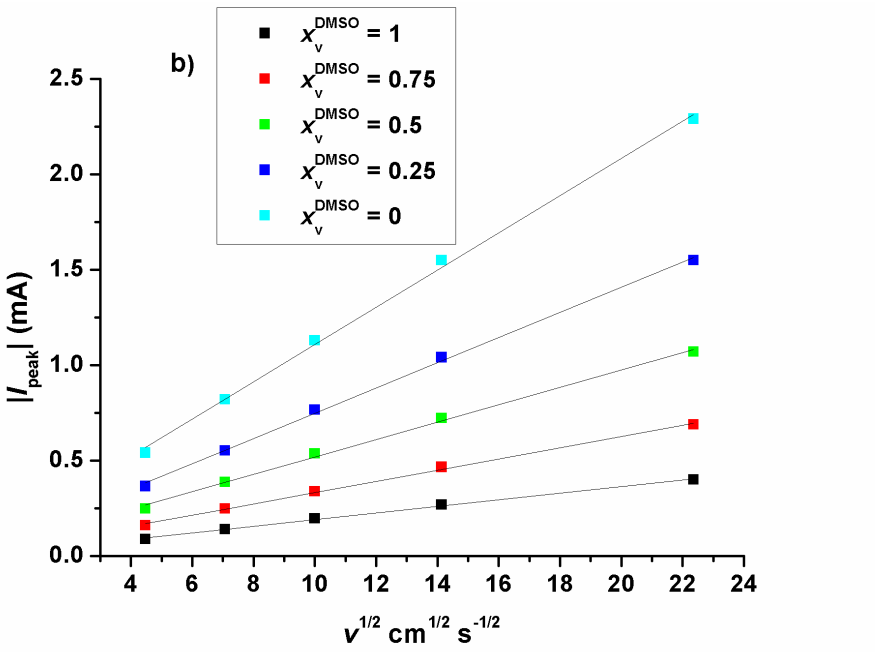

Figure IV.6. a) Cyclic voltammetries at different scan rates in oxygen saturate DMSO. b) Randles-Sevcik treatment of the peak potentials obtained at different scan rates *v* in Acn-DMSO mixtures with different volume fraction of DMSO x_v^{DMSO}.

$$I_{\mathrm{peak}} = 268.6 n^{3/2} F S D_O^{1/2} C_{\mathrm{O}} v^{1/2} \qquad \text{(IV.5)}$$

with n the number of electrons exchanged, I_{peak} the peak current, S the geometric surface of the electrode, D_{O} the diffusion coefficient of the oxidant, C_O its bulk concentration and v the scan rate

The transfer activity coefficient of superoxide from DMSO to other solvents can be estimated according to equation (III.10), considering the transfer activity coefficient of oxygen as negligible (Table IV.2). It is also considered that the difference in half-peak potentials between two different solvents is equal to the difference in the standard potentials of the first reduction of oxygen in the same solvents. This can be a rather rough approximation since the half-peak potential depends also on the relative diffusion coefficients for oxygen and superoxide, and on the reaction kinetics. Of course, both of these elements might vary from one solvent to another, which could lead to uncertainty up to several tenths of millivolts.

Table IV.2. Physicochemical parameters estimated from cyclic voltammetries in different solvents and solvent mixtures. *the transfer activity coefficient proposed for pyridine might be underestimated due to ion-pairing with TBA^+.

Solvent	$E_{1/2}^{TBA^+}$ *vs* Ref /V	$C_{O_2}^*(D_{O_2})^{1/2}$ /mol.cm^{-2}.s$^{-1/2}$	$\gamma_t(O_2^{\cdot-}, DMSO \rightarrow S)$
DMSO	-1.16	0.011	0
DMSO 3:1 Acn	-1.16_5	0.020	1.2
DMSO 1:1 Acn	-1.16_5	0.031	1.2
DMSO 1:3 Acn	-1.17	0.046	1.5
Acn	-1.18_5	0.067	2.6
DMA	-1.28	0.033	100
DMSO 1:1 DMA	-1.18	0.019	2.1
Acn 1:1 DMA	-1.20	0.045	5.1
Py	-1.24	0.032	21*
Py 1:1 Acn	-1.19	0.047	3.2
NMP	-1.29	0.016	150

Conclusion

On the basis of electrochemical measurements presented in this chapter, it has been demonstrated that the interactions between TAA^+ cations and the superoxide anion $O_2^{\cdot-}$ are limited in high-permittivity solvents, partly invalidating the hypothesis of a stabilization of superoxide in solution by the large ammonium cations. In addition, in such high-permittivity solvents, the nature of the anion associated to the TAA^+ cation (ClO_4^-, PF_6^- or BF_4^-) and the overall salt concentration also play minor role on the first reduction of oxygen. The important effect of the permittivity of the solvent on the oxygen reduction reaction has also been addressed. In high-permittivity solvents, the solvation of the superoxide has been linked to the acceptor number of the solvent, in accordance with the literature. Finally, transfer activity coefficients of superoxide from DMSO to other solvents have been estimated.

The fact that TAA^+ have proven to be non-interacting cations supports their use as supporting electrolyte to study the interactions between larger charge-density alkali metal cations and $O_2^{\cdot-}$. Thus the following chapter will be dedicated to the understanding of the influence of alkali metal cations on the ORR mechanism.

Bibliography:

1. Laoire, C. O.; Mukerjee, S.; Abraham, K. M.; Plichta, E. J.; Hendrickson, M. A., Influence of Nonaqueous Solvents on the Electrochemistry of Oxygen in the Rechargeable Lithium−Air Battery. *The Journal of Physical Chemistry C* **2010**, *114*, 9178-9186.

2. Bryantsev, V. S.; Giordani, V.; Walker, W.; Blanco, M.; Zecevic, S.; Sasaki, K.; Uddin, J.; Addison, D.; Chase, G. V., Predicting Solvent Stability in Aprotic Electrolyte Li–Air Batteries: Nucleophilic Substitution by the Superoxide Anion Radical (O2•–). *The Journal of Physical Chemistry A* **2011**, *115*, 12399-12409.

3. Bryantsev, V. S.; Faglioni, F., Predicting Autoxidation Stability of Ether- and Amide-Based Electrolyte Solvents for Li–Air Batteries. *The Journal of Physical Chemistry A* **2012**, *116*, 7128-7138.

4. Bryantsev, V. S.; Uddin, J.; Giordani, V.; Walker, W.; Addison, D.; Chase, G. V., The Identification of Stable Solvents for Nonaqueous Rechargeable Li-Air Batteries. *Journal of the Electrochemical Society* **2013**, *160*, A160-A171.

5. Tsushima, M.; Tokuda, K.; Ohsaka, T., Use of Hydrodynamic Chronocoulometry for Simultaneous Determination of Diffusion Coefficients and Concentrations of Dioxygen in Various Media. *Analytical Chemistry* **1994**, *66*, 4551-4556.

6. Tissot, P.; Yadav, A. K., The Electrochemically Generated Superoxide: Some Kinetic Measurements and Its Use for the Fragmentation of Some Tosylhydrazones. *Electrochimica Acta* **1986**, *31*, 71-77.

7. Ue, M.; Sasaki, Y.; Tanaka, Y.; Morita, M., Nonaqueous Electrolytes with Advances in Solvents. In *Electrolytes for Lithium and Lithium-Ion Batteries*, Jow, T. R.; Xu, K.; Borodin, O.; Ue, M., Eds. Springer New York: **2014**; Vol. 58, pp 93-165.

8. Izutsu, K., *Electrochemistry in Non-Aqueous Solutions*, First ed., **2002**.

9. Ahire, S.; Chaudhari, A.; Lokhande, M.; Mehrotra, S., Complex Permittivity Spectra of Binary Pyridine–Amide Mixtures Using Time–Domain Reflectometry. *Journal of Solution Chemistry* **1998**, *27*, 993-1008.

10. Patil, U. N.; Keshri, S.; Tembe, B. L., Solvation Structure of Sodium Chloride (Na+–Cl−) Ion Pair in Dimethyl Sulfoxide–Acetonitrile Mixtures. *Journal of Molecular Liquids* **2015**, *207*, 279-285.

11. Kim, J. I.; Duschner, H., Preferential Solvation of Single Ions: The Medium Effects of the Ag+, Agcln1—N), and Cl— Ions in Mixed Acetonitrile-Water Solvents. In *Zeitschrift für Physikalische Chemie*, **1977**; Vol. 106, p 1.

Chapter V. Oxygen Reduction Reaction Mechanism in DMSO in Presence of Alkali Metal Cations

The previous chapter demonstrated that tetraalkylammonium cations (TAA^+) interact very weakly with superoxide anions ($O_2^{\bullet-}$) in DMSO-based electrolyte solutions, and that the nature of the anion associated to the TAA^+ cation (ClO_4^-, PF_6^- or BF_4^-) negligibly influences the first reduction of oxygen [i]. Furthermore, DMSO has high permittivity, acceptor number (AN) and MCB values (Table III.1). Thus, it has been considered as a perfect solvent to study the impact of alkali metal cations on the ORR mechanism. This chapter is principally devoted to the qualitative development of the mechanism; it is mainly based on experimental findings and, as such, contains only few calculations.

1. General overview of the ORR/OER in presence of alkali metal cations

The addition of small amounts of alkali metal cations (Li^+, Na^+ and K^+) in a DMSO + $TEAPF_6$ supporting electrolyte leads to major changes on the ORR/OER voltammograms (Figure V.1), though similarities between the three systems can be observed. On the forward scan (ORR, toward negative potentials), the peak associated to the first reduction process is mildly affected and slightly shifts to higher potentials when the charge-density of the cation increases (*i.e.* in the order $K^+ < Na^+ < Li^+$). It is followed by a second wave, appearing at higher potentials also when the charge-density of the cation increases ($K^+ < Na^+ < Li^+$). This second reduction process forms a defined peak only in the presence of K^+. When going to even lower potentials (typically below -2 V *vs*. Ref), the current is gradually decreasing to 0 in presence of Li^+ and Na^+, which can be related to the precipitation of non–conductive solid products at the electrode surface, which "passivates" it. The formation of solid reduction products at the electrode surface is further supported by the higher OER anodic charge observed on the backward scan (toward positive potentials), as compared to the measurements in the absence of alkali metal cations. In order to understand these effects, the first and second reduction processes will be studied separately in the following sections of the chapter.

[i] In the present chapter, the higher chemical purity salt was the criterion of choice, therefore alkali metal cations associated with different anions were used.

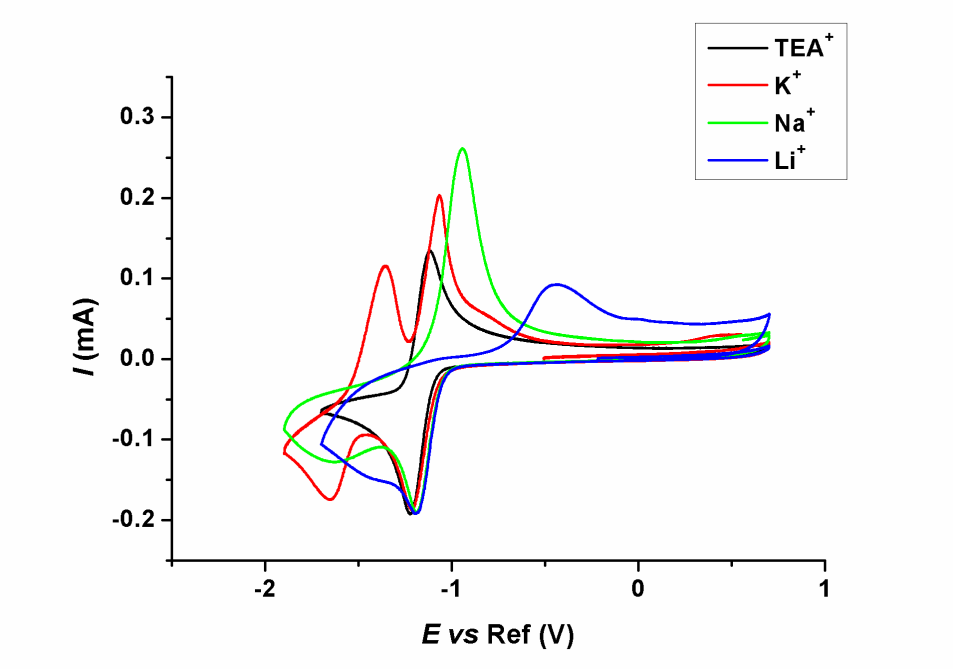

Figure V.1. Cyclic voltammetries at v = 100 mV s^{-1} in oxygen-saturated DMSO in presence of 150 mM $TEAPF_6$ and 25 mM KPF_6 (red), $NaClO_4$ (green) or LiTf (blue).

2. First reduction process

Upon addition of increasing amounts of alkali metal cations M^+, regardless of their nature, the potential of the first reduction process is gradually shifting positive (Figure V.2).

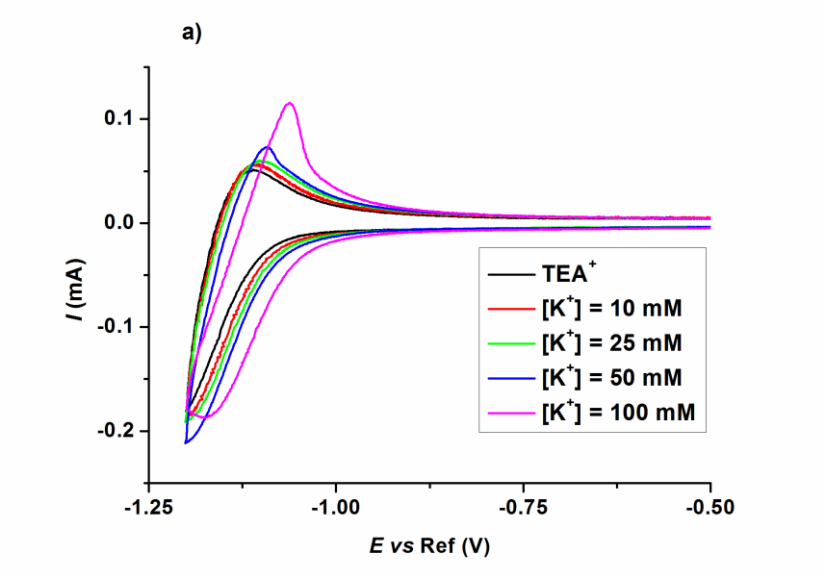

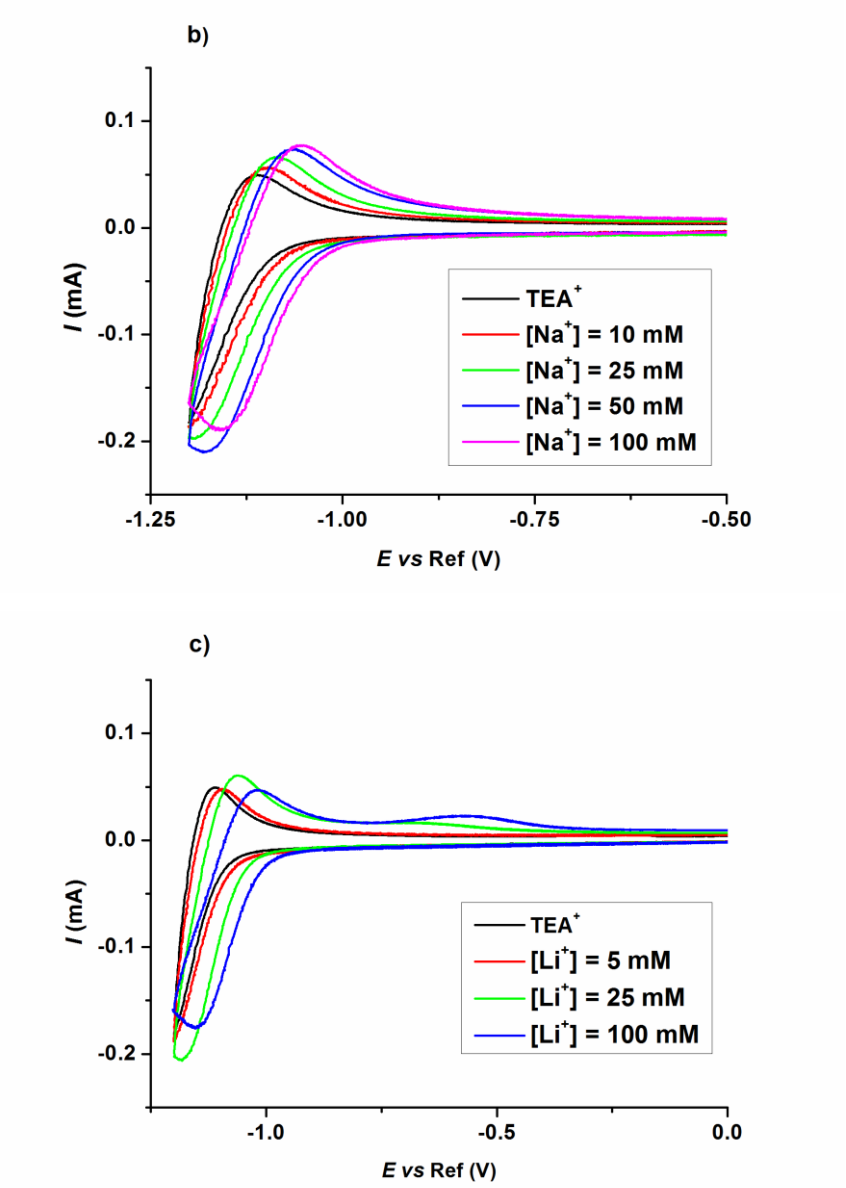

Figure V.2. Cyclic voltammetries at v = 100 mV s^{-1} in oxygen saturated DMSO and 150 mM $TEAPF_6$ in presence of increasing concentration in KPF_6 (a), $NaClO_4$ (b) or LiTf (c). The negative vertex potential is set to limit the reactions to the first reduction process.

At equal concentrations in alkali metal cations, the positive shift of the first ORR peak is larger in the order $K^+ < Na^+ < Li^+$, as forecast by Figure V.1. As stated in chapter II, such a shift has already been observed in presence of Li^+[1] and harder Lewis acids, its magnitude being related to the charge-density of the cation[2-3]. The present results demonstrate that this relation can be extended to Na^+ and K^+. Three explanations can in principle be proposed to account for the charge-density-related positive shift of the first oxygen reduction process in presence of alkali metal cations: it can be due (i) to the precipitation of solid alkali metal superoxide (MO_2), (ii) to ion-pairing in solution and/or (iii) to the disproportionation of superoxide into peroxide species, which could be favored in

presence of interacting cations. This last proposition is not likely for K^+, since K_2O_2 is less stable than KO_2[4]. Thus, for K^+, the shift is at least due to one of the two first propositions. Moreover, the anodic charge on the backward scan in presence of 50 mM K^+ (Figure V.3a) exceeds that observed in presence of 50 mM Na^+ (Figure V.3b), although in the forward (negative) scan, the peak coulometry values were similar. From this simple comparison, one can assert that the first oxygen reduction in the presence of potassium is not a pure solution-based mechanism and that it produces species that remain at the electrode surface upon formation (in the presence of sodium, this is less likely). More specifically, one can conclude that solid products (most likely KO_2) to some extent form during the first oxygen reduction in the presence of K^+ (case (i) above); in addition, the less-likely formation of solid products in the case of Na^+ signs that the solubility of NaO_2 exceeds that of KO_2. In the same manner, the disproportionation of superoxide into peroxide species (proposition (iii) above) in presence of Na^+ would lead to the formation of highly insoluble Na_2O_2 on the electrode surface, which is not compatible with the results of Figure V.3b.

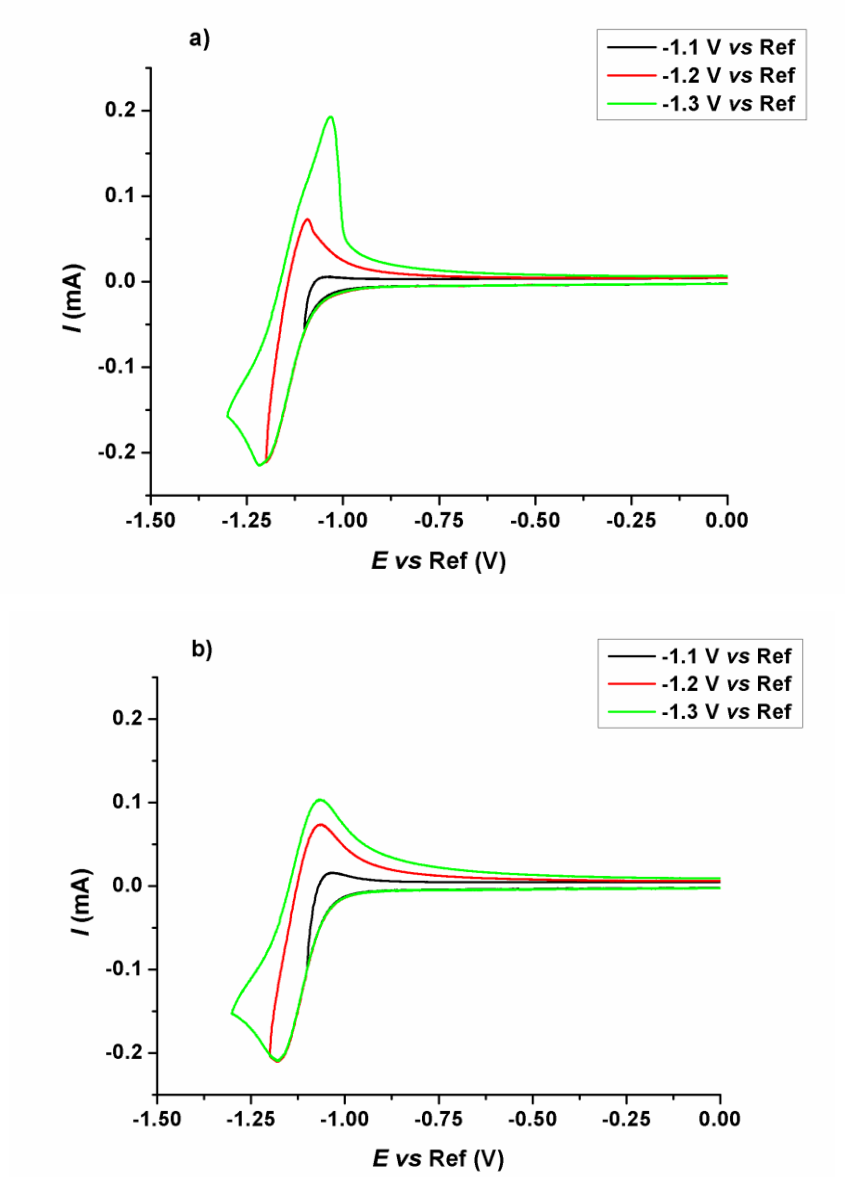

Figure V.3. Cyclic voltammetries at v = 0.1 V s^{-1} in oxygen saturated DMSO and 0.15 M $TEAPF_6$ in presence of 50 mM of K^+ (a) or Na^+ (b), at different cathodic return potentials

These results lead to an apparent incompatibility between the positive shift in potential, which is obviously larger in presence of Na^+ as compared to K^+, and the solubility of NaO_2, which would be higher than that of KO_2. This apparent inconsistency can be resolved by considering that the shift in potential is mainly due to the formation of ion-pairs between $O_2^{\cdot-}$ and the alkali metal cations in presence (case (ii) above), and especially for Na^+. This is further corroborated by the fact that, in order for a precipitation to occur, oversaturation concentrations have to be reached in $O_2^{\cdot-}$ and M^+ at the electrode interface. Thus, if the salt has a partial solubility, the reduction onset potential should not be influenced by precipitation, but solely by ion-pairs formation. To summarize,

at least in presence of Na^+, the ORR in presence of alkali metal cations involves the formation of ion-pairs between the superoxide anion $O_2^{\cdot-}$ and the alkali metal cation.

When the experiments were performed with a rotating ring-disk electrode (RRDE[ii]) configuration (Figure V.4), a current plateau is reached in presence of K^+ both for the disk current (oxygen reduction) and the ring current (re-oxidation of $O_2^{\cdot-}$-like species). A wave corresponding to the second reduction process could not be clearly observed in presence of Na^+: it is considered here that the first reduction process is still highly predominant at low potential values (large ORR overpotentials), in agreement with the voltammograms on static electrodes (Figure V.1). The potential range has thus been chosen as to limit the influence of the second reduction process (Figure V.4b). RRDE results in presence of Li^+ will be discussed in the section devoted to the second reduction process, owing to the very poor separation observed between the first and second reduction process in presence of Li^+ (Figure V.1): in this case, the influence of the second reduction process can indeed not assuredly be ruled out, even at low overpotentials.

[ii] Usually, rotating disk electrode (RDE) is used as a tool to achieve quasi-stationary conditions, and current plateaus are directly related to mass-transport control, which depends, among other parameters, on the rotation rate. Here, the situation is considerably complicated by the precipitation of partially soluble salts on the surface of the electrode. Thus, not only the kinetics of the electrochemical reactions or the mass-transport phenomena have to be taken into account but also the deposition, dissolution and solid-state transformations kinetics. The use of RRDE can thus lead to particularly interesting features, and might be of use to determine these solid-state related parameters. However, this determination requires modelling of the system. Without it, even a qualitative interpretation of the results is complicated, and can be subject to incomplete statements.

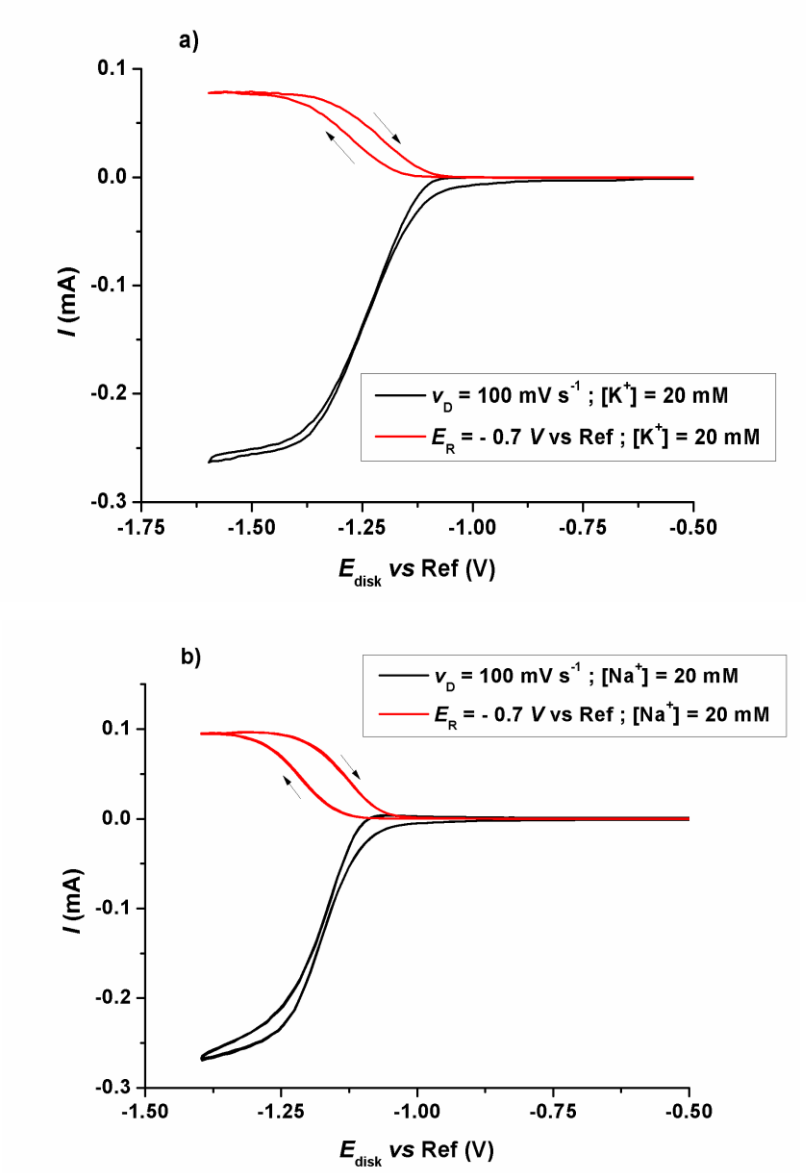

Figure V.4. RRDE response in oxygen-saturated DMSO containing 150 mM $TEAPF_6$. A cyclic voltammetry was performed on the disk at v = 0.1 V s^{-1} while the potential of the ring was set at E_R = - 0.7 V vs. Ref at Ω = 1000 rpm in presence of 20 mM KPF_6 (a) (IR uncorrected) or 20 mM $NaClO_4$ (b) (IR corrected).

The ratio of the ring current on the disk current is slightly larger in presence of Na^+ ($\frac{I_{\text{ring}}}{I_{\text{disk}}} = 0.36$) as compared to K^+ ($\frac{I_{\text{ring}}}{I_{\text{disk}}} = 0.31$), but lower than in their absence ($\frac{I_{\text{ring}}}{I_{\text{disk}}} = 0.38$). This can be due to the precipitation of MO_2 on the surface, with then, NaO_2 having a larger solubility than KO_2, in agreement with the conclusions made above. The detection of superoxide intermediates in solution on the ring is also a direct proof of the non-negligible solubility of KO_2. As stated before for Na^+, this partial solubility leads to the necessity to introduce ion-pairs $K^+ - O_2^-$ to account for the shift in the onset potential of the first reduction of oxygen in presence of K^+.

It is concluded from these elements that the shift of potential of the first reduction process in DMSO in presence of Na^+ and K^+ is, at least partially and most likely mainly, due to the formation of $M^+ - O_2^{\cdot-}$ ion-pairs between the superoxide anion ($O_2^{\cdot-}$) and the alkali metal cations. It is also concluded that NaO_2 has a larger solubility as compared to KO_2, the precipitation of which is experimentally observed.

3. Second reduction process

In order to further characterize the influence of the charge-density of the alkali metal cation on the second reduction wave, an additional experiment was performed in presence of Cs^+ (Figure V.5a). Whatever the alkali metal cation in presence (Figure V.5b), a second wave is observed at increasing potentials in the order $Cs^+ < K^+ < Na^+ < Li^+$, *i.e*. for increasing cation charge-density, as noticed above.

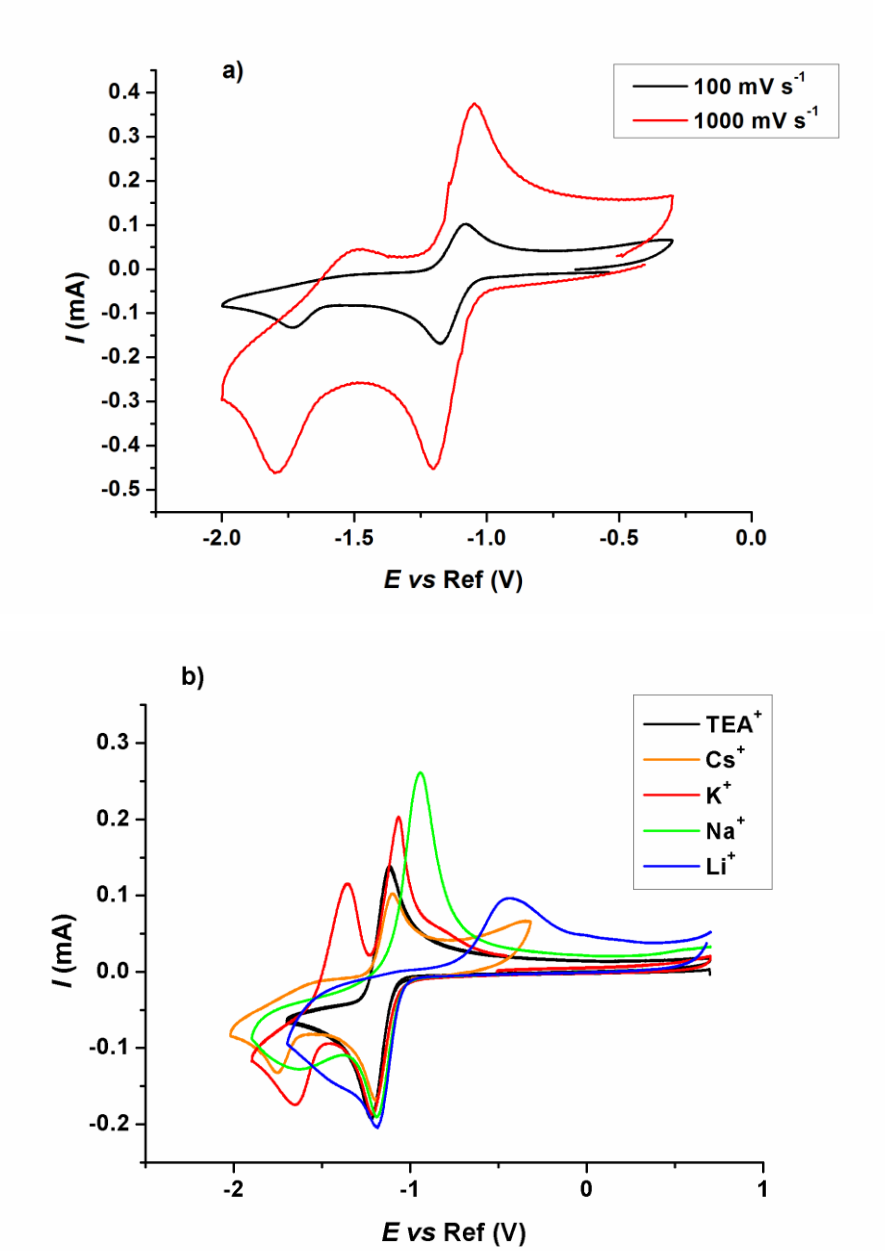

Figure V.5. (a) Cyclic voltammetry at *v* = 0.1 V s^{-1} (black) or *v* = 1 V s^{-1} (red) in oxygen-saturated DMSO containing 150 mM $TEAPF_6$ in presence of 50 mM CsI. (b) Cyclic voltammetries at *v* = 0.1 V s^{-1} in oxygen-saturated DMSO in presence of 150 mM $TEAPF_6$ and 25 mM KPF_6 (red), $NaClO_4$ (green) or LiTf (blue), or 50 mM CsI (orange).

The second wave is forming a defined peak only in presence of the lowest charge-density cations (K^+ and Cs^+). A high degree of reversibility is observed for the two oxygen reduction processes in presence of K^+. On the contrary, no sign of reversibility is witnessed in presence of Na^+ and Li^+, whatever the potential scan rate. In presence of Cs^+, increasing reversibility is observed with increasing scan rate. It should be noted that scanning the potential on this second wave irreversibly deteriorates the working electrode, due to the formation of either solid degradation products or

non-conductive insoluble products (or both), which cannot be fully oxidized on the backward (OER) scan.

Assuming the occurrence of a one-electron reduction of the ion-pairs $M^+ - O_2^{\cdot-}$ accounts well for these observations. Indeed, as stated in chapter II, the second reduction of $O_2^{\cdot-}$ into peroxide dianion O_2^{2-} is observed at much lower potentials in presence of TAA^+, cations that do not make ion-pairs with $O_2^{\cdot-}$ (Chapter IV). Measuring the value of standard potential for this second reduction is difficult, owing to the very high reactivity of the peroxide dianion with both the carbon working electrode and the electrolyte. Nevertheless, it can roughly be estimated as being 1.5 to 2 V lower than the first reduction potential[5-6]. Experiments in those two references were done in ammonia and acetonitrile. An influence of the solvent on the reduction potential of $O_2^{\cdot-}$ is expected, but was considered as included in this very rough approximation, which will not be at the basis of any calculations.

The standard potential associated to the reduction of the ion-pairs $M^+ - O_2^{\cdot-}$ can be determined by the standard potential associated to the reduction of the superoxide anion $O_2^{\cdot-}$ and the ratio of the association constants of $O_2^{\cdot-}$ and O_2^{2-} with M^+ (equations V.1-5).

$$O_2^{\cdot-} + e^- = O_2^{2-} \quad \text{(V.1)}$$

$$M^+ - O_2^{\cdot-} + e^- = M^+ - O_2^{2-} \quad \text{(V.2)}$$

$$O_2^{\cdot-} + M^+ = M^+ - O_2^{\cdot-} \quad \text{(V.3)}$$

$$O_2^{2-} + M^+ = M^+ - O_2^{2-} \quad \text{(V.4)}$$

$$E^o_{V.2} - E^o_{V.1} = \frac{RT}{F}\ln\left(\frac{K_{V.4}}{K_{V.3}}\right) \quad \text{(V.5)}$$

It can reasonably be assumed that $K_{V.4}$ should be considerably larger than $K_{V.3}$, and that their ratio is increasing with the charge-density of the cation M^+, since O_2^{2-} is a much harder base than $O_2^{\cdot-}$. Therefore, the standard potential of the reduction of the ion-pairs $M^+ - O_2^{\cdot-}$ shall significantly exceed that of the reduction of the superoxide anion $O_2^{\cdot-}$, and increase with the charge-density of the cations. This in agreement with the present experimental findings: the second wave/peak was clearly observed at somewhat higher potential values in the sequence $Cs^+ < K^+ < Na^+ < Li^+$, with the second reduction being very poorly separated in potential from the first one in the case of Li^+, the highest charge-density alkali cation (Figure V.5b).

The observations made here are very similar to results obtained for the second reduction of *o*-quinones (Q)[7]. Their second reduction leads to the formation of reactive dianions Q^{2-}, which undergo polymerization, hence a non-reversible second reduction peak on voltammograms. A peak separation of about 0.8 V was observed between the first and second reduction processes. Addition

of Na^+ into the electrolyte leads to a decrease of the peak separation to 0.4 V and a reversible second reduction. This has been explained by the formation of ion-pairs $Na^+ - Q^{\cdot -}$ between the one-electron reduced quinone $Q^{\cdot -}$ and Na^+, which is reduced at higher potentials as compared to $Q^{\cdot -}$, and the decrease of the reactivity of $Na^+ - Q^{2-}$ as compared to Q^{2-}.

This analogy could explain the results obtained in presence of Cs^+ and K^+: a larger interaction between K^+ and O_2^{2-} leads to less reactive ion-pairs $K^+ - O_2^{2-}$ as compared to $Cs^+ - O_2^{2-}$, the latter being less reactive than O_2^{2-}.

In presence of Li^+ and Na^+, the peak separation, even though it is rather complicated to assess, is even lower than in presence of K^+. Associated with the distorted shape of the wave, these phenomena can be explained by the formation of solid peroxides M_2O_2 according to equation (V.6). A faster reaction in the presence of cations of larger charge-density can be expected. The relative thermodynamic stability of solid oxides (MO_x) has been described in chapter II: KO_2 is more stable than K_2O_2, whereas Na_2O_2 and Li_2O_2 are more stable than NaO_2 and LiO_2 respectively. Thus, K_2O_2 formation on the electrode by general equation (V.6) should be limited by its synproportionation with O_2 (equation (V.7)), whereas Li_2O_2 and Na_2O_2 could precipitate on the surface without restrictions.

$$M^+ - O_2^{2-} + M^+ = M_2O_2 \quad \text{(V.6)}$$

$$M_2O_2 + O_2 = 2\,MO_2 \quad \text{(V.7)}$$

During RRDE experiments (Figure V.5a), a well-defined plateau is observed for the second reduction process in presence of K^+. In presence of Na^+, such second reduction wave is not clearly observed. The current is slightly rising (in absolute value) starting at -1.3 *V vs* Ref, and the second reduction process is thus considered as negligible at higher potentials, in agreement with the cyclic voltammetries on static electrodes. When potentials corresponding to the second reduction process are reached on the disk during cyclic voltammetries, the ratio of the ring current to the disk current is decreasing. This decrease is significantly more important in presence of K^+ ($\frac{I_{\text{ring}}}{I_{\text{disk}}} = 0.11$) than Na^+ ($\frac{I_{\text{ring}}}{I_{\text{disk}}} = 0.30$).

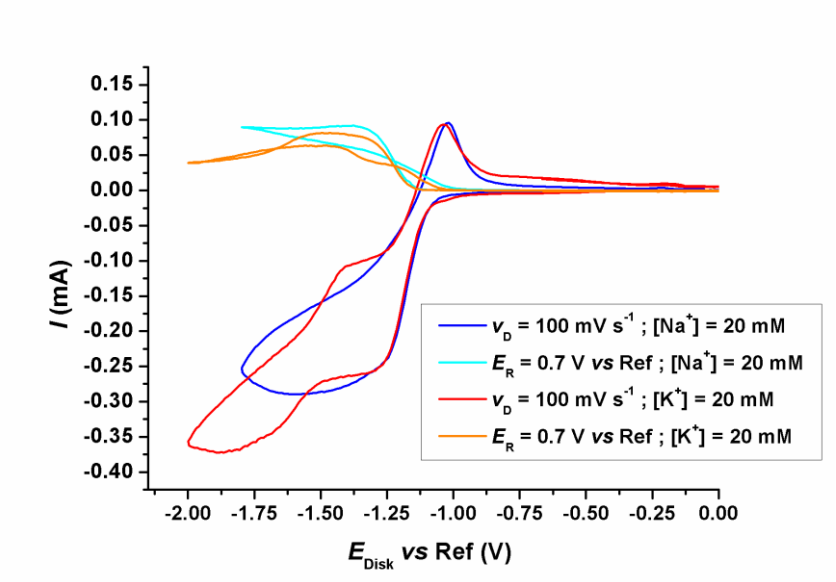

Figure V.6. RRDE response in oxygen-saturated DMSO containing 150 mM $TEAPF_6$. A cyclic voltammetry was performed on the disk at v = 0.1 V s^{-1} while the potential of the ring was set at E_R = - 0.7 V vs. Ref at Ω = 1000 rpm in presence of 20 mM KPF_6 (red and orange) or 20 mM $NaClO_4$ (light and dark blue) (both are IR corrected).

On the backward scan in presence of K^+ and Na^+, an anodic peak is observed only when the second reduction has been performed on the forward scan (Figures V.4 and V.6), indicating the formation of solid products (from the second reduction process) on the electrode. In presence of K^+, the anodic charge corresponding to this oxidation peak is nearly independent on the rotating rate, while it is influenced by the scan rate (Figure V.7). This can be a sign that reactions related to solid products (precipitation, dissolution, synproportionation) are limited by their kinetics rather than by mass-transport.

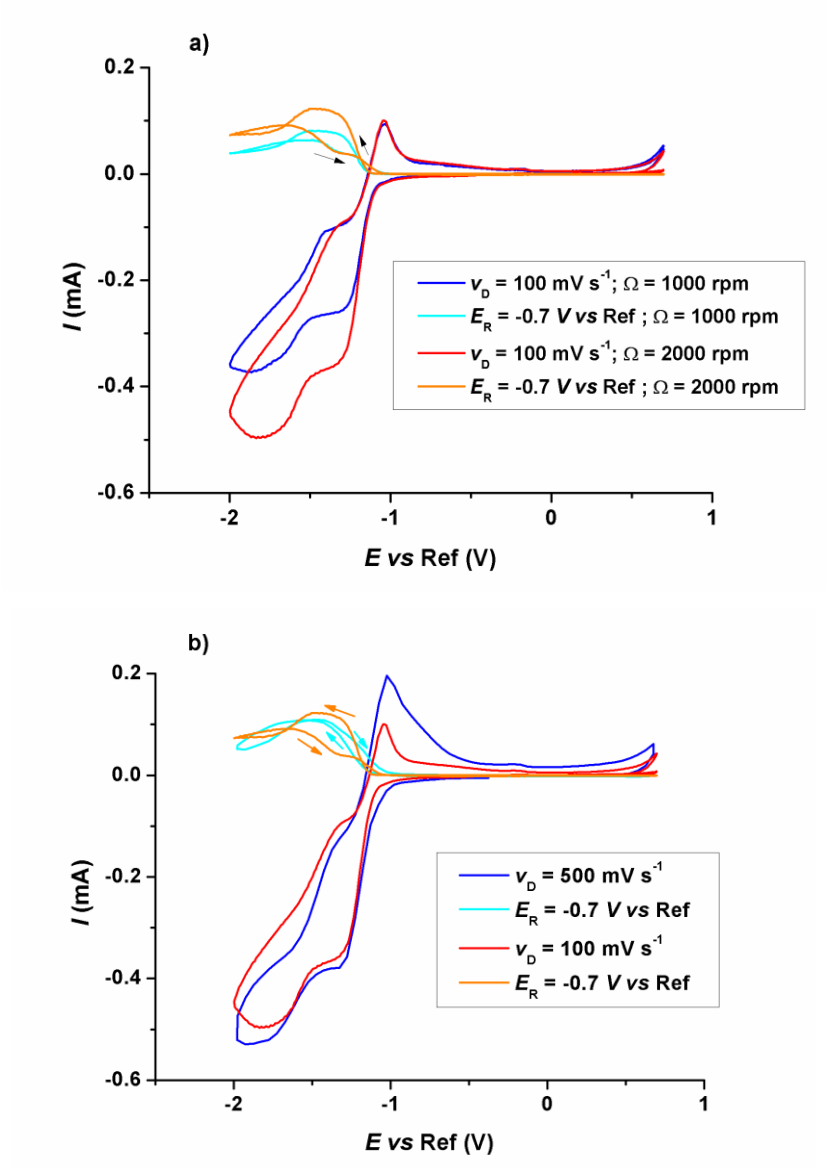

Figure V.7. RRDE response in oxygen-saturated DMSO containing 150 mM $TEAPF_6$ and 20 mM KPF_6. a) A cyclic voltammetry was performed on the disk at v = 0.1 V s^{-1} while the potential of the ring was set at E_R = - 0.7 V vs. Ref at Ω = 1000 rpm (light and dark blue) or Ω = 2000 rpm (red and orange) (both are IR corrected). b) A cyclic voltammetry was performed on the disk at v = 0.5 V s^{-1} (light and dark blue) or v = 0.1 V s^{-1} (red and orange) while the potential of the ring was set at E_R = - 0.7 V vs. Ref at Ω = 2000 rpm (both are IR corrected).

At disk potentials where oxygen can be reduced into superoxide species and $M^+ - O_2^{2-}$ can be oxidized (between – 1.5 *V vs* Ref and – 1.2 *V vs* Ref), a reduction current plateau can be observed on the backward scan (Figure 7.a), for both the disk and the ring. The ratio of the ring current on the disk current ($\frac{I_{ring}}{I_{disk}} = 0.45$) is larger than the geometric collection coefficient ($\frac{I_{ring}}{I_{disk}} = 0.42$), and both plateaus are independent on the rotating rate of the electrode. Conclusions on this feature would be

highly hypothetical, since many parameters could be involved, in particular the dissolution or solid state reactions of two different solid phases (KO_2 and K_2O_2). Modelling these phenomena was not achieved in the course of this work, and it will therefore[iii] not be discussed further here.

RRDE measurements have thus evidenced the formation of solid products during the second reduction process. Considering that the second reduction process in presence of K^+ has been attributed to the formation of $K^+ - O_2^{2-}$ in solution, its precipitation as K_2O_2 is very likely. By extension, and according to the results obtained on static electrode, the second reduction of $Na^+ - O_2^{\cdot-}$ to $Na^+ - O_2^{2-}$ and its precipitation as Na_2O_2 is also anticipated to account for the second reduction process in presence of Na^+.

As stated before, it was not possible to separate the two oxygen reduction processes in presence of Li^+ on RRDE measurements (figure V.8). Interestingly, the ratio of the ring current on the disk current is in the same order as those obtained in presence of the other alkali metal cations. However, the electrode passivation occurs whatever the reduction potential, and the anodic charge obtained on the corresponding backward scans remains very similar. This result can be explained by the formation of solid Li_2O_2 either from the chemical disproportionation of LiO_2, or the electrochemical second reduction of the ion-pairs $Li^+ - O_2^{\cdot-}$. A disproportionation in solution of $Li^+ - O_2^{\cdot-}$ seems unlikely, since the resulting ratio of ring current to disk current would be expected to be much smaller in that case.

Furthermore, the anodic charge measured on the backward scans remains very similar whatever the values of the negative vertex potential or the revolution rate, as long as the electrode has been passivated during reduction (figure V.8b). It seems that there is no specific potential needed to achieve such a passivation. This anodic charge could correspond to the oxidation of a compact insulating Li_2O_2 layer on the electrode. In that case, the average thickness of the layer would be of *ca*. 1.5 nm, which is sensibly lower than the values proposed in reference [8] in dimethoxyethane as a solvent (5 to 10 nm). Interestingly, the charge measured during the backward scan (OER) on Figure V.1 would correspond to a thicker layer (5 nm). The formation of a more uniform deposit when rotating the electrode is a probable explanation. On this basis, it is therefore possible that the actual insulating capability of Li_2O_2 has been slightly underestimated.[iv]

[iii] (sadly)

[iv] As a side note, it appears thus even more clearly that a solution-based mechanism is mandatory to achieve high energy density in practical LiOB.

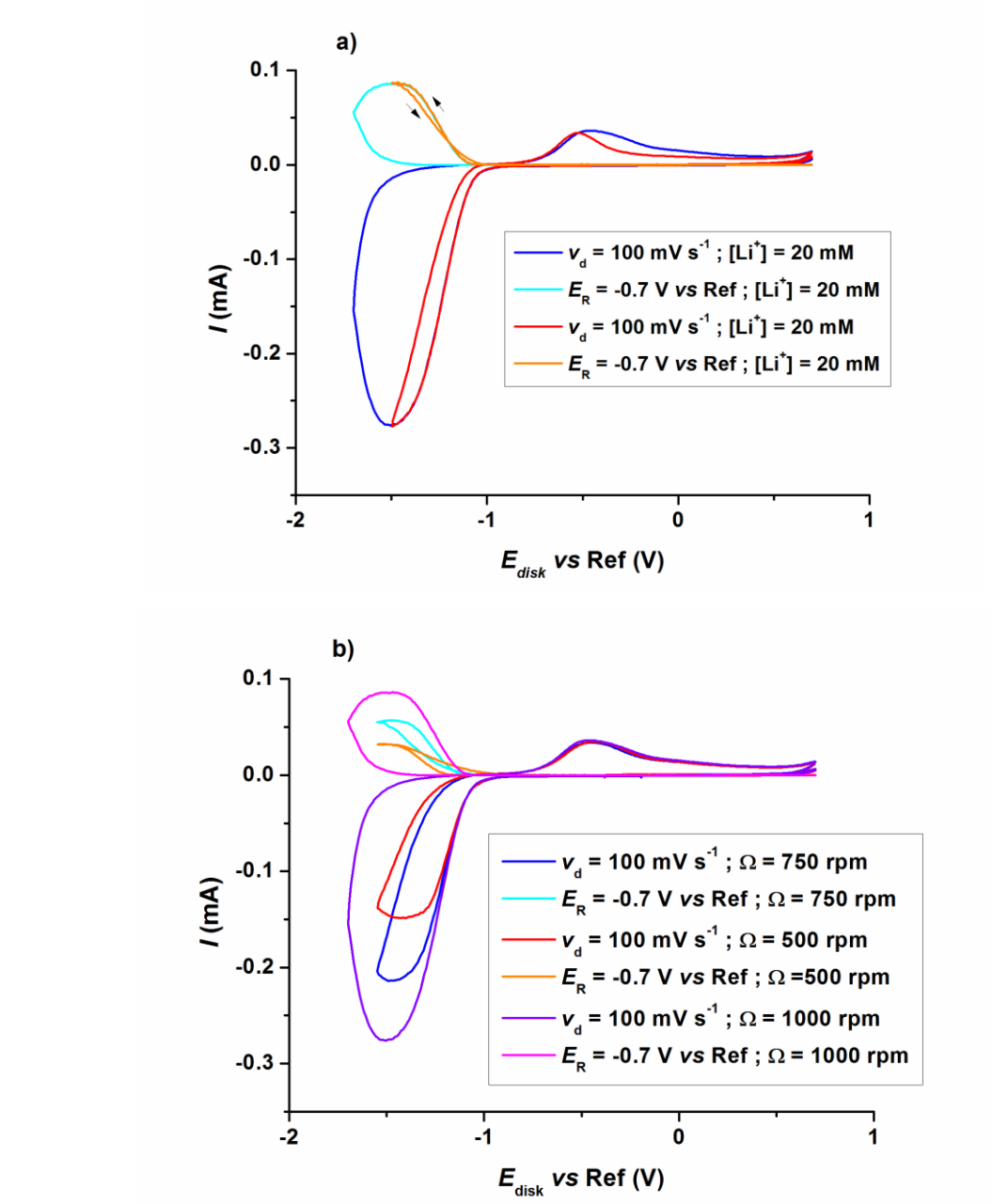

Figure V.8. RRDE response in oxygen-saturated DMSO containing 150 mM $TEAPF_6$ and 20 mM $LiPF_6$ (IR uncorrected). a) A cyclic voltammetry was performed on the disk at *v* = 0.1 V s^{-1} while the potential of the ring was set at E_R = - 0.7 V vs. Ref at Ω = 1000 rpm to - 1.5 *V vs* Ref vertex potential (red and orange) or to - 1.7 *V vs* Ref vertex potential (light and dark blue). b) A cyclic voltammetry was performed on the disk at *v* = 0.1 V s^{-1} while the potential of the ring was set at E_R = - 0.7 V vs. Ref at Ω = 500 rpm (red and orange) or Ω = 750 rpm (dark and light blue) to - 1.5 *V vs* Ref vertex potential, or Ω = 1000 rpm (violet and pink) to - 1.7 *V vs* Ref vertex potential.

From these elements, the second reduction process undergone by the superoxide species is thus accounted for by the one-electron reduction of the ion-pair $M^+ - O_2^-$ and its precipitation into solid

peroxide M_2O_2. The solid-phase equilibrium between MO_2 and M_2O_2 has also been introduced in order to account for the formation of Li_2O_2, as well as the difference in waves associated to the second reduction process in presence of K^+ and Na^+ or Li^+.

Proposed oxygen reduction mechanism and conclusions

From the crossed-analysis of the results in presence of different alkali metal cations in DMSO, a single mechanism can be proposed, which takes into account all the experimentally observed features (scheme V.1).

$$MO_{2,s} + MO_{2,s} \overset{K_{disp}}{=} M_2O_{2,s} + O_2$$

$$K_{s1} \,||\, M^+$$

$$O_2 + e^- \overset{E^\circ_1}{=} O_2^{\cdot -} + e^- \overset{E^\circ_2}{=} O_2^{2-}$$

$$K_{f1} \,||\, M^+ \qquad K_{f2} \,||\, M^+$$

$$O_2 + M^+ + e^- = M^+\text{-}O_2^{\cdot -} + e^- = M^+\text{-}O_2^{2-}$$

$$K_{s2} \,||\, M^+$$

$$M_2O_{2,s}$$

Scheme V.1. Proposed ORR mechanism in DMSO in presence of alkali metal cations.

This mechanism appears to be relatively simple, with only four electrochemical reaction (but only two independent standard potentials, E_1^o and E_2^o) and two chemical reactions (with two association constants), which are fixing two other standard potentials, as well as two solubility products and one solid-phase chemical constant. It is also important to note here that this mechanism does not involve any second electrochemical reduction in solid phase, or any oxido/reduction reaction of adsorbed species.

Furthermore, the experimental results presented in this chapter have shown how important it is to take into account the solubility of the solid phases precipitated during the reduction processes, and the complex phenomena related. In particular, RRDE seems to be a perfect way to understand these effects, and might lead to efficient determination of underlying mechanisms and thermodynamic constants.

Two related particular interesting points have been noticed and might have implications for LiOB. At low concentrations in Li^+, the disproportionation of superoxide into peroxide has only been

attributed to solid-phase disproportionation or electrochemical reduction of the ion-pairs $Li^+ - O_2^{\cdot-}$. Homogeneous solution-phase disproportionation has been directly ruled out by the RRDE results. Also, the highly insulating nature of Li_2O_2 has been confirmed.

Finally, since the mechanism has been developed in a particular solvent (DMSO for the time being), it has to be checked whether it can be extended to other solvents, which is the purpose of the next chapter.

Bibliography:

1. Johnson, L.; Li, C.; Liu, Z.; Chen, Y.; Freunberger, S. A.; Ashok, P. C.; Praveen, B. B.; Dholakia, K.; Tarascon, J.-M.; Bruce, P. G., The Role of Lio2 Solubility in O2 Reduction in Aprotic Solvents and Its Consequences for Li–O2 Batteries. *Nature Chemistry* **2014**, *6*, 1091-1099.

2. Sawyer, D. T.; Chiericato, G.; Angelis, C. T.; Nanni, E. J.; Tsuchiya, T., Effects of Media and Electrode Materials on the Electrochemical Reduction of Dioxygen. *Analytical Chemistry* **1982**, *54*, 1720-1724.

3. Johnson, E. L.; Pool, K. H.; Hamm, R. E., Polarographic Reduction of Oxygen in Dimethylsulfoxide. *Analytical Chemistry* **1966**, *38*, 183-185.

4. Zhuravlev, Y. N.; Kravchenko, N. G.; Obolonskaya, O. S., The Electronic Structure of Alkali Metal Oxides. *Russ. Journal of Physical Chemistry B* **2010**, *4*, 20-28.

5. Uribe, F. A.; Bard, A. J., Electrochemistry in Liquid Ammonia. 5. Electroreduction of Oxygen. *Inorgic Chemistry* **1982**, *21*, 3160-3163.

6. Guo, Z.; Lin, X., Kinetic Studies of Dioxygen and Superoxide Ion in Acetonitrile at Gold Electrodes Using Ultrafast Cyclic Voltammetry. *Journal of Electroanalytical Chemistry* **2005**, *576*, 95-103.

7. René, A.; Evans, D. H., Electrochemical Reduction of Someo-Quinone Anion Radicals: Why Is the Current Intensity So Small? *Journal of Physical Chemistry C* **2012**, *116*, 14454-14460.

8. Viswanathan, V.; Thygesen, K. S.; Hummelshoj, J. S.; Norskov, J. K.; Girishkumar, G.; McCloskey, B. D.; Luntz, A. C., Electrical Conductivity in Li2o2 and Its Role in Determining Capacity Limitations in Non-Aqueous Li-O2 Batteries. *Journal of Chemical Physics* **2011**, *135*, 214704.

Chapter VI. Extension of the Oxygen Reduction Reaction Mechanism to Other Aprotic Solvents

« On va bien plus facilement par les bouts, là où l'extrémité sert de borne d'arrêt et de guide, que par la voie du milieu large et ouverte, mais bien moins noblement et de façon moins estimable. »

Montaigne, Essais, III.13, ***1580***

The mechanism proposed in chapter V for the non-aqueous oxygen reduction reaction (ORR) in presence of alkali metal cations (Scheme VI.1) has been developed for DMSO, and could therefore be limited to that particular solvent.

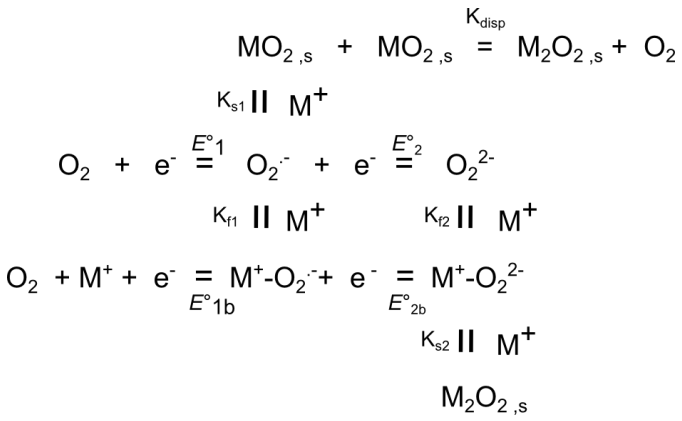

Scheme VI.1. Non-aqueous ORR mechanism in presence of alkali metal cations

If it can be extended to other solvents without involving the introduction of other reactions, then the solvent effects might be rationalized by using the solvation parameters described in chapter III (recalled in Table VI.1). In that frame, this chapter targets three important goals:

- demonstrate that the proposed ORR mechanism can indeed account for the impact of alkali metal cations in the other solvents tested;
- study the effects of preferential solvation in solvent mixtures;
- relate the observed properties of the solvents to their solvation parameters, in order to predict the behavior of other solvents and solvent mixtures.

Table VI.1. Parameters related to the solvents studied.

	ε_r	AN	DN	LiCB (kJ mol^{-1})	NaCB (kJ mol^{-1})	KCB (kJ mol^{-1})
Acn	37.5	18.9	14.1	142	98.7	75.3
DMSO	46.7	19.3	29.8	175.1	129.7	104.6
DMA	37.8	13.6	27.8	179.1	132.8	100.4
Py	12.4	14.2	33.1	146.7	100	64.6
DME	7.2	10.2	20	187.9	133	86.6
NMP	32.2	13.3	27.3	ND	ND	ND

1. ORR in Acn and Acn-DMSO mixtures

As demonstrated in chapter IV, the affinity of Acn for $O_2^{\cdot-}$ is similar to that of DMSO. However, its affinity for alkali metal cations should be much lower, as measured by both its DN and MCB. A strong positive shift in potential of the reduction wave is observed on ORR voltammograms in Acn with respect to TBA^+ (Figure VI.1), when alkali metals cations are added to the electrolyte, in the order $K^+ < Na^+ < Li^+$.

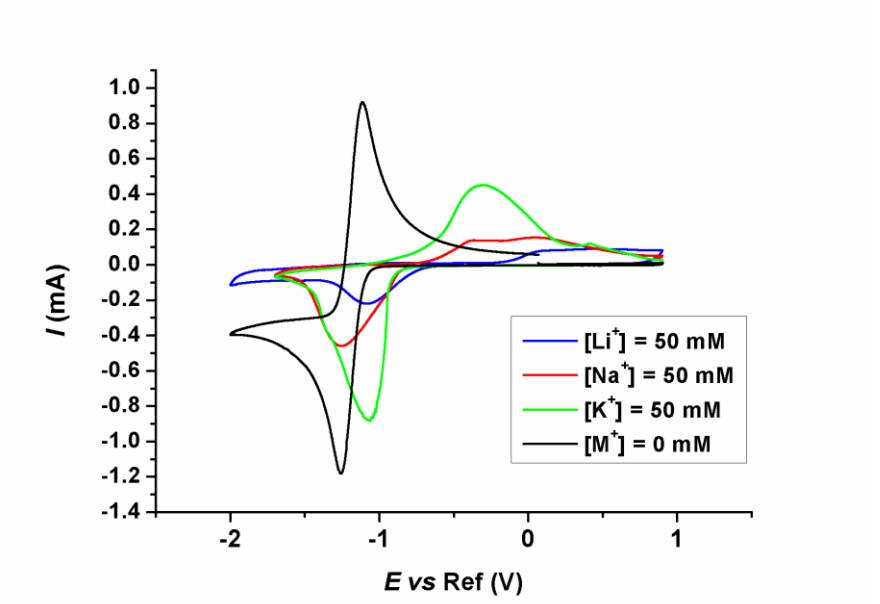

Figure VI.1. Cyclic voltammetries at *v* = 100 mV s^{-1} in oxygen-saturated Acn containing 150 mM $TBAPF_6$ (black) in presence of 50 mM KPF_6 (green), $NaClO_4$ (red) or LiTf (blue).

This shift is much larger as compared to similar experiments in DMSO. Furthermore, the shape of the reduction wave is distorted: in presence of K^+, the slope brutally increases at low reduction overpotentials, while in presence of Na^+ and Li^+, a lower quasi-linear slope is observed, as compared to DMSO. The peak currents are decreasing (in absolute value) in the order $K^+ > Na^+ > Li^+$, and are smaller than that obtained in the absence of alkali metal cations. At higher reduction overpotentials, the (absolute) current is dropping to a value considerably lower than the diffusion plateau observed in the absence of alkali metal cations. Finally, the anodic charge on the backward scan is nearly equivalent to the cathodic charge in presence of K^+ ($\frac{I_{\text{anodic}}}{I_{\text{cathodic}}} = 0.99$), which can sign the precipitation of very poorly soluble products during reduction (and if so would mean that these solid products can be quantitatively oxidized in the backward (OER) scan). This ratio is lower in presence of Na^+ ($\frac{I_{\text{anodic}}}{I_{\text{cathodic}}} = 0.82$) and Li^+ ($\frac{I_{\text{anodic}}}{I_{\text{cathodic}}} = 0.72$). The difference can be explained either by higher solubility, irreversible degradation reactions (which could form non-reoxidizable products) or

the larger difficulty to re-oxidize the products formed during oxygen reduction in presence of Na^+ and Li^+. This last proposition is corroborated both by the poorer cyclability observed in presence of Na^+ and Li^+ as well as the pronounced current "tailing" observed at high potential values during the backward scan (OER). This "tailing" might be a sign that some products formed during oxygen reduction would require high overpotentials for their re-oxidation: indeed, sweeping the potential to high values (> 1 V *vs* Ref) leads to a partial recovery of the electrode.

All these elements militate in favor of the formation of non-soluble, or very poorly soluble, solid products on the electrode in Acn, even for the first oxygen reduction process. There is also no evidence of a second reduction process in Acn, at least in the potential domain scanned here.

These elements can be accounted for by a much lower solubility of alkali metal superoxides (MO_2) in Acn as compared to DMSO. In the former solvent, according to scheme VI.1, the formation of soluble intermediates, either $O_2^{\cdot-}$ or $M^+ - O_2^{\cdot-}$ would be limited, which, together with the passivation of the surface by the formation of non-conductive solid products, can explain the absence of the wave corresponding to the second reduction process. The difference in solubility products of MO_2 in DMSO and Acn can be estimated from equation (III.9) (Table VI.2), since transfer activity coefficients for $O_2^{\cdot-}$ have been measured in chapter IV and those tabulated for M^+ in the literature have been listed in chapter III. However, this calculation is not taking the formation of ion-pairs into account, and can thus not serve as a direct estimation of the actual difference in solubility of MO_2.

Table VI.2. Difference in solubility products ($pK_{s1,S} - pK_{s1,DMSO}$) of MO_2 between solvents S and DMSO, calculated using $\log(\gamma_t(O_2^{\cdot-}, DMSO \rightarrow S))$ (chapter IV) and $\log(\gamma_t(M^+, DMSO \rightarrow S))$ (chapter III).

Solvent	$pK_{s1,S} - pK_{s1,DMSO}$ LiO_2	$pK_{s1,S} - pK_{s1,DMSO}$ NaO_2	$pK_{s1,S} - pK_{s1,DMSO}$ KO_2
DMSO	0	0	0
Acn	7.4	5.4	3.8
DMA	ND	1.7	1.7

When mixing DMSO with increasing contents of Acn (Figure VI.2), electrolytes with intermediate properties can be obtained. Whatever the alkali metal cation in presence, the positive shift in ORR potential is increasing with increasing content in Acn. Furthermore, the ratio of the peak

current of the first oxygen reduction on the peak current obtained in the absence of alkali metal cations ($\frac{I_{\text{peak}}^{\text{M}^+}}{I_{\text{peak}}^{\text{TBA}^+}}$) is decreasing with increasing content in Acn.

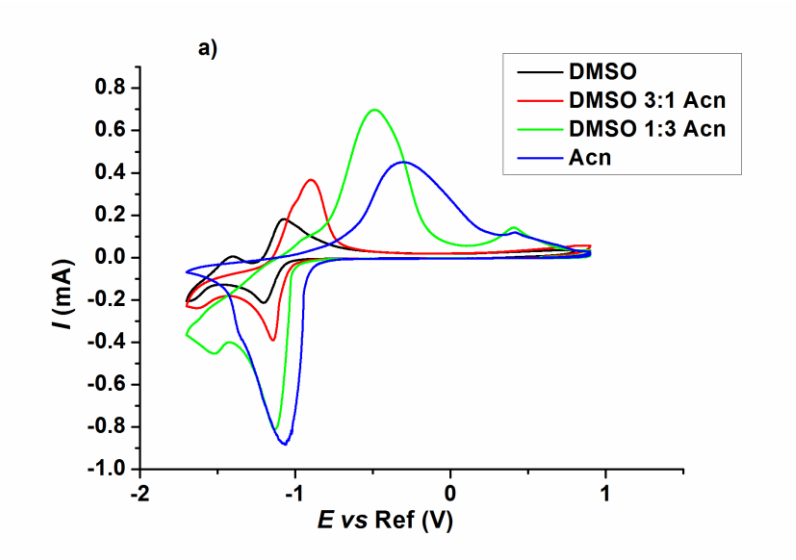

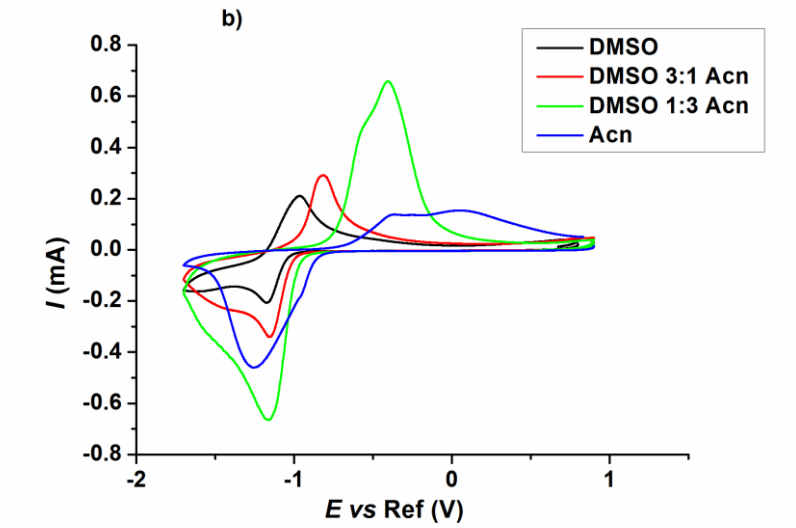

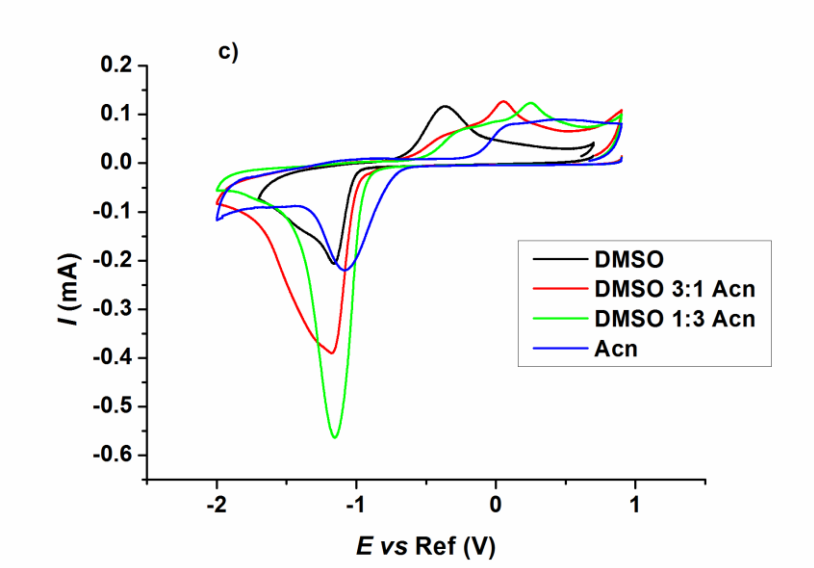

Figure VI.2. Cyclic voltammetries at *v* = 100 mV s^{-1} in oxygen-saturated Acn-DMSO mixtures and 150 mM $TBAPF_6$ in presence of 50 mM KPF_6 (a), $NaClO_4$ (b) or LiTf (c).

In presence of K^+ (Figure VI.2a), the current at which the slope steeply increases is sensibly larger (in absolute value) at lower proportion in Acn. This particular change of slope can be explained by the nucleation of solid MO_2. Indeed, if the salt has a partial solubility in the electrolyte, an over-saturation concentration in $O_2^{\cdot-}$ has to be achieved at the electrode to trigger the nucleation of MO_2. Once nucleation has occurred, $O_2^{\cdot-}$ in solution will be consumed to form the precipitated solid phase.

Thus, the electrochemical reaction forming $O_2^{\cdot-}$ will be accelerated, since its product is being consumed, which prompts the steep increase of the slope. Since the solubility of KO_2 might be lower with higher contents in Acn, the concentration in $O_2^{\cdot-}$ required to saturate the solution at the electrode interface should be lower, provoking nucleation at lower currents (in absolute value) and lower overpotential [i]. This phenomenon will require kinetic modelling in order to be confirmed (which has been attempted in chapter VII). With addition of Acn into DMSO, the second oxygen reduction is also becoming irreversible, even in the Acn 1:3 DMSO mixture, and the ratio of its peak current to the peak current of the first reduction process is decreasing with increasing content in acetonitrile.

In the presence of Na^+ and Li^+ (Figure VI.2b and c), similar trends are observed, except the steep change of slope of the first reduction wave, which only proceeds in presence of K^+. The similarity between the voltammograms obtained in presence of Na^+ in the Acn 1:3 DMSO mixture and in presence of Li^+ in pure DMSO can also be noted. Similarities between voltammograms cannot

[i] The ratio of the diffusion coefficients of O_2 and $O_2^{\cdot-}$ ($D_{O_2}/D_{O_2^{\cdot-}}$) is supposed to remain more or less the same between the mixtures and pure acetonitrile.

be considered as a sound evidence of actual similarities in mechanisms. However, the main difference between those two electrolytes is the presence of a larger charge-density cation, Li^+, in a better cation-solvating solvent, pure DMSO.

This section demonstrates that the mechanism developed for DMSO can also be applied to describe the ORR in Acn and mixtures of both solvents. The discussion was essentially based on the much lower solubility of MO_2 in Acn: in Acn, MO_2 easily precipitates on the electrode surface, therefore rendering the reduction of $M^+ - O_2^{\cdot -}$ unlikely, owing both to the electrode passivation and the decrease of the ion-pairs concentration. These results are in agreement with the literature[1-2], where no or little intermediates in solution have been observed during the ORR in presence of Li^+ in Acn on rotating ring-disk electrode (RRDE).

However, it can be argued here that this second reduction has only been observed in presence of DMSO, and could thus be related to the solvent. Furthermore, the presence of ion-pairs is not mandatory to account for the ORR in Acn, and, again, they might be related to the presence of DMSO. This hypothesis is examined below.

2. ORR in DMA and DMA-DMSO mixtures

Similar experiments have thus been performed using DMA, which has a similar capacity to solvate cations as DMSO, but a lower affinity for $O_2^{\cdot -}$. In pure DMA (Figure VI.3), an irreversible second reduction wave is observed in presence of K^+. The shift in potential of the first reduction process remains in the order $K^+ < Na^+ < Li^+$. However, the difference in the shift in presence of Na^+ and Li^+ is much less apparent than in Acn. A steep change of slope at low overpotentials is observed in presence of K^+.

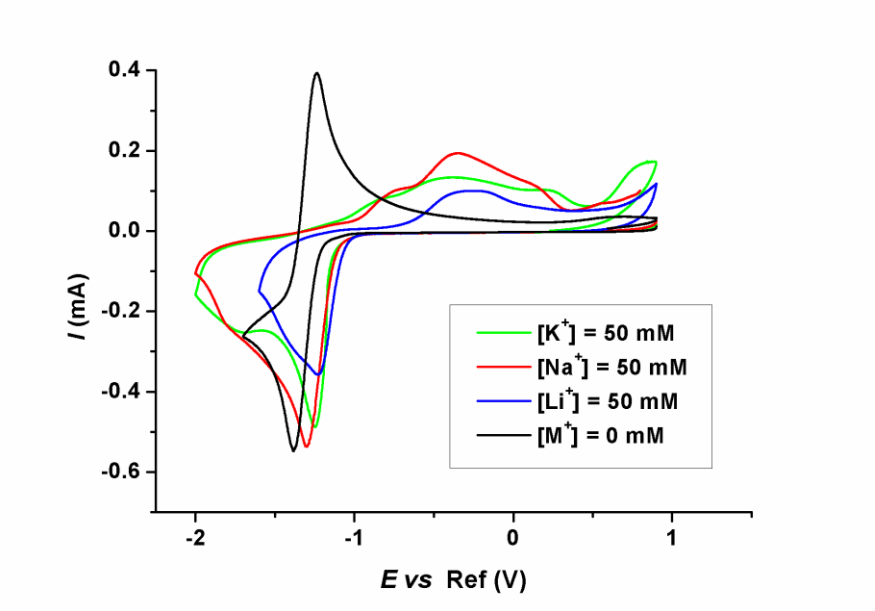

Figure VI.3. Cyclic voltammetries at *v* = 100 mV s^{-1} in oxygen-saturated DMA containing 150 mM $TBAPF_6$ (color) in presence of 50 mM KPF_6 (color), $NaClO_4$ (color) or LiTf (color).

The difference in solubility product of MO_2 in DMA and DMSO is estimated in the same manner as for Acn. The solubility products of MO_2 compounds in DMA is intermediate between those in DMSO and Acn, which is consistent with the intermediate ORR wave shapes observed on the cyclic voltammetries.

In DMA-DMSO mixtures in presence of K^+ (Figure VI.4a), the steep change of slope is observed at lower current (in absolute value) with increasing content in DMA. The reversibility of the second reduction process as well as the ratio of its peak current on the peak current associated to the first reduction process is decreasing with increasing content in DMA. In presence of Na^+ and Li^+, the second wave is becoming less apparent with increasing content in DMA. Passivation, reflected by the gradual decrease of the current (in absolute value) when scanning to lower potentials, is also more pronounced with increasing content in DMA.

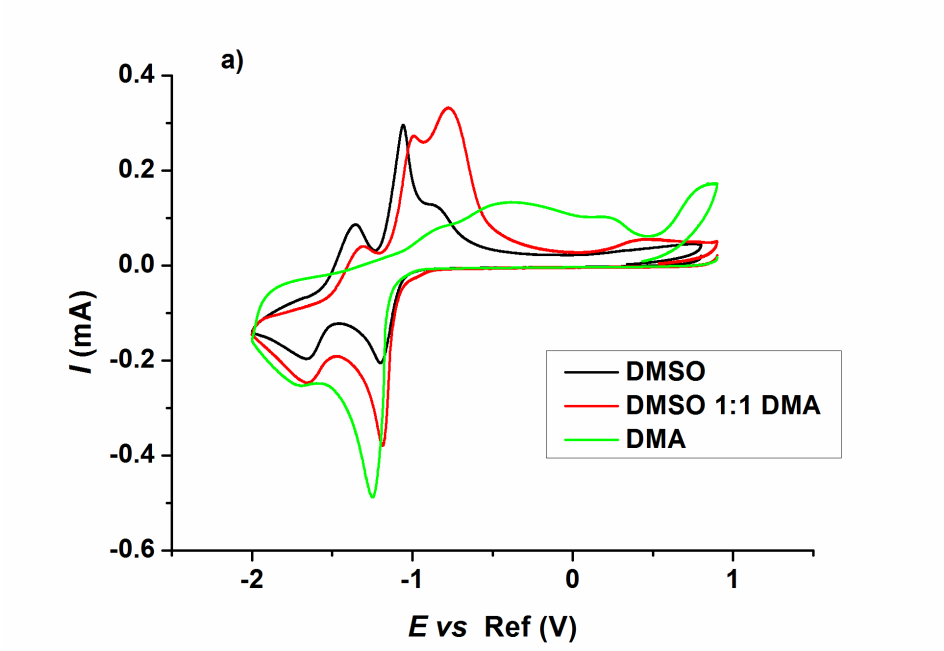
a)
0.4
0.2
0.0
-0.2
-0.4
-0.6
I (mA)
-2
-1
0
1
E vs Ref (V)
DMSO
DMSO 1:1 DMA
DMA

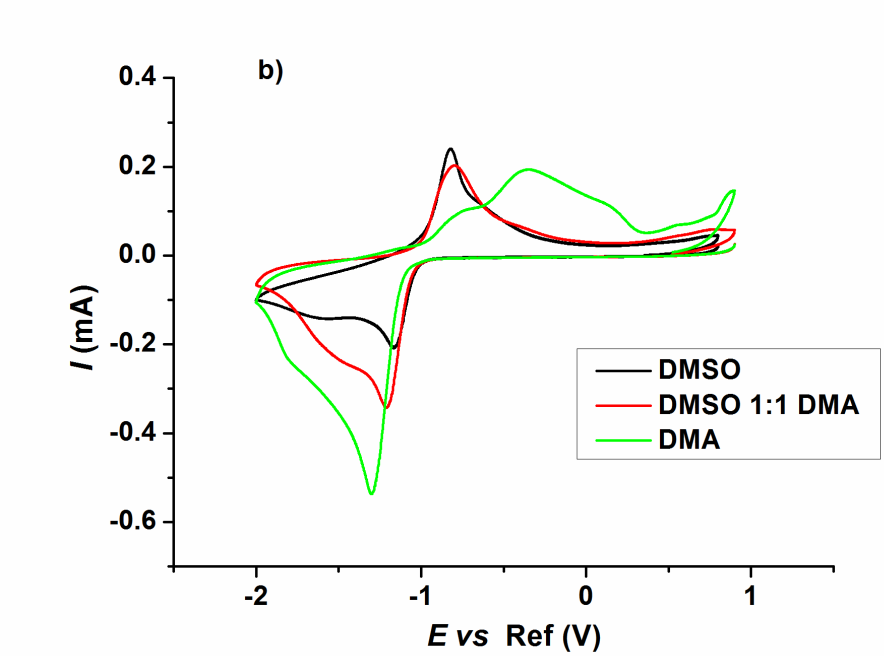
b)
0.4
0.2
0.0
-0.2
-0.4
-0.6
I (mA)
-2
-1
0
1
E vs Ref (V)
DMSO
DMSO 1:1 DMA
DMA

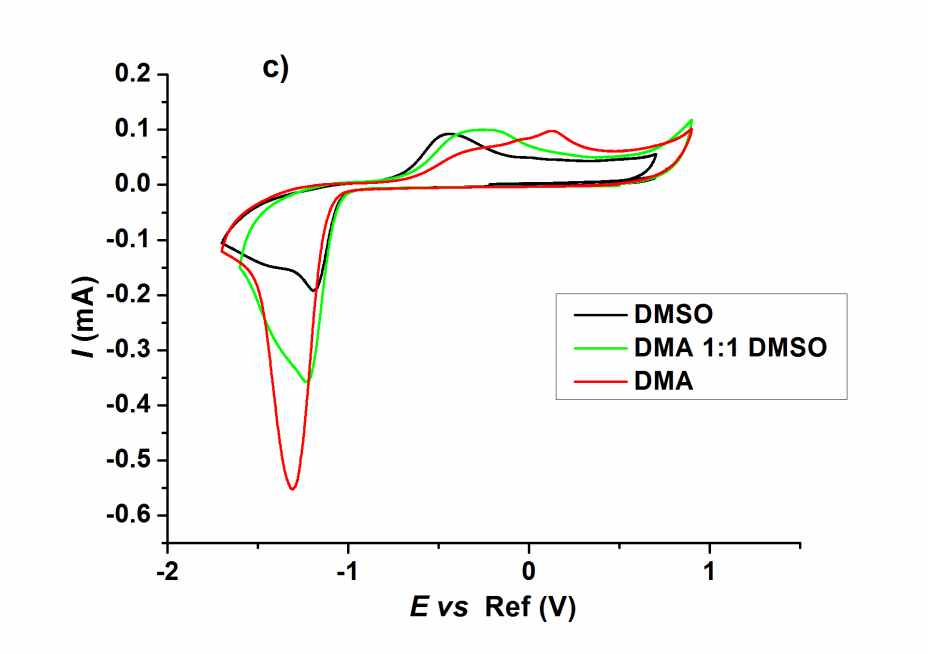

Figure VI.4. Cyclic voltammetries at *v* = 100 mV s^{-1} in oxygen-saturated DMA-DMSO mixtures containing 150 mM $TBAPF_6$ in presence of 50 mM KPF_6 (a), $NaClO_4$ (b) or LiTf (c).

These observations demonstrate that the mechanism developed for DMSO can also be applied for DMA, if one considers that the solubility of MO_2 species in DMA are intermediate between those in Acn and DMSO. Since the second reduction process is also clearly observed in pure DMA, it is also confirmed that the formation of ion-pairs $M^+ - O_2^{\cdot-}$ and their one-electron reduction is possible in other solvents than DMSO. Thus, it will be considered in the following that the mechanism depicted in scheme VI.1 applies to any solvent; this mechanism will therefore be used to understand the non-aqueous ORR in presence of alkali metal cations.

3. Effect of the solvent on the ORR: solvation of M^+ and $O_2^{\cdot-}$

The shift in the potential of the first oxygen reduction in presence of alkali metal cations can be related to $E°_1$ and K_{f1} (scheme VI.1), as long as saturation concentrations in M^+ and $O_2^{\cdot-}$ have not been reached, *e.g.* at low ORR overpotential values.

Differences in this shift between different solvents at a fixed concentration in alkali metal cations can be understood from the thermodynamic calculations developed in chapter III, and related to transfer activity coefficients according to equation (VI.1).

$$\Delta E^{o}_{1b-1,S} - \Delta E^{o}_{1b-1,R} = \log(\ 0.06\ \log(\frac{K_{f1,S}}{K_{f1,R}})) \qquad \text{(VI.1)}$$

The difference in the potential shift directly depends on the ion-pairs formation constants. A useful alternative representation of the ORR voltammograms in presence of alkali metal cations is thus proposed: plotting the ratio of the measured current in presence of alkali metal cation divided by the peak current of the first oxygen reduction in the absence of alkali metal cations (noted $I_{\mathrm{corr}} = \frac{I^{\mathrm{M}^+}}{I_{\mathrm{peak}}^{\mathrm{TBA}^+}}$) *vs* the applied potential referred to the half-peak potential of the first reduction process in the absence of alkali metal cations (*E vs* $E_{1/2}^{\mathrm{TBA}^+}$). The deviation of the mechanism from a one-electron reduction process of oxygen in solution can directly be observed from the peak value of I_{corr} in the first reduction process. Using this representation also enables to directly compare the shift of the first reduction process between different solvents.

Figure VI.5 further supports the uniqueness of the mechanism in the three different solvents.

- the larger the shift in potential, the lower the first peak value of I_{corr}, thus the larger the surface passivation;
- the higher the shift in potential, the less apparent the second reduction process;
- these two elements do not seem to depend on the solvent mixtures, although the amplitude of the variations can be solvent-dependent.

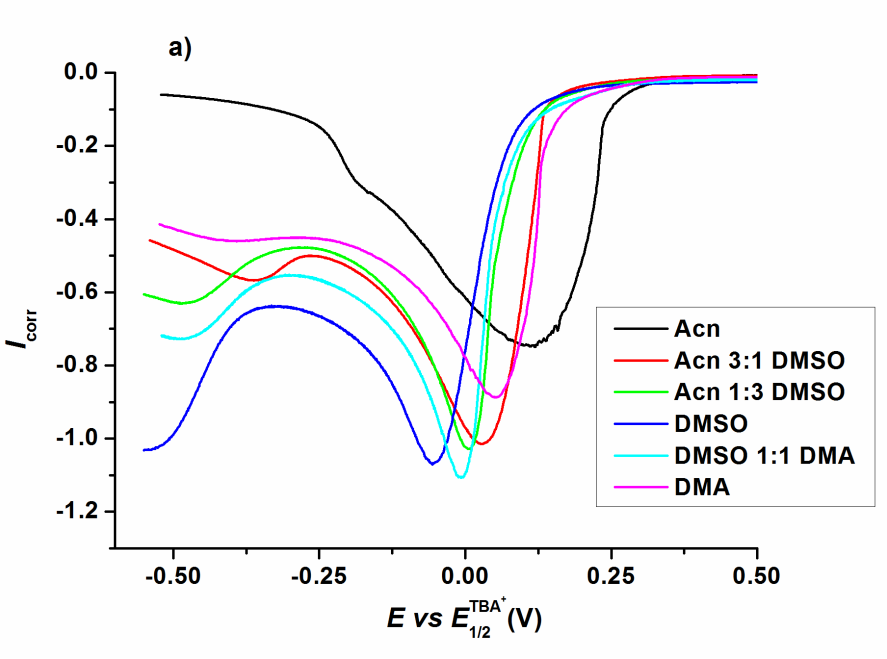

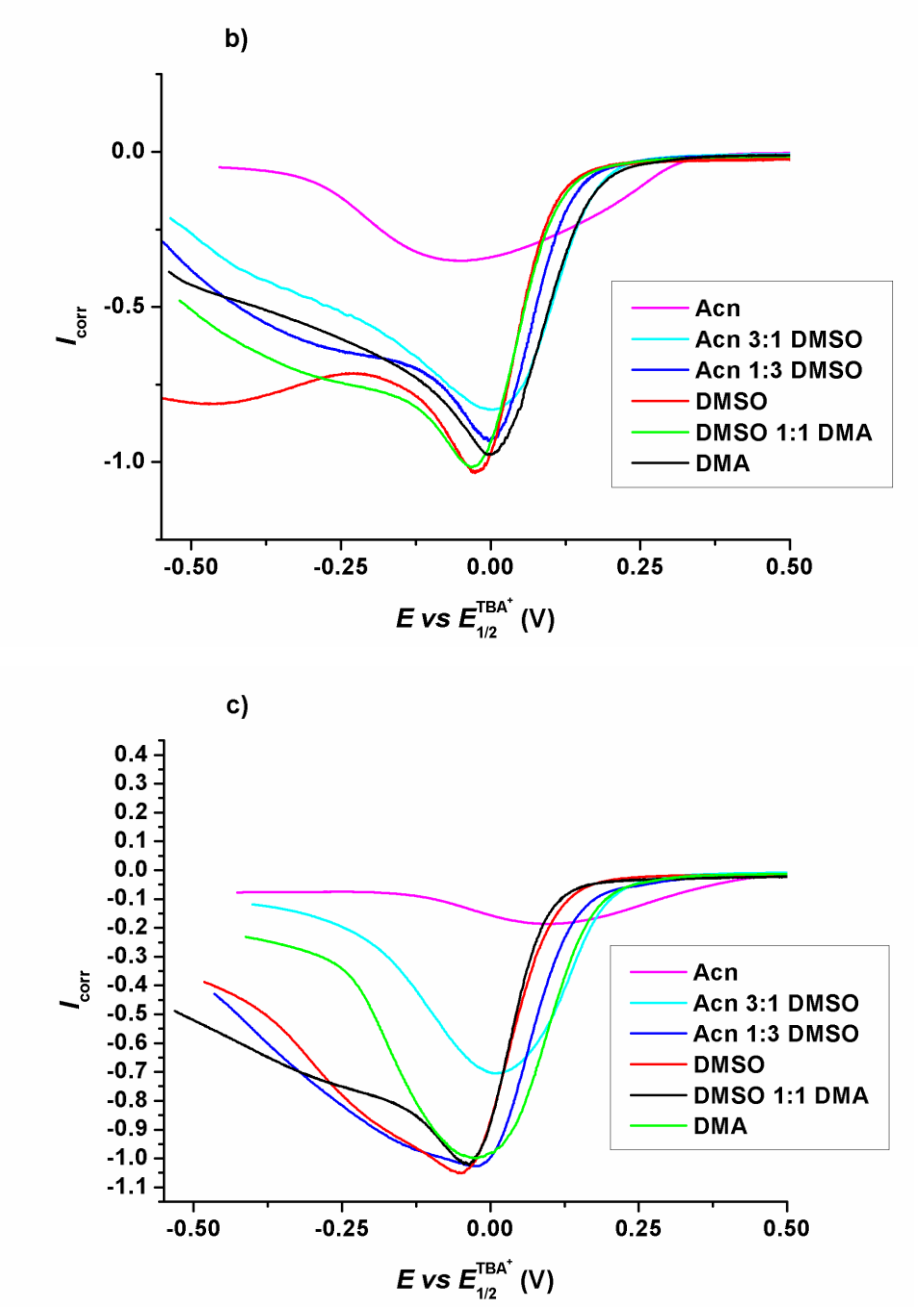

Figure VI.5. I_{corr} vs (*E vs* $E_{1/2}^{\mathrm{TBA}^+}$) representation of the ORR in different solvents in presence of 150 mM $TBAPF_6$ and 50 mM K^+ (a), Na^+ (b) or Li^+ (c).

In presence of K^+ (Figure VI.5a), the difference in potential shifts can be estimated from *E vs* $E_{1/2}^{\mathrm{TBA}^+}$ measured at I_{corr} = -0.1 (*i.e.* corresponding to a shift of $E_{10\%}$). The Acn 3:1 DMSO mixture is an exception: nucleation has already occurred at these small currents. It is important to note here that the nucleation depends on the concentration in $O_2^{\cdot-}$ and M^+ and thus comparison between solvents should be made on the absolute current and not the ratio I_{corr}. This issue is related to a specific fundamental difficulty inherent to the present mechanism: it is intermediate between a solution-

based mechanism with mass-transport limitations and a surface-based mechanism limited by the active surface (and actually also by solid crystal growth and solid-state chemical reactions, the analysis of which might differ from the classical analysis of surface-based mechanisms).[ii]

This representation of the voltammograms is also useful to compare the results obtained in presence of different cations in different electrolytes. By varying both the cation charge-density and its solvation (Figure VI.6), similar shifts in $E_{10\%}$ can be obtained:

- in presence of Li^+ and Na^+ (a lower charge-density cation) in, respectively, DMSO and the DMSO 1:1 DMA mixture (which has a lower solvation capability for $O_2^{\cdot-}$);
- In presence of Li^+ and K^+ (which has a considerable lower charge-density) in, respectively, the Acn 1:3 DMSO mixture and DMA (which has a considerable lower solvation capability for $O_2^{\cdot-}$, but a possible higher capability to solvate cations).

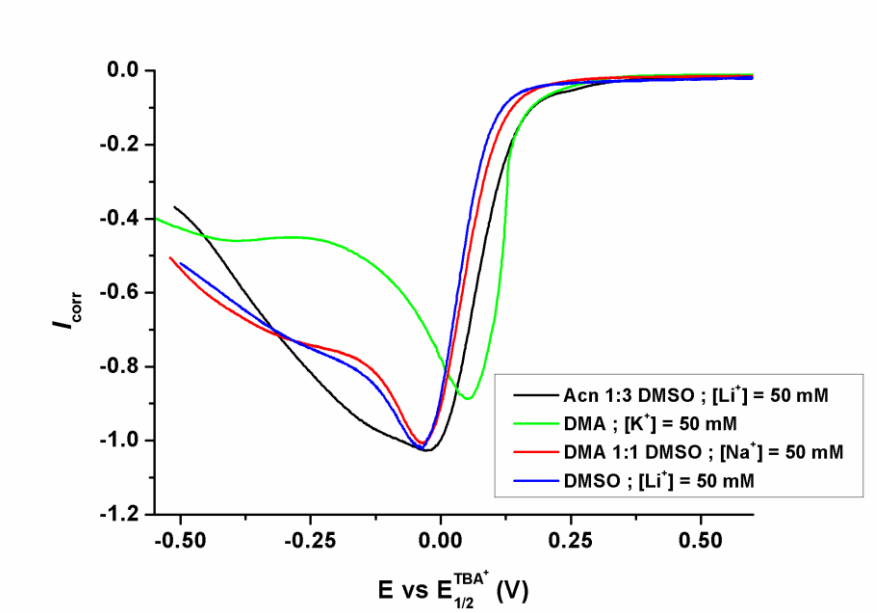

Figure VI.6. Comparison of the I_{corr} vs (E *vs* $E_{1/2}^{TBA^+}$) representation of the ORR in different electrolytes.

[ii] This difficulty can be observed in Reference [3] where a diffusion coefficient for O_2 is estimated by applying the Nicholson and Shain (irreversible version of the Randles-Sevcik) equation on the peak corresponding to a (Acn +Li^+) system on static electrode, which is not simply due to a limitation of diffusion of oxygen. Thus, the diffusion coefficient measured is one order of magnitude lower than the diffusion coefficient of oxygen measured in the absence of Li^+. Such a difference for an uncharged species is most likely a direct evidence of the non-applicability of Nicholson and Shain analysis on a peak which is not due to a limitation by mass-transport of oxygen.

Estimated values for the difference in potential shifts are given in Table VI.3: the higher the $\Delta E_{1b-1,S}^{10\%} - \Delta E_{1b-1,DMSO}^{10\%}$ value, the more favored the formation of ion-pairs $M^+ - O_2^{\cdot-}$ in solvent S as compared to DMSO.

Table VI.3. Potential shifts measured at I_{corr} = 0.1 upon addition of 50 mM M^+ in different solvents + 150 mM $TBAPF_6$.

Solvent	Cation	$\log(\gamma_t(O_2^{\cdot-}, DMSO \rightarrow S))$	$\log(\gamma_t(M^+, DMSO \rightarrow S))$	$\Delta E_{1b-1,S}^{10\%}$	$\Delta E_{1b-1,S}^{10\%} - \Delta E_{1b-1,DMSO}^{10\%}$ (V)
DMSO	Li^+	0	0	0.06	0
	Na^+		0	0.05	0
	K^+		0	0.02	0
Acn 1:3 DMSO	Li^+	0.08	ND	0.10	0.04
	Na^+		ND	0.07	0.01
	K^+		ND	0.05	0.03
Acn 3:1 DMSO	Li^+	0.18	ND	0.13	0.07
	Na^+		ND	0.10	0.05
	K^+		ND	0.06 *estimated at 5 %*	0.04
Acn	Li^+	0.42	7	0.28	0.21
	Na^+		5	0.19	0.14
	K^+		3.7	0.15	0.13
Acn 1:1 DMA	Na^+	1	ND	0.11	0.06
DMA	Li^+	2	ND	0.11	0.05
	Na^+		-0.3	0.10	0.035
	K^+		-0.3	0.08	0.060
DMA 1:1 DMSO	Li^+	0.32	ND	0.06	0
	Na^+		ND	0.06	0.01
	K^+		ND	0.05	0.03

The formation of ion-pairs $M^+ - O_2^{\cdot-}$ is much more favored in Acn as compared to DMSO. This can be directly related to the much better solvation of M^+ in the latter, since solvation of $O_2^{\cdot-}$ is similar in both solvents. Considering Na^+ and K^+, the formation of ion-pairs $M^+ - O_2^{\cdot-}$ is more favored in DMA as compared to DMSO. This can be directly related to the better solvation of $O_2^{\cdot-}$ in

the latter, since the solvation of M^+ should be similar (and even a sensibly superior), in DMA as compared to DMSO. Thus, it is necessary to take both the difference in solvation of M^+ and $O_2^{\cdot-}$ from one solvent to another to account for the differences in the thermodynamic and kinetic constants of ORR mechanism; to summarize, the higher the solvation of both ions, the less favorable the formation of the ion-pairs.

The behavior of mixtures can be understood in terms of preferential solvation: in a binary mixture, an ion is preferentially solvated by the solvent having the higher affinity for it. Thus, in an Acn-DMSO binary mixture, cations M^+ will be preferentially solvated by DMSO, even at low proportions of DMSO in the mixture, whereas $O_2^{\cdot-}$ will be almost equally solvated by DMSO and Acn. This accounts well for the pronounced decrease in the formation constant of ion-pairs upon addition of DMSO in the mixture. Similarly, DMSO preferentially solvates $O_2^{\cdot-}$ in a DMA-DMSO mixture: this is the reason for the intermediate ion-pairs formation constant. Finally, an Acn 1:1 DMA mixture containing Na^+ has an ion-pairs formation constant much closer to that of pure DMA than Acn: Na^+ is preferentially solvated by DMA, while Acn solvates preferentially $O_2^{\cdot-}$. For this last mixture, it might be possible to reach a composition where $M^+ - O_2^{\cdot-}$ ion-pairs formation is even less favorable than in both pure solvents taken separately.

It is interesting to also note that the shift in potential $\Delta E_{1b-1,S}^{10\%}$ is always larger in the order $K^+ < Na^+ < Li^+$, whatever the solvent mixture. This means that the larger the charge-density of the cation, the larger its interaction with $O_2^{\cdot-}$; if so, the superoxide anion cannot be considered as a soft base, whatever the solvent. Furthermore, the better the general solvation of the alkali metal cations, the lower this difference in the shifts, especially when comparing Na^+ and Li^+.

As a conclusion, the effect of the solvent on the ORR mechanism in presence of alkali metal cations has been related to its capacity to solvate both M^+ and $O_2^{\cdot-}$: the larger the solvation of both ions, the lower the ion-pairs $M^+ - O_2^{\cdot-}$ formation constant. An interpretation of the behavior of binary mixtures is also proposed, based on the concept of preferential solvation. These elements can lead to the development of electrolytes with tailored properties, and even predict their behavior. However, this would require the prior knowledge of the transfer activity coefficients of both M^+ and $O_2^{\cdot-}$ in the solvents of interest. It would thus be interesting to correlate the solvation of M^+ and $O_2^{\cdot-}$ to solvation scales or solvents structure-related parameters.

4. Proposition of parameters to predict the behavior of solvents and solvent mixtures

The discussion until here was based on solvents with similar high permittivity. As discussed in chapter III, the permittivity of the solvent accounts for the majority of the solvation-energy of ions. However, it was considered that differences in solvation of ions between different solvents of high permittivity (typically superior to 20) was mostly influenced by other parameters, such as the Lewis acidity and basicity of the solvent.

The most widely used solvent basicity scale is the Donor Number (DN)[1, 3-4]. Its use as an indicator of alkali metal cation solvation can be criticized, since coordination to the large $SbCl_5$ complex might not reflect coordination to much smaller cations, like alkali metal cations[5]. In particular, the DN of pyridine has shown to be highly overestimated when considering association to alkali metal cations[6]. Another scale to study the intrinsic interactions between cations and Lewis bases, the gas-phase Metal Cation Basicity (MCB)[5], has also been introduced in chapter III.

Since the ORR mechanism is similar in presence of all alkali metal cations, it is proposed here to study the use of the proposed solvent parameters specifically in presence of Na^+, for the following reasons:

- measuring $\Delta E_{1b-1,S}^{10\%}$ is generally more precise in presence of Na^+ as compared to K^+;
- in presence of Li^+, an effect of the second reduction on $\Delta E_{1b-1,S}^{10\%}$, either electrochemical or chemical, of LiO_2 cannot be completely ruled out.

Values of $\Delta E_{1b-1,S}^{10\%}$ are listed in Table VI.4. As discussed before, the amplitude of the shift cannot be accounted for by the capacity of the solvent to solvate Na^+. Indeed, the DN of DMSO lies between those of NMP and DMA. However, the potential shift in DMSO is half those of NMP and DMA, which are similar. This is accounted for by the higher AN of DMSO, compared to those of NMP and DMA, which are similar.

Table VI.4. Potential shifts measured at I_{corr} = 0.1 upon addition of 50 mM Na^+ in different solvents + 150 mM $TBAPF_6$.

Solvent	ε_r	AN	DN	NaCB (kJ.mol^{-1})	$\Delta E_{1b-1,S}^{10\%}$ (mV)
DMSO	46.5	19.3	29.8	129.7	55
Acn	35.9	18.9	14.1	98.7	195
DMA	37.8	13.6	27.8	132.8	105
NMP	32.2	13.3	27.3	ND	110
Py	12.9	14.2	33.1	100	220
Acn 1:3 DMSO					85
Acn 3:1 DMSO					135
DMA 1:1 DMSO					60
Acn 1:1 Py					200
Acn 1:1 DMA					110
DME 1:1 DMSO	(7.2_{DME})	(10.2_{DME})	(20_{DME})	(133_{DME}) *(bidendate)*	90

DN and NaCB values are generally well correlated with one-another; Py, which has a DN higher than DMSO but a NaCB comparable to that of Acn, makes exception. However, Py also has a low permittivity. Thus, the very high $\Delta E_{1b-1,S}^{10\%}$ in presence of Py could be related to either the low permittivity of the solvent or its low Na^+ solvation capacity. A way to discriminate between those two elements is to consider solvent mixtures. Indeed, the permittivity of a solvent mixture lies in between that of the two solvents taken separately. In particular, a linear dependence of the permittivity with the composition is found in N,N-dimethylformamide (DMF)-Py mixtures. In the case of Acn 1:1 Py, the resulting permittivity of the mixture could reasonably be estimated as superior to 20, although no values have been measured here. The $\Delta E_{1b-1,S}^{10\%}$ remains very high in the Acn 1:1 Py mixture, similar to that in Acn. This is more consistent with the NaCB value of Py than with its DN: if Py had a capability to solvate Na^+ superior to that of DMSO or DMA, the $\Delta E_{1b-1,S}^{10\%}$ in the Acn 1:1 Py

mixture would be expected to be much lower than the one obtained in pure Acn, and even lower than the one obtained in the Acn 1:1 DMA mixture.

1,2-dimethoxyethane (DME) is another example of solvent with a marked difference between its DN and NaCB values. However, its permittivity value is even lower than that of Py. In this low-permittivity solvent, salts are usually poorly dissociated and readily form ion-pairs. This explains the low conductivity of pure DME-based electrolytes at low and intermediate concentrations in salt (usually below 0.5 M, but this value depends on the salt). At higher concentration in salt, the conductivity of the solution increases, owing to the formation of triple ion-pairs. Considering the set-up used in the present study, measures in pure DME were subjected to large ohmic drop. A similar difficulty is most likely the reason for the non (or partial)-correction of the ohmic drop in [3] in presence of DME. As stated in chapter IV, interactions between TAA^+ and $O_2^{\cdot-}$ have to be taken into account in low-permittivity solvents, which considerably complicates the mechanism of ORR. Furthermore, the formation of ion-pairs between M^+ and its counter-anion also has to be taken into account. Thus, a comparison of the ORR mechanism between solvents of high and low permittivity is not proposed in this work, and is, to the author's belief, not straightforward.

Even mixtures of DME and Acn or DMA cannot be considered as having sufficiently high permittivity values as to compare their results with the other mixtures presented here. Thus, only the study of a DME 1:1 DMSO mixture is proposed in the present chapter. In that case, the half-peak potential of the first oxygen reduction in the absence of alkali metal cations is $E_{1/2}^{TBA^+}$ = -1.215 V *vs* Ref. This value is consistent with the very low AN of DME and a preferential solvation of $O_2^{\cdot-}$ by DMSO. Since the $\Delta E_{1b-1,S}^{10\%}$ value could be related to the much lower AN of DME, it is not evident to discriminate between DN and NaCB value in that case by only qualitative reasoning. Thus, quantitative correlations between solvent parameters and $\Delta E_{1b-1,S}^{10\%}$ will be proposed.

5. Extrapolation of solvent and mixtures parameters

A linear relation between $E_{1/2}^{\mathrm{TAA}^+}$ and the AN of the solvents is proposed on Figure VI.7. Similar relationships have already been proposed in the literature[7]. The relation proposed is calculated using the two extreme points (DMSO and NMP)[iii]. It shows a good correlation with the results obtained in the other solvents (R^2 = 0.985). The $E_{1/2}^{\mathrm{TBA}^+}$ calculated in DMA is equal to the one

[iii] This choice has been made here due to the highest confidence on the value obtained in DMSO. The best fit involving all high-permittivity solvents lead to a sensibly higher, but comparable R^2 = 0.989. I also have doubts on the actual ORR mechanism in Acn, as a chemical reaction between O_2 and Acn is possible in my opinion, and could account for the results on Au or Pt electrodes (discussed briefly in chapter II) by catalytic reactions. However, I did not find any sound evidences of such phenomena.

measured experimentally (Table VI.5). In Py, the underestimation of the calculated half-wave potential can be explained by the interaction between TBA^+ and $O_2^{\cdot-}$ as discussed in chapter IV. By using this relation, an AN value for solvent mixtures can be estimated. The value calculated is the direct reflection of $E_{1/2}^{\mathrm{TBA}^+}$, and as such, follows directly the same conclusions in term of preferential solvation as those made in chapter IV. It is interesting to note that the AN of DME 1:1 DMSO mixture is significantly lower than that of the DMA 1:1 DMSO mixture, which reasonably accounts for the lower AN of DME as compared to DMA.

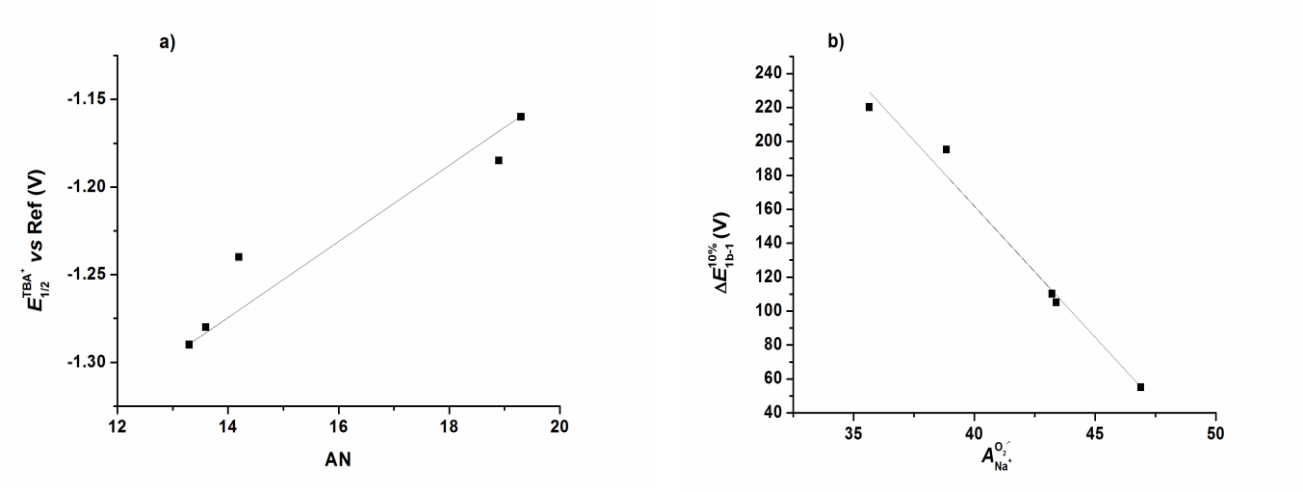

Figure VI.7. (a) Relation between $E_{1/2}^{TBA^+}$ the AN of the solvents. (b) Relation between $\Delta E_{1b-1,S}^{10\%}$ measured in presence of 50 mM Na^+ and the parameter $A_{Na^+}^{O_2^{\cdot-}}$ = 0.75 NaCB + 0.25 AN.

Table VI.5. Extrapolation of AN and $NaCB_{eq}$ values for different solvents.

Solvent	AN	$E_{1/2}^{TBA^+}$ (V *vs* Ref)	$\Delta E_{1b-1,S}^{10\%}$ (V *vs* Ref)	NaCB (or $NaCB_{eq}$ for mixtures) (kJ mol^{-1})
DMSO	19.3		55	129.7
Acn	18.9	-1.18_5 $(-1.169)_{calc}$	195	98.7
DMA	13.6	-1.28 $(-1.283)_{calc}$	105	132.8
NMP	13.3		110	$(133)_{calc}$
Py	14.2	-1.24* $(-1.270)_{calc}$	220	100
Acn 1:3 DMSO	$(19.1)_{calc}$		70	$(126)_{calc}$
Acn 3:1 DMSO	$(18.9)_{calc}$		100	$(119)_{calc}$
DMA 1:1 DMSO	$(18.4)_{calc}$		60	$(131)_{calc}$
Acn 1:1 Py	$(17.9)_{calc}$		200	$(96)_{calc}$
Acn 1:1 DMA	$(17.4)_{calc}$		110	$(123)_{calc}$
DME 1:1 DMSO	$(16.8)_{calc}$		90	$(128)_{calc}$

A relation between $\Delta E_{1b-1,S}^{10\%}$ and the parameter $A_{Na^+}^{O_2^{\cdot-}}$ = 0.75 NaCB + 0.25 AN is then proposed in Figure VI.7b. A correlation coefficient of R^2 = 0.982 is found when using the measured values obtained in pure solvents. Equivalent values of NaCB ($NaCB_{eq}$) for mixtures [iv] can thus be estimated using this relation and the calculated values of AN. This estimate is very rough considering the very little amount of points that have been used for the linear relations that allowed the calculation of both the AN and the NaCB. This can explain the lower value obtained in the Acn 1:1 Py mixture as compared to the NaCB of the two pure solvents. However this value is still comparable to that of the pure solvents, which thus further corroborates the use of NaCB over DN. The effect of preferential solvation is clearly observed in the Acn-DMSO mixture (Figure VI.8), with a $NaCB_{eq}$ closer to that of pure DMSO even in the Acn 3:1 DMSO mixture. Similarly, the $NaCB_{eq}$ value in Acn 1:1 DMA is sensibly closer to that of pure DMA. Finally, the $NaCB_{eq}$ value calculated for the DME 1:1 DMSO mixture is comparable to that of DMSO, which is a further evidence of the better reliability of NaCB as compared to DN when considering Na^+ solvation.

[iv] The NaCB refers to the association between two particular molecules. It is considered here that a mixture of solvents at a particular composition has a particular affinity for Na^+, thus referred as an "equivalent" NaCB ($NaCB_{eq}$).

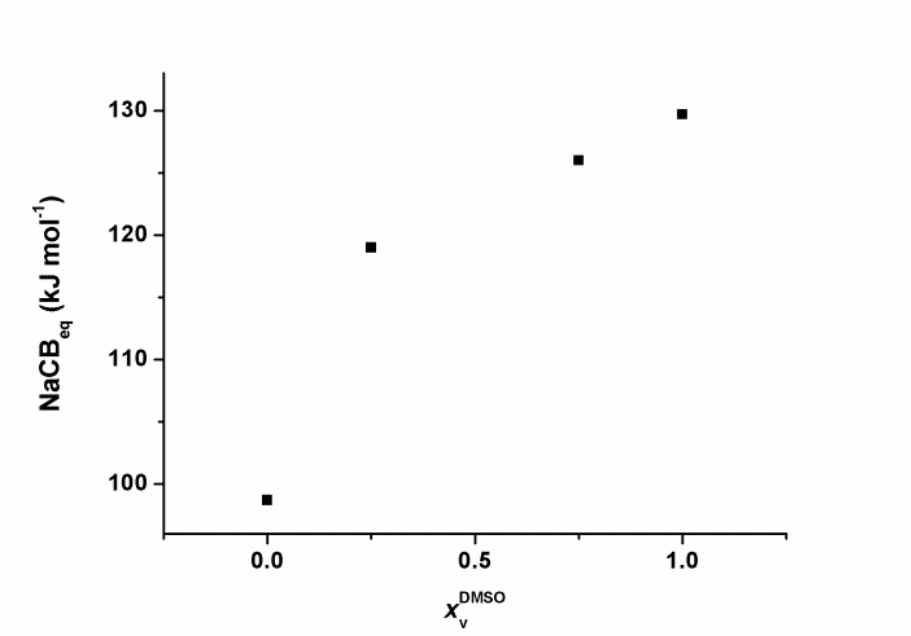

Figure VI.8. Variation of $NaCB_{eq}$ values calculated for Acn-DMSO mixtures with the content in DMSO.

This section demonstrated that $\Delta E_{1b-1,S}^{10\%}$ could be linearly related to a simple parameter $A_{Na^+}^{O_2^{\cdot-}}$ = 0.75 NaCB + 0.25 AN. This parameter has been optimized on very few experimental points, and could thus certainly be improved. Still, its use allowed the extrapolation of solvation parameters for Na^+ in solvent mixtures which are consistent with the preferential solvation concept. The linear relation between $\Delta E_{1b-1,S}^{10\%}$ and $A_{Na^+}^{O_2^{\cdot-}}$, which is the sum of a parameter related to the solvations of Na^+ and $O_2^{\cdot-}$ in solvents is also consistent with the physical meaning attributed to $\Delta E_{1b-1,S}^{10\%}$: the capability of high-permittivity solvents to separate ion-pairs is linked to the capability of the solvent to solvate both the anion and the cation.

Due to the lack of experimental points, definite conclusions on a similar treatment of the results obtained in presence of Li^+ and K^+ cannot reliably made. Still, based on the measures obtained in DMA, Acn and DMSO, the following parameters are estimated: $A_{Li^+}^{O_2^{\cdot-}}$ = 0.7 LiCB + 0.7 AN and $A_{K^+}^{O_2^{\cdot-}}$ = 0.7 KCB + 0.3 AN. The calculated values of $LiCB_{eq}$ and KCB_{eq} using these parameters are proposed in Table VI.6.

Table VI.6. Calculated $LiCB_{eq}$ and KCB_{eq} for different solvents.

	LiCB (or KCB_{eq} for mixtures) ($kJ.mol^{-1}$)	KCB (or KCB_{eq} for mixtures) ($kJ.mol^{-1}$)
DMSO	175	104
Acn 1:3 DMSO	170	97
Acn 3:1 DMSO	166	95
Acn	142	74
DMA	179	101
DMA 1:1 DMSO	177	98

Preferential solvation effects are also marked in Acn-DMSO mixtures in presence of Li^+ and K^+ (Figure VI.9). It is also interesting to note that the $A_{M^+}^{O_2^{\cdot-}}$ coefficients are nearly equal. MCB values for a particular solvent are lower in the order $Li^+ > Na^+ > K^+$. Thus, the relative importance of MCB in the parameters $A_{M^+}^{O_2^{\cdot-}}$ is in the order $Li^+ \geq Na^+ > K^+$. This can be related to the larger interactions between $O_2^{\cdot-}$ and higher charge-density cations: solvation of the cation will have a more pronounced effect on the association of $O_2^{\cdot-}$ with Li^+ than on K^+.

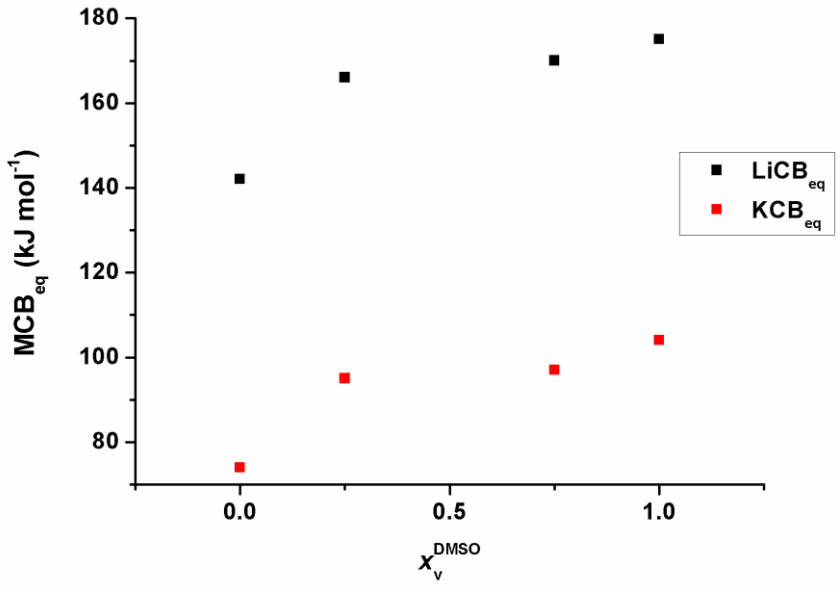

Figure VI.9. Variation of KCB_{eq} (red) and $LiCB_{eq}$ (black) values calculated for Acn-DMSO mixtures with the content in DMSO.

It is thus concluded that the parameters $A_{M^+}^{O_2^{\cdot-}}$ are promising descriptors to understand the effect of the solvent on the non-aqueous ORR in presence of alkali metal cations. Solvation effects can be predicted simply using the MCB and AN values of the solvents.

6. Proposition of a solvent structure-related parameter to predict $O_2^{\cdot-}$ solvation: hydrogen bond donicity

The solvation of $O_2^{\cdot-}$ has already been related to the AN of the solvent. However, this scale is limited in terms of potential candidates. In that case, it could be interesting to relate the solvation of $O_2^{\cdot-}$ to a particular structural effect of the solvent: its capability to provide hydrogen bonding. Indeed, anions are generally prone to accept hydrogen bonds. This tendency is stronger for smaller anions with more localized negative charge. Since the charge in $O_2^{\cdot-}$ is delocalized between two oxygen atoms, it could have been expected to have a low tendency to accept hydrogen bonds: I^- and ClO_4^- for example are considered as very poor hydrogen bond acceptors. However, the particular structure of $O_2^{\cdot-}$ (discussed in chapter II) and the (related) fact that it seems to behave much more like a hard base, would make the assumption of a high hydrogen bonding acceptance more likely. Therefore, a high hydrogen bond donor solvent, which can be measured by its A* parameter in [8], could make a perfect solvent for $O_2^{\cdot-}$. However, such solvents are also usually prone to H-abstraction, as mentioned in [9], with the exceptions of amines (pKa_{NH3} = 41 in DMSO).

The study of ORR in presence of K^+ in an ethylene diamine (EN) 1:4 DMA mixture is thus proposed as an experimental conclusion of this chapter (Figure VI.10). Ethylene diamine has a high A* value, owing to the hydrogen bond donor capacity of the N-H bonds. A ratio of 1:4 should be enough between EN and DMA, owing to the expected much preferential solvation of $O_2^{\cdot-}$ by EN. It should be noted here that EN is rather difficult to purify: a small quantity of the solvent has been dried on molecular sieves for 2 days. Although the exact concentration of water in EN is not known, it is estimated that the overall water content in the electrolyte remains below 50 ppm. Furthermore, EN has a very high affinity for Ag^+, and thus a very slight pollution of the reference electrode leads to considerable shift in the reference potential. Therefore, at the moment of the writing, a reliable value of the potential shift had not been measured. Thus, only a qualitative description is proposed here.

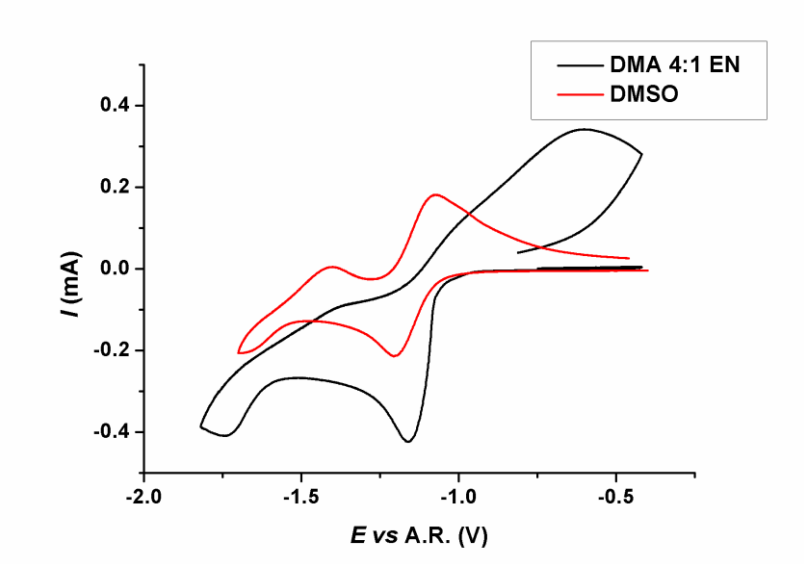

Figure VI.10. Cyclic voltammetry at *v* = 100 mV s^{-1} in oxygen-saturated EN 1:4 DMA mixture (black) or DMSO (red) and 150 mM $TBAPF_6$ in presence of 50 mM KPF_6. Precision on the reference electrode cannot be assured due to a possible contamination by EN. Thus the potentials are presented versus the resulting arbitrary reference noted A.R..

The second reduction wave is better defined in the mixture as compared to pure DMA. The peak separation between the first and second reduction process is similar to that obtained in DMSO. A low degree of reversibility is observed for the second reduction process. Thus, by addition of a small amount of EN, which has a high capability to solvate $O_2^{\cdot-}$ by hydrogen bonding, into DMA, which has a high capability to solvate K^+, a mixture with a high capability to separate $K^+ - O_2^{\cdot-}$ ion-pairs in solution has been designed. In this mixture, which does not contain DMSO, reversibility for the second reduction process has been demonstrated, which validates our concept.

Finally, as stated in chapter II, a reversible second reduction of oxygen in presence of K^+ has been observed in ammonia[10]. Ammonia has a KCB of 55 and an A* similar to that of alcohols, which have AN superior to 35. Thus a value of $A_{K^+}^{O_2^{\cdot-}}$ in the order of 50 is expected, which would mean a shift in potential in the order of 100 mV in presence of 50 mM K^+. The measure is rather complicated on the curves from[10], but a value of 100-150 mV is nevertheless estimated in presence of 100 mM K^+.

From these two last examples, it would appear that the reversibility of the second oxygen reduction is more related to the anion-solvation capability of the solvent, and most likely its ability to solvate $M^+ - O_2^{2-}$. If a similar parameter $A_{M^+}^{M^+-O_2^{2-}}$ is proposed, it would thus have a higher coefficient related to AN (and lower for MCB by construction) as compared to $A_{M^+}^{O_2^{\cdot-}}$.

Conclusion

This chapter demonstrated that the mechanism developed to account for the ORR in presence of alkali metal cations in DMSO can also be used to understand the ORR in other high-permittivity solvents. The shift in first oxygen reduction potential observed on cyclic voltammetries upon addition of alkali metal cations has been attributed to the formation of ion-pairs $M^+ - O_2^{\cdot-}$ and its extent has been related to the capability of a solvent to solvate both M^+ and $O_2^{\cdot-}$. The second reduction wave observed on voltammograms has been attributed to the reduction of ion-pairs $M^+ - O_2^{\cdot-}$, which precipitate as M_2O_2 on the electrode. This process is less reversible when the charge-density of the cation M^+ is higher and the capability of the solvent to solvate both M^+ and $O_2^{\cdot-}$ is lower. Furthermore, this mechanism allowed to understand the behavior of solvent mixtures in terms of preferential solvation of ions.

The differences in the solvation capability of the solvents have been related to their AN or A* and MCB. Simple parameters $A_{M^+}^{O_2^{\cdot-}}$ have been proposed to predict the behavior of solvents and thus design solvent mixtures with tailored properties.

Using these results, a mixture which allowed to demonstrate that the reversibility of the second oxygen reduction in presence of K^+ is not specific to DMSO has been designed. The reversibility of this second reduction process could be accounted for by a second parameter $A_{M^+}^{M^+-O_2^{2-}}$ which is expected to have a larger dependence in solvation capabilities of the solvent as compared to $A_{M^+}^{O_2^{\cdot-}}$.

It would also be interesting to study the impact of the concentration in M^+ on the coefficients of the parameters $A_{M^+}^{O_2^{\cdot-}}$, and thus propose parameters $A_{M^+,c}^{O_2^{\cdot-}}$.

Finally, this study has enabled a much better understanding of the ORR in presence of alkali metal cations: it demonstrated that a unique mechanism accounts for the effects of all alkali metal cations, based on their charge-density, and solvents, based on their capability to solvate both M^+ and $O_2^{\cdot-}$.

The next and final chapter is devoted to the modelling of this mechanism, to further confirm it and account for the particular shape of the oxygen reduction voltammograms in non-aqueous solvents.

Bibliography:

1. Johnson, L.; Li, C.; Liu, Z.; Chen, Y.; Freunberger, S. A.; Ashok, P. C.; Praveen, B. B.; Dholakia, K.; Tarascon, J.-M.; Bruce, P. G., The Role of Lio2 Solubility in O2 Reduction in Aprotic Solvents and Its Consequences for Li–O2 Batteries. *Nature Chemistry* **2014**, *6*, 1091-1099.

2. Trahan, M. J.; Mukerjee, S.; Plichta, E. J.; Hendrickson, M. A.; Abraham, K. M., Studies of Li-Air Cells Utilizing Dimethyl Sulfoxide-Based Electrolyte. *Journal of the Electrochemical Society* **2012**, *160*, A259-A267.

3. Laoire, C. O.; Mukerjee, S.; Abraham, K. M.; Plichta, E. J.; Hendrickson, M. A., Influence of Nonaqueous Solvents on the Electrochemistry of Oxygen in the Rechargeable Lithium−Air Battery. *Journal of Physical Chemistry C* **2010**, *114*, 9178-9186.

4. Luntz, A. C.; McCloskey, B. D., Nonaqueous Li–Air Batteries: A Status Report. *Chemical Reviews* **2014**.

5. Laurence, C.; Gal, J.-F., *Lewis Basicity and Affinity Scales*, Wiley, 2010.

6. Gritzner, G.; Sperker, S., Solvent Donor and Acceptor Properties of Pyridine. *Journal of Solution Chemistry* **1990**, *19*, 543-553.

7. Bryantsev, V. S.; Giordani, V.; Walker, W.; Blanco, M.; Zecevic, S.; Sasaki, K.; Uddin, J.; Addison, D.; Chase, G. V., Predicting Solvent Stability in Aprotic Electrolyte Li–Air Batteries: Nucleophilic Substitution by the Superoxide Anion Radical (O2•–). *The Journal of Physical Chemistry A* **2011**, *115*, 12399-12409.

8. Oliferenko, A. A.; Oliferenko, P. V.; Huddleston, J. G.; Rogers, R. D.; Palyulin, V. A.; Zefirov, N. S.; Katritzky, A. R., Theoretical Scales of Hydrogen Bond Acidity and Basicity for Application in Qsar/Qspr Studies and Drug Design. Partitioning of Aliphatic Compounds. *Journal of Chemical Information and Computer Sciences* **2004**, *44*, 1042-1055.

9. Khetan, A.; Luntz, A.; Viswanathan, V., Trade-Offs in Capacity and Rechargeability in Nonaqueous Li–O2 Batteries: Solution-Driven Growth Versus Nucleophilic Stability. *Journal of Physical Chemistry Letters* **2015**, *6*, 1254-1259.

10. Uribe, F. A.; Bard, A. J., Electrochemistry in Liquid Ammonia. 5. Electroreduction of Oxygen. *Inorganic Chemistry* **1982**, *21*, 3160-3163.

Chapter VII. Kinetic Modelling of the Oxygen Reduction Reaction Mechanism

"Those who have handled sciences have been either men of experiment or men of dogmas. The men of experiment are like the ant, they only collect and use; the reasoners resemble spiders, who make cobwebs out of their own substance. But the bee takes a middle course: it gathers its material from the flowers of the garden and of the field, but transforms and digests it by a power of its own. Not unlike this is the true business of philosophy; for it neither relies solely or chiefly on the powers of the mind, nor does it take the matter which it gathers from natural history and mechanical experiments and lay it up in the memory whole, as it finds it, but lays it up in the understanding altered and digested. Therefore from a closer and purer league between these two faculties, the experimental and the rational (such as has never yet been made), much may be hoped"

Bacon, Francis ; The New Organon, Book One, **1620**

The mechanism proposed to understand the non-aqueous ORR in presence of alkali metal cations (scheme VII.1) is basically a variation of a double square scheme. However, it also involves solubility equilibriums, which considerably complicates the study of the experimental curves. In this chapter, we will focus on the development of a kinetic model to account for the effects of both the ion-pairs formation and the precipitation of solid products with partial solubility.

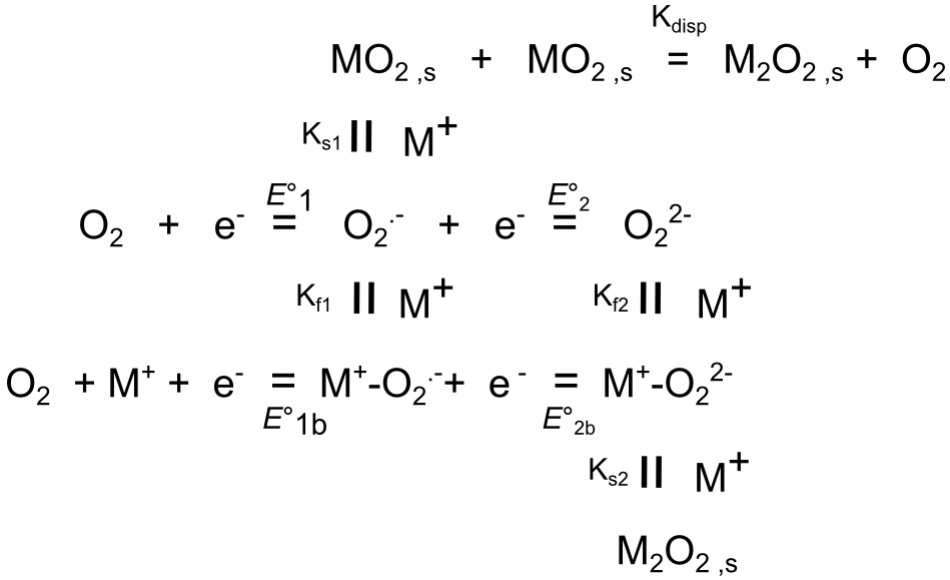

Scheme VII.1. Proposed mechanism to account for the ORR in presence of alkali metal cations M^+ in aprotic solvents

After the presentation of the general methods and approximations used, the first section of this chapter will be devoted to the study of the effect of ion-pairs formation on the first reduction of oxygen. The correlations proposed in the chapter VI are based on a shift of the potential of the first reduction process upon addition of alkali metal cations, M^+, and a fundamental study of the reasons of this shift is needed to justify these empirical correlations.

As also stated in chapter VI, the precipitation of solid MO_2 leads to particular shapes of the voltammograms. Thus, a model involving solubility equilibrium, solid phase growth and dissolution as well as surface passivation will be proposed, based on simple assumptions.

1. Kinetic equations, linear system formulation and resolution[1-2]

We will consider here the modelling of cyclic voltammetry or chronoamperometry on a uniform electrode with a 1D semi-infinite diffusion in solution, without solid or adsorbed species (Figure VII.1).

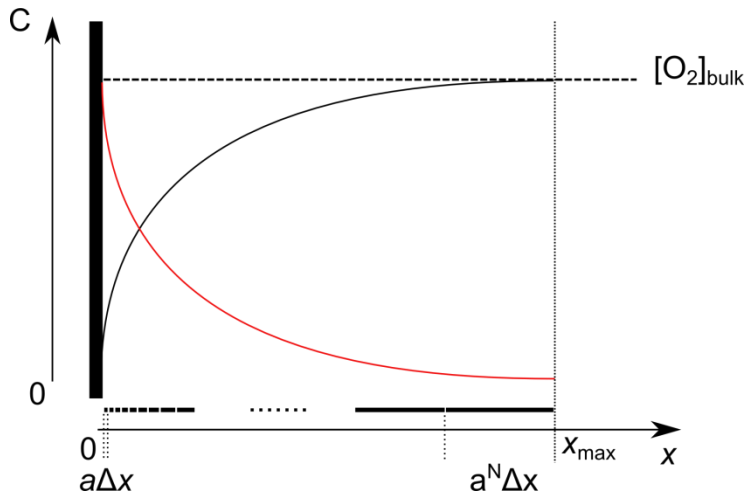

Figure VII.1. Schematic representation of the basic principles of the kinetic model in the case of a simple reduction of oxygen. Since the steepest variations in concentrations are located near the electrode, non-equal intervals in *x* with a geometric growth have been used. This allows for a maximal precision at the electrode|electrolyte interface, while limits the number of intervals far from the electrode and thus the computational time. Both *a* and *x* can be adjusted to meet the precision required (which is generally higher in presence of fast homogeneous chemical reactions).

Let us consider a general electrochemical mechanism involving *P* species A_i, composed of *L* heterogeneous electrochemical reactions and *M* homogeneous chemical reactions, written as:

$$\sum_{i=1}^{P} a_{i,j} A_i + n_j e^- = \sum_{i=1}^{P} b_{i,j} A_i \quad \text{, for } j = 1,..,L \tag{VII.1}$$

$$\sum_{i=1}^{P} a_{i,j} A_i = \sum_{i=1}^{P} b_{i,j} A_i \quad \text{, for } j = L+1,..,L+M \tag{VII.2}$$

The reaction rates can be expressed by:

$$v_j(t) = k_{r,j} \prod_{i=1}^{P} A_i^{a_{i,j}}(0,t) \exp\left(-\alpha_{r,j} n_j f\left(E(t) - E_j^o\right)\right) - k_{o,j} \prod_{i=1}^{P} A_i^{b_{i,j}}(0,t) \exp\left(-\alpha_{o,j} n_j f\left(E(t) - E_j^o\right)\right) \quad \text{, for } j = 1,..,L \tag{VII.3}$$

$$v_j(x,t) = K_{d,j} \prod_{i=1}^{P} A_i^{a_{i,j}}(x,t) - K_{g,j} \prod_{i=1}^{P} A_i^{b_{i,j}}(x,t) \quad \text{, for } j = L+1,..,L+M \tag{VII.4}$$

With $f = \frac{F}{RT}$, $\alpha_{r,j} + \alpha_{o,j} = 1$ the symmetry coefficients, n_j the number of electrons involved, $k_{r,j}$ ($k_{o,j}$) the reduction (oxidation) rate constant of electrochemical reaction *j*, $K_{d,j}$ ($K_{g,j}$) the direct (inverse) rate constant of chemical reaction *j*. For the sake of simplicity, symmetry coefficients are considered constant and equal to 0.5, and the number of electrons exchanged in each electrochemical step is $n_j = 1$, whatever *j*. $A_i(x,t)$ corresponds to the activity of species A_i at a

distance *x* from the electrode interface and at time *t*. For species in solution, $A_i(x,t)$ corresponds to the concentration. *E*(t) corresponds to the applied potential, either fixed (chronoamperometry) or constantly varying according to (VII.5) (voltammetry). $E°_j$ corresponds to the standard potential of electrochemical reaction *j*.

$$\frac{dE}{dt} = \pm v \tag{VII.5}$$

The current *I* on an electrode of surface *S* can be related to the electrochemical reaction rate by equation (VII.6).

$$I(t) = -FS \sum_{j=1}^{L} (n_j v_j(t)) \tag{VII.6}$$

Thus, $I(t)$ depends on the applied potential *E*(t) and the interfacial concentrations, which follow equation (VII.7).

$$-D_{A_i} \frac{\partial A_i(0,t)}{\partial x} = \sum_{j=1}^{L} \left((a_{i,j} - b_{i,j}) v_j(t)\right) \tag{VII.7}$$

The variation of the concentrations in solution can be calculated using Fick's law, for $x > 0$:

$$\frac{\partial A_i(x,t)}{\partial t} = D_{A_i} \frac{\partial^2 A_i(x,t)}{\partial^2 x} + \sum_{j=L+1}^{L+M} \left((a_{i,j} - b_{i,j}) v_j(x,t)\right) \tag{VII.8}$$

In order to solve these coupled equations, the time and position are discretized. Discretization of the time is straightforward by introducing a unique discrete interval Δt. It could have been chosen to adapt this discrete interval dynamically depending on the precision required by the model. This would have led to a considerable optimisation of the model, but was not required here.

The precision in distance required near the electrode is considerable, due the very fast variations in interfacial concentrations. An interval of 10 to 50 nm is generally required at the electrode interface. Since a maximal distance superior to the millimetre has to be taken into account to keep valid the approximation of semi-infinite diffusion, the number of uniform intervals required would have been too large for reasonable computational time. Thus a non-uniform discretization of space with a geometric growth of the intervals with the distance has been undertaken. Practically, position intervals are defined according to equation (VII.9) with *N* the number of intervals.

$$a^n \Delta x\,, \qquad n \in [\![1; N]\!] \tag{VII.9}$$

Using these definitions, derivatives can be linearized according to equations (VII.10) and (VII.11), introducing the notation $A_i|_n^t$ to represent the concentration of species A_i at the instant *t* and the position *n*. It is also needed to linearize products of variables, in particular for bimolecular reactions, which is done according to equation (VII.12). Similar reasoning can lead to the linearization of higher order products.

$$\frac{\partial^2 A_i}{\partial x^2}|_n^t \cong \frac{1}{0.5\Delta x(a^n + a^{n-1}).a^n} A_i|_{n-1}^t - \frac{1}{0.5\Delta x(a^n + a^{n-1})}\left(\frac{1}{a^n} + \frac{1}{a^{n-1}}\right) A_i|_{n-1}^t + \frac{1}{0.5\Delta x(a^n + a^{n+1}).a^n} A_i|_{n+1}^t \quad \text{(VII.10)}$$

$$\frac{\partial A_i}{\partial t}|_n^{t+1} \cong \frac{A_i|_n^{t+1} - A_i|_n^t}{\Delta t} \quad \text{(VII.11)}$$

$$A_i|_n^{t+1} A_j|_n^{t+1} = A_i|_n^{t+1} A_j|_n^t + A_i|_n^t A_j|_n^{t+1} - A_i|_n^t A_j|_n^t \quad \text{(VII.12)}$$

If linear functions of variables must be used, as it will be when studying precipitation, a simple linearization using first-order Taylor development is proposed (equation (VII.13)).

$$f(A_i|_n^{t+1}) = f(A_i|_n^t) + \frac{\partial f(A_i|_n^t)}{\partial t} \quad (A_i|_n^{t+1} - A_i|_n^t) \quad \text{(VII.13)}$$

This approximation generates a relatively large error, and thus requires shorter intervals in order to keep sufficient precision. A second-order Taylor development could be used if higher precision, or shorter computational time, is needed.

The concentrations at each instant *t* can now be calculated by resolving a system of linear equations. It can be written in a matrix form (equation (VII.14)), with $C|^{t+1}$ the concentrations vector, and solved by matrix inversion. The build-in matrix inversion function of Scilab (open source equivalent to Matlab) has directly been used.

$$GC|^{t+1} = H \quad \text{(VII.14)}$$

The current is finally calculated at each instant *t* by equation (VII.6), and modelled voltammograms or chronoamperograms can be plotted.

2. Study of the impact of ion-pairs formation on the resulting voltammograms

In this section, the study will be limited to scheme (VII.2), which corresponds to the first oxygen reduction process in the absence of precipitation. The concentration in M^+ will be considered

as constant, which is reasonable for concentrations at least 10 times larger than the concentration in oxygen.[i] The following parameters will be held constant during the study: v = 0.1 V s^{-1}; $D_{O_2} = 2\ 10^{-5}$ $cm^2\ s^{-1}$; $D_{O_2^{\cdot-}} = 5\ 10^{-6}$ $cm^2\ s^{-1}$; $D_{M^+} = 5\ 10^{-6}$ $cm^2\ s^{-1}$; $(O_2)_{bulk} = 2$ mM; T = 300 K; S = 0.2 cm^2; E_1^o = -1.2 V; $K_{d,1f}$ = 10^{12} cm^{-3} $mol\ s^{-1}$. It is also worth noting that since the reduction reaction of step (1b) is bimolecular, the unit of k_{r1b} is [$mol^{-1}\ cm^4\ s^{-1}$]. The actual comparable value of rate constant for this reduction step is $k_{r1b}C°$, the unit of which is [$cm\ s^{-1}$], with $C°$ = 10^{-3} $mol\ cm^{-3}$.

$$O_2 + e^- \overset{E°1}{=} O_2^{\cdot-}$$

$$K_{f1} \ \text{II} \ M^+$$

$$O_2 + M^+ + e^- = \underset{E°1b}{M^+\text{-}O_2^{\cdot-}}$$

Scheme VII.2. First reduction of oxygen in aprotic solvents in the absence of precipitation and in the presence of alkali metal cations M^+

As already mentioned in the previous chapters, the standard potential E_{1b}^o is fixed by the values of E_1^o and K_{f1}. Thus, if electrochemical and chemical reactions are considered as fast enough, then the shift in the half-peak potential will be directly linked to the difference in standard potentials between the two electrochemical steps, and thus determined by the thermodynamic constants and the concentration in M^+ (Figure VII.2 and equation (VII.15)).

[i] Modelling non-constant concentrations in M^+ has also been attempted: it considerably complicates the elaboration of the model as well as the matrix inversion, and is therefore not presented here.

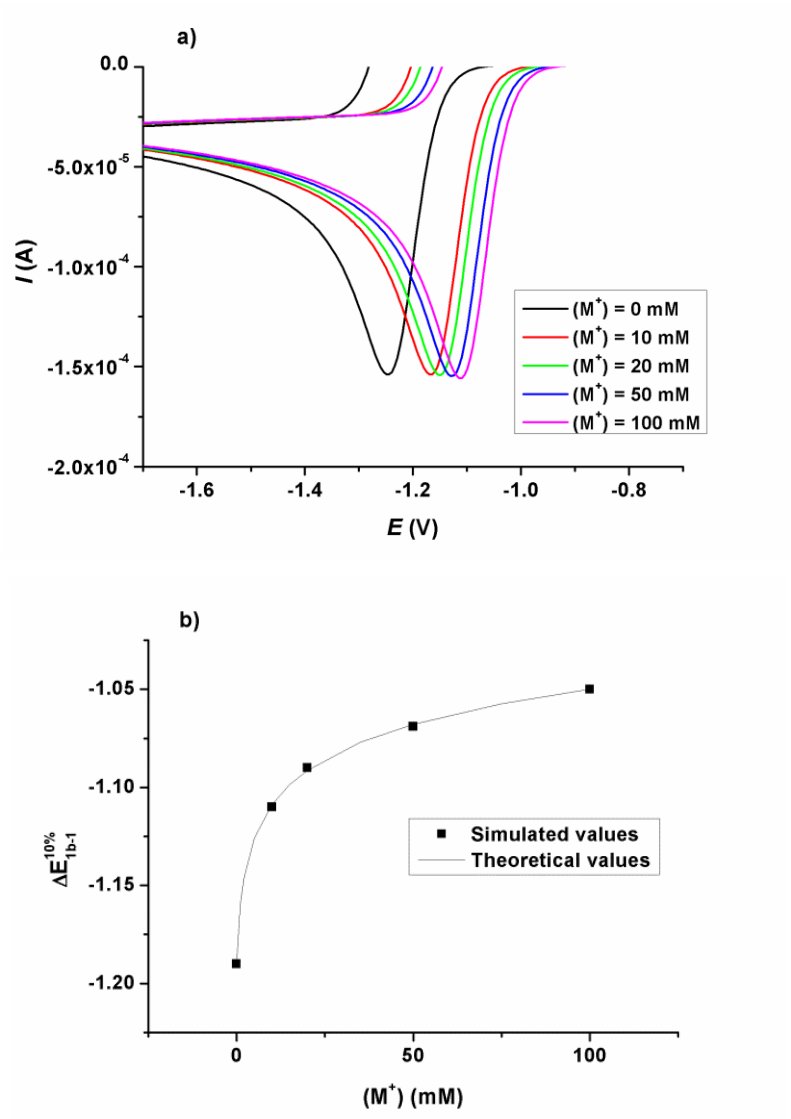

Figure VII.2. (a) Influence of the concentration in M^+ on the ORR voltammograms with $k_{r1} = k_{o1}$ = 10 cm s^{-1}; k_{r1b} $C°$= k_{o1b} = 0 cm s^{-1}; $\Delta E^{0}_{1b-1,S}$ = 0.2 V; (M^+) = 0 mM (black), 10 mM (red), 20 mM (green), 50 mM (blue), 100 mM (violet).

$$\Delta E^{1/2}_{1b-1,S} = \Delta E^{10\%}_{1b-1,S} = \frac{RT}{F}\ln(1 + K_{f1}(M^+)) \qquad \text{(VII.15)}$$

Furthermore, in that case, the voltammograms will be independent on the pathway: $M^+ - O_2^{\cdot-}$ can be formed either from the direct reduction (1b) (electrochemical pathway) or by the chemical reaction (1f) from $O_2^{\cdot-}$, itself formed by the reduction of oxygen (1) (chemical pathway), and their origin on the voltammograms cannot be discriminated. Thus electrochemical step 1b is not mandatory to account for the shift in potential of the shape of the voltammograms (Figure VII.2a). However, the situation is much more complicated if either the electrochemical or the chemical reactions are considered to have a slower rate.

Here we consider the chemical reaction (1f) fast enough, so that its rate will not influence the following results. This is supported by the consideration that ion-pairs formation should indeed occur at a significantly high rate. It is also considered that the rate constants of the reduction and oxidation reactions of an electrochemical step are always equal, except when one of them is set to 0. Let us first consider the influence of the electrochemical rate constants on the chemical pathway (Figure VII.3a). The direct formation of the ion-pairs is forbidden, but their direct oxidation is still possible (oxidation reaction of step (1b)). It can be observed that the rate of the electrochemical reaction (1) can become limiting. Interestingly, the anodic peak potential on the positive scan is independent on the electrochemical rate constant. This phenomenon has been studied in detail in [3] and is of particular importance when considering the ORR. Indeed, the first reduction of oxygen in non-aqueous solvents is generally considered as a quasi-reversible process. If a corresponding electrochemical rate constant is used in the model (Figure VII.3b), it can be observed that the cathodic wave becomes independent on the concentration in M^+, even at moderate concentrations. Since the anodic peak potential on the backward (positive) scan depends on the concentration in M^+, the difference in potential between the cathodic and anodic peak is varying with the concentration in M^+. Such behaviour has not been observed experimentally. Therefore, it can be concluded that either the electrochemical rate constant is considerably underestimated, or that it is needed to take the electrochemical pathway (reduction step in 1b) into account.

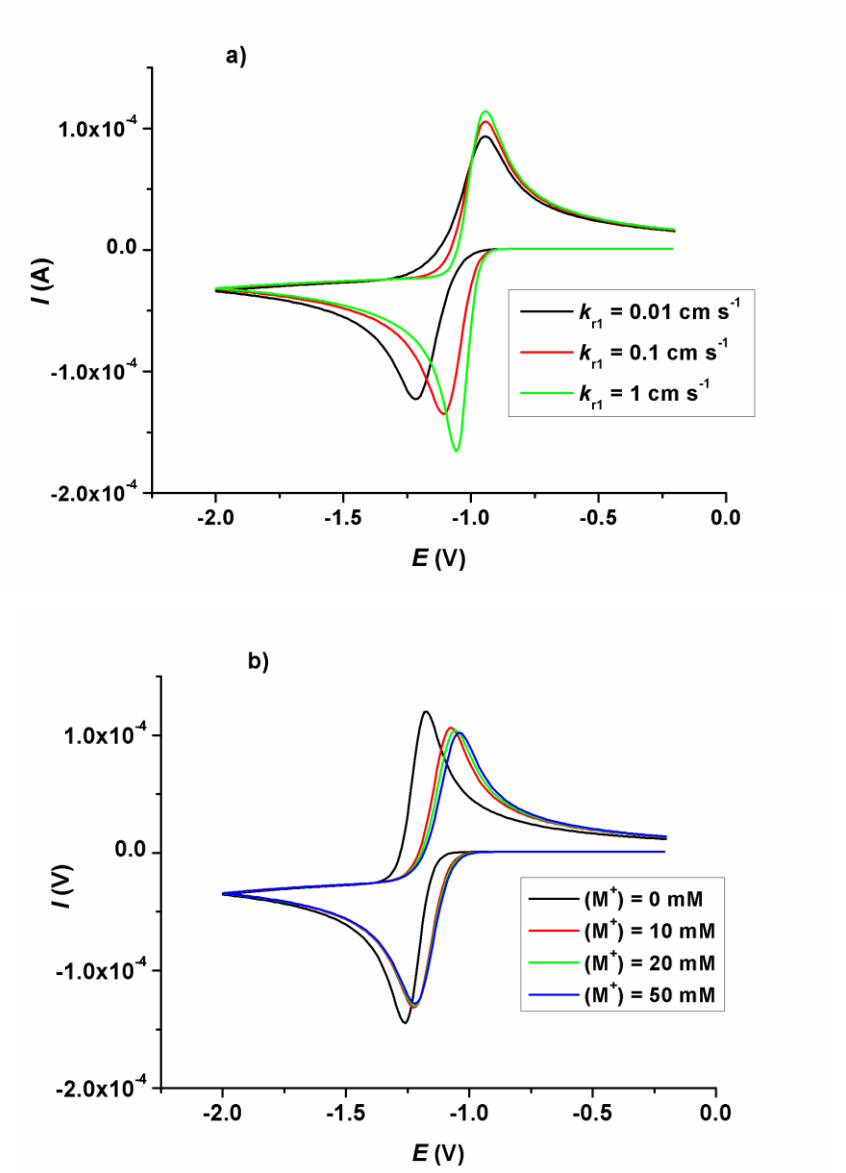

Figure VII.3. (a) Influence of the electrochemical rate constant of step (1) on the simulated voltammograms with (M^+) = 50 mM; b) Influence of the concentration in M^+ on the ORR voltammograms with k_{r1} = k_{o1} = 0.01 cm s^{-1}. For both simulations: $\Delta E^{o}_{1b-1,S}$ = 0.2 V ; k_{r1b} C^{o}= 0 cm s^{-1}; k_{o1b} = 0.01 cm s^{-1}.

When taking the electrochemical pathway into consideration, the limitation due to the rate constant of reaction (1) can be overcome (Figure VII.4).

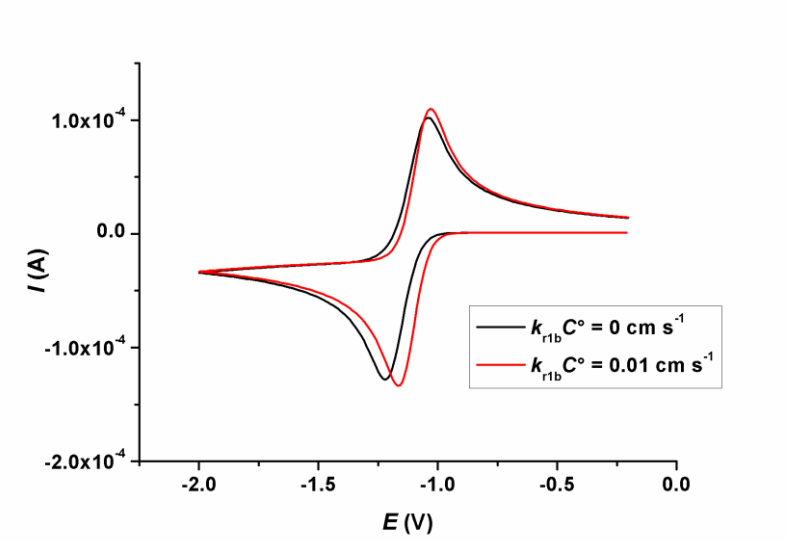

Figure VII.4. Influence of the electrochemical rate constant of step (1) on the simulated voltammograms with (M^+) = 50 mM; $\Delta E^{o}_{1b-1,S}$ = 0.2 V ; $k_{r1} = k_{o1}$ = 0.01 cm s^{-1}; k_{r1b} $C°$= 0 cm s^{-1} (a) or k_{r1b} $C°$= 0.01 cm s^{-1} (b); k_{o1b} = 0.01 cm s^{-1} .

However, the question of the value of the electrochemical rate constant of the direct reduction of the ion-pairs (reaction 1b) arises. Since the reaction rate of (1b) depends on the concentration in M^+, a clear effect of the alkali metal concentration on the voltammograms can be observed (Figure VII.5). This phenomenon could be characterized by the decrease of the cathodic peak current or the change in the slope of the current.

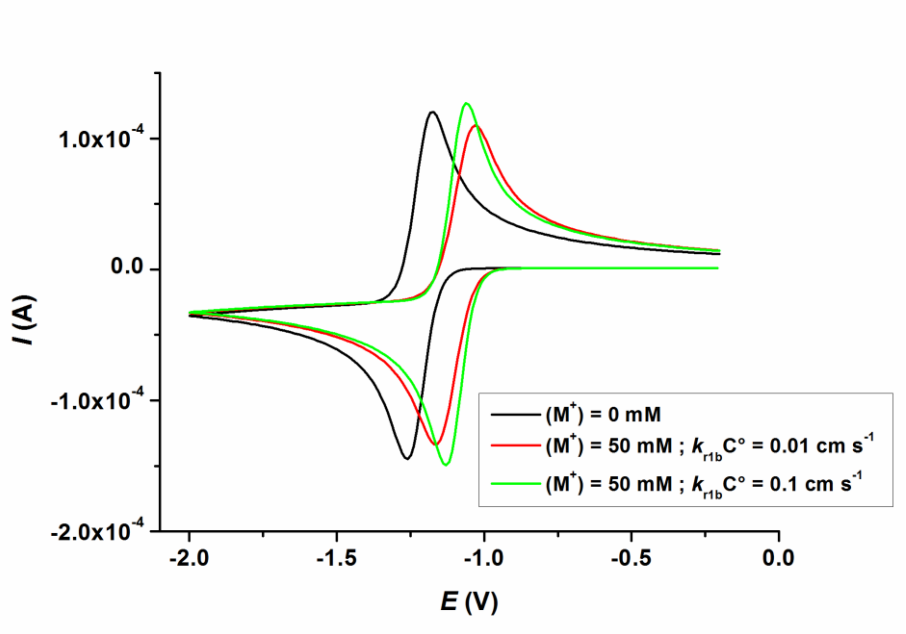

Figure VII.5. Influence of the electrochemical rate constant of step (1b) on the simulated voltammograms with (M^+) = 50 mM; $\Delta E^{o}_{1b-1,S}$ = 0.2 V ; k_{r1} = k_{o1} = 0.01 cm s^{-1}; k_{r1b} $C°$= k_{o1b} =0.1 cm s^{-1} (green) or k_{r1b} $C°$= k_{o1b} = 0.01 cm s^{-1} (red). Comparison with the simulated voltammograms in the same conditions but in absence of alkali metal cation: (M^+) = 0 mM (black).

However, the experimental observation of this phenomenon is complicated, since a large ion-pairs formation constant is also associated with a low solubility of MO_2, which results in distorted voltammograms. It can still be noticed that, in the presence of 50 mM Na^+, which allows higher shifts in potential compared to K^+ and more limited precipitation effects, neither change in the slope nor in the peak current is observed in DMSO or DMA (Figure VII.6). This could mean that, either the rate constant of reaction (1) is underestimated, or the rate constant of (1b) is larger than that of (1). In this last case, it would be remarkably improbable that the change in the rate constant of (1b) leads to the exact same peak current. It is thus proposed to re-examine the rate constant of the reduction of oxygen to superoxide in non-aqueous solvents on glassy carbon micro-electrodes in order to obtain more accurate values in the relative absence of ohmic drop, before making any definitive conclusions at that stage. This study, despite its interest, could not be achieved in the present work.

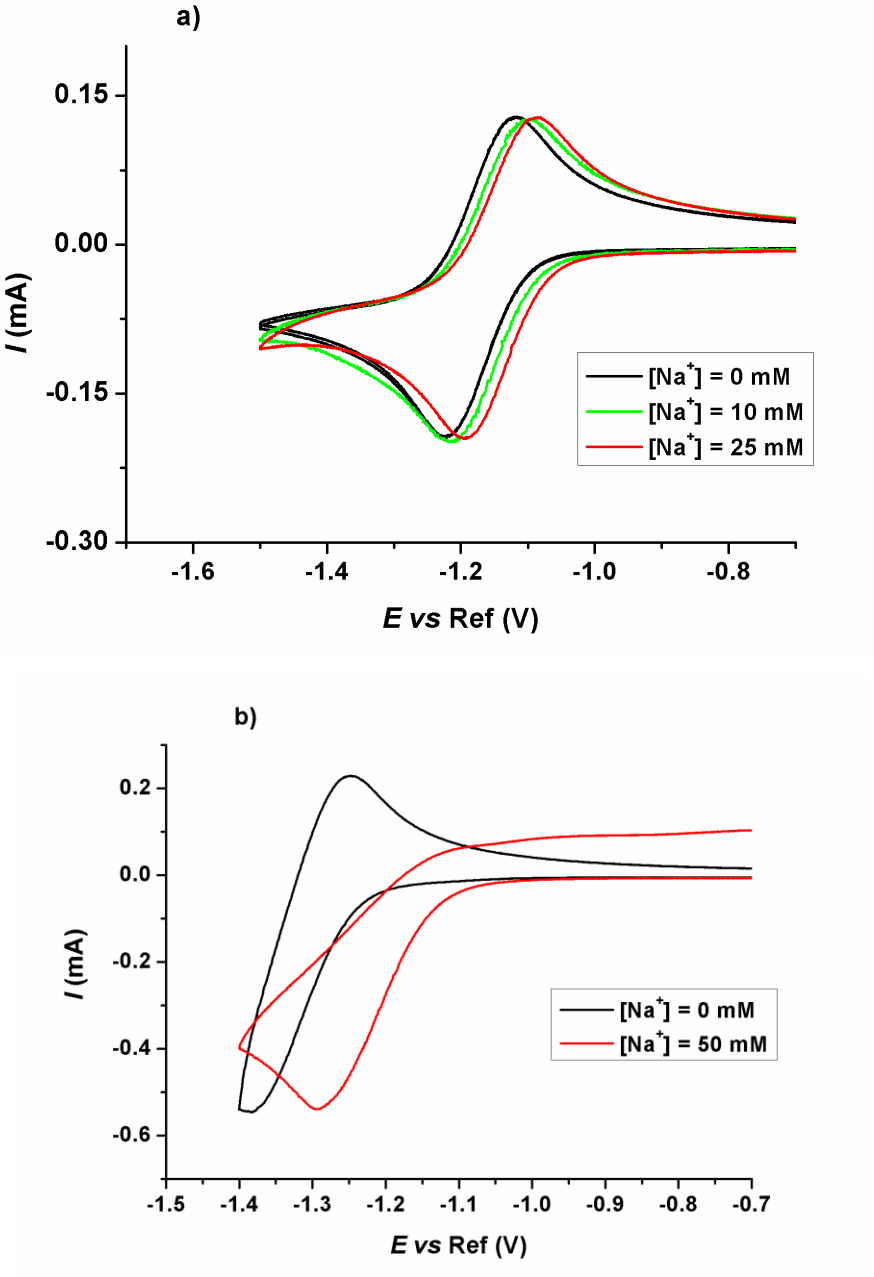

Figure VII.6. Cyclic voltammetries at *v* = 100 mV s^{-1} in O_2-saturated DMSO (a) or DMA (b) containing 150 mM $TBAPF_6$ (black) in presence of different concentrations in $NaClO_4$ (red and/or green).

As mentioned before, passivation prevents any measurement of the peak current associated to the first oxygen reduction process at low solubilities in MO_2. However, it might be possible to demonstrate the effect on the current slope by a measurement at very low overpotentials, where precipitation should be limited, and compare it to the slope measured at the same currents in the absence of Na^+. As observed in Table VII.1, the ratio of the average slope measured at I_{corr} = 0.05 in

presence of Na^+ on the average slope measured in its absence is lower than 1 in Acn and Py, as well as in their mixture.

Table VII.1. Ratio of the slopes of the ORR voltammograms measured at low overpotentials in the presence of 50mM Na^+ and in the absence of alkali metal cations.

Solvent	$\Delta E_{1b-1,S}^{10\%}$ (mV)	$\dfrac{\Delta I_{corr,Na^+}^{5\%}/\Delta E}{\Delta I_{corr,TBA^+}^{5\%}/\Delta E}$
DMSO	55	1
DMA	105	1
NMP	110	1
Acn	195	0.8
Py 1:1 Acn	200	0.75
Py	220	0.82
Acn 1:1 DMA	110	1
Simulation: $k_{r1} = k_{o1} = 0.01$ cm s^{-1}; $k_{r1b}\ C^\circ = k_{o1b} = 0.01$ cm s^{-1}; $(M^+) = 50$ mM	$\Delta E_{1b-1,S}^{o} = 300$ mV $\Delta E_{1b-1,S}^{10\%} = 210$ mV	*0.91*
	$\Delta E_{1b-1,S}^{o} = 200$ mV $\Delta E_{1b-1,S}^{10\%} = 115$ mV	*0.98*

The principle of the measurement at $\Delta E_{1b-1,S}^{10\%}$ was based on the assumption that the shift in potential of the wave corresponding to the first oxygen reduction process upon addition of M^+ cations was almost constant at any current. However, it appears that this assumption could be wrong at high association constants K_{f1}. The resulting underestimation of the actual shift in standard potentials seems to be limited to 5 to 10 mV, according to the model.

However, it should be noted that the slopes observed at low overpotentials in presence of Na^+ in Acn and Py are significantly lower than the slopes expected from the model. Again, a more accurate measure of the actual rate constant in the absence of alkali metal cations is needed to conclude here. A lower rate constant of step (1) in Acn and Py as compared to DMSO, NMP and DMA is a possible explanation. Another possible, but much more hypothetical, explanation could be related to the actual structure of the ion-pairs formed during the first reduction process.

It has been considered until here, without physical evidence, that the ion-pairs, mainly formed by the interaction between M^+ and $O_2^{\cdot-}$, were of the simplest form $M^+ - O_2^{\cdot-}$. This can now be corroborated in DMSO in presence of Na^+ by the fact that equation (VII.15) efficiently fits the shift in potential $\Delta E_{1b-1,DMSO}^{1/2}$ (Figure VII.7).

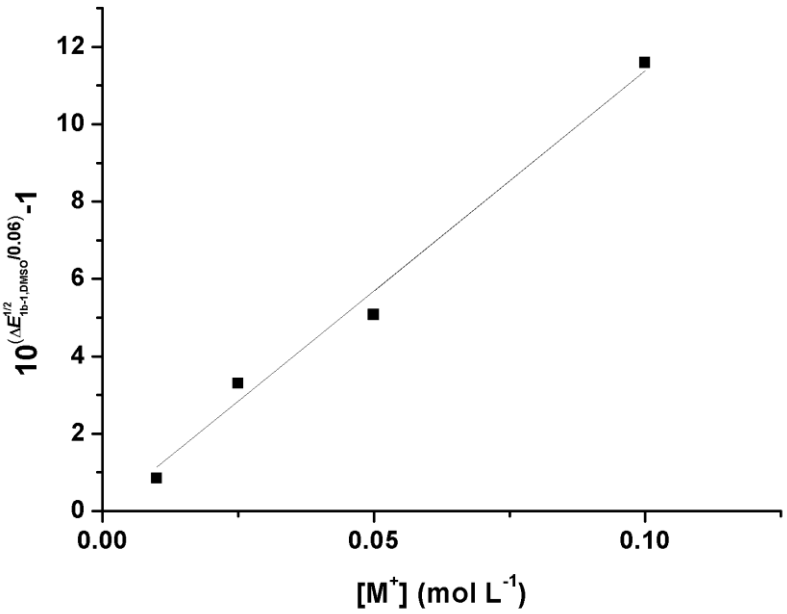

Figure VII.7. Evolution of $10^{\frac{1}{0.06}(\Delta E_{1b-1,DMSO}^{1/2})} - 1$ versus the concentration in Na^+. A linear fit is proposed in agreement with equation (VII.11) (R^2 = 0.989). A value of K_f = 114 mol^{-1} L^3 is thus found.

However, other ion-pairs could also be taken into account, and in particular triple ion-pairs: $M^+ - O_2^{\cdot-} - M^+$. This formation is probable considering the structure of the $O_2^{\cdot-}$ radical, and could be favoured in solvents that poorly solvate alkali metal cations, such as Py and Acn. In that case, equation (VII.15) would no longer be valid and the mechanism would be much more complicated. From a very qualitative and approximated first approach, let us consider that only $M^+ - O_2^{\cdot-} - M^+$ are formed. The only change in the model is a square of the constant concentration in M^+ in the reaction rates, which leads to lower slopes in the cyclic voltammetries (Figure VII.8).

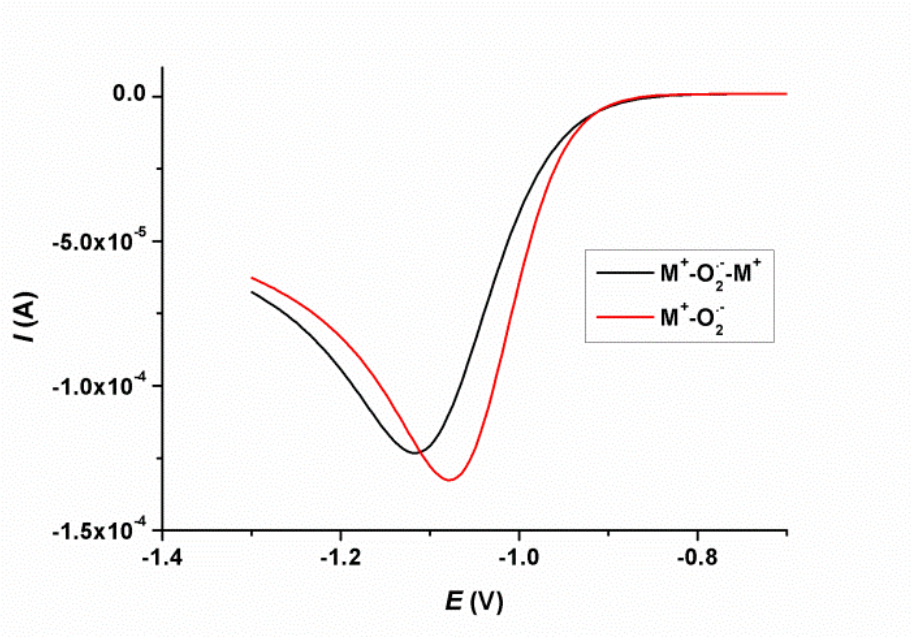

Figure VII.8. First approximation of the effect of the formation of triple ion-pairs $M^+ - O_2^{\cdot-} - M^+$ on the ORR voltammogram. (M^+) = 50 mM; $\Delta E^{o}_{1b-1,S}$ = 0.3 V ; k_{r1} = k_{o1} = 0.01 cm s^{-1}; k_{r1b} $C°$= 0.1 cm s^{-1} (red) or k_{r1b} $C°$ $C°$= 0.1 cm s^{-1} (black); k_{o1b} = 0.1 cm s^{-1}.

The direct electrochemical reduction of oxygen in presence of 2 cations M^+ is highly unlikely; thus, a mechanism including two subsequent additions of M^+ to form the ion-pair $M^+ - O_2^{\cdot-} - M^+$ has to be modelled and studied, which was not achieved at the moment of the writing.

3. Modelling of the precipitation of MO_2

In this section we will use the same mechanism as in the previous section, but adding the solubility equilibrium (1s) (scheme VII.3).

$$MO_{2,s}$$

$$K_{s1} \; \| \; M^+$$

$$O_2 + e^- \overset{E°1}{=} O_2^{\cdot-}$$

$$K_{f1} \; \| \; M^+$$

$$O_2 + M^+ + e^- \underset{E°1b}{=} M^+\text{-}O_2^{\cdot-}$$

Scheme VII.3. First reduction of oxygen in aprotic solvents involving precipitation and in the presence of alkali metal cations M^+.

Modelling the precipitation of solid products and their dissolution involves several theoretical difficulties related to the uniqueness of the solubility product. For a classical chemical reaction, equilibrium is reached at any concentration in the different species composing the equilibrium. Thus, the calculation of these concentrations is always possible, even if it involves concentrations that correspond to less than a single molecule/ion (which does not make sense physically, but remains mathematically correct). On the contrary, precipitation involves the formation of a new phase, which leads to non-linearity at the moment of its appearance and disappearance. A nucleation step is needed in order for the growth of the new phase to occur, and nucleation is only possible when oversaturation has been reached.

In the present study, no means have been found to use the existing nucleation and growth theories to model cyclic voltammetries. Thus, another, but very simplified, theory is proposed. Crystals are considered as half-spheres (Figure VII.9), which are growing from a definite number of points N_s, and are homogeneously distributed on the electrode surface. Two surfaces are then defined, which are time-dependent but non-classically depending on one-another (they differ from classical surface coverages):

- the active surface of the electrode S_{act}, which is the surface not covered by the half-spheres. Electrochemical reactions can proceed on this surface;
- the half-spheres surface S_{MO2}, which is proportional to the interfacial concentration in MO_2. Cristal growth and dissolution can proceed on this surface, the area of which is the sum of the areas on all the half-spheres (see Figure VII.9).

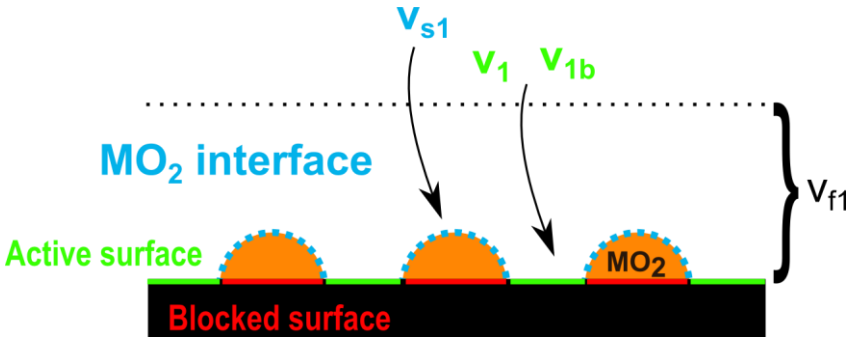

Figure VII.9. Representation of the electrode interface as considered in the model.

The volume of the spheres can be related to the amount of MO_2 deposited on the electrode according to equation (VII.16), with M_{MO_2}, ρ_{MO_2} and n_{MO_2} the molar mass, bulk density and number of moles of MO_2, respectively. It is then possible to relate the surface of the spheres to the amount of MO_2 (equation (VII.17), introducing B_{MO_2} a deposition parameter. This surface is roughly proportional (equation (VII.18)) to the interfacial concentration in MO_2, by introducing $C_{MO_2}^{surf,o}$ the

surfacic concentration of MO_2 in a crystalline MO_2 plane. Finally, the active surface is calculated according to equation (VII.19).[ii]

$$V_{MO_2}^{total} = \frac{M_{MO_2}}{\rho_{MO_2}} n_{MO_2} \tag{VII.16}$$

$$S_{MO_2}^{total} = 2SN_s^{\frac{1}{3}}\pi^{\frac{1}{3}}\left(\frac{3}{2}\frac{M_{MO_2}}{\rho_{MO_2}}\right)^{2/3} {n_{MO_2}}^{2/3} = SB_{MO_2}{n_{MO_2}}^{2/3} \tag{VII.17}$$

$$C_{MO_2}^{surf} = \frac{C_{MO_2}^{surf,o} S_{MO_2}^{total}}{S} \tag{VII.18}$$

$$S_{active} = S(1 - \frac{1}{2}B_{MO_2}{n_{MO_2}}^{2/3}) \tag{VII.19}$$

These equations are based on a single unknown variable: the quantity of MO_2 precipitated at the electrode: n_{MO_2}.

Now that the geometry is set, the reaction rate of the solubility equilibrium (1s) can be written as:

$$v_{1s} = K_{d,1s}(O_2^{\cdot-})(M^+) - K_{g,1s}C_{MO_2}^{surf} \tag{VII.20}$$

Since the concentration in M^+ is constant, when the concentration in $O_2^{\cdot-}$ reaches the saturation concentration, then the reaction rate of (1s) is equal to 0, forcing the value of $K_{d,s}$ to be set as (VII.21). The reaction rate of (1s) is then equal to (VII.22).

$$K_{d,s} = \frac{K_{g,s}C_{MO_2}^{surf}}{K_s} \tag{VII.21}$$

$$v_{cs} = \frac{K_{g,s}C_{MO_2}^{surf}}{K_s}(O_2^{\cdot-})(M^+) - K_{g,s}C_{MO_2}^{surf} \tag{VII.22}$$

It is interesting to note here that this rate is different from 0 only when $C_{MO_2}^{surf}$ is different from 0. This means, as stated before, that there is a non-linearity due to the fact that nucleation has not been taken into account.

The boundary conditions at the electrode interface can now be written as:

$$-D_{O_2}\frac{\partial O_2(0,t)}{\partial x} = S_{active}(-v_1(t) - v_{1b}(t)) \tag{VII.23}$$

[ii] It can be noted here that the geometry chosen can be changed/adapted relatively easily.

$$-D_{O_2^-}\frac{\partial O_2^-(0,t)}{\partial x} = S_{\text{active}}(v_1(t)) - v_{1s}(t) \quad \text{(VII.23)}$$

$$-D_{M^+-O_2^-}\frac{\partial (M^+ - O_2^-)(0,t)}{\partial x} = S_{\text{active}} v_{1b}(t) \quad \text{(VII.24)}$$

$$\frac{\partial n_{MO_2}(t)}{\partial t} = v_{1s}(t) \quad \text{(VII.25)}$$

And the current can be calculated according to:

$$I = -FS_{\text{active}}(v_1(t) + v_{1b}(t)) \quad \text{(VII.26)}$$

After linearization of the equations, in particular the crystals' surface-related terms for which a first-order Taylor development is needed, the linear system can finally be solved.

Since the reaction rate of (1s) is different from 0 only when MO_2 is present at the electrode, n_{MO_2} has to be set different from 0 at the initial potential (before the ORR has been initiated). Since the concentration in O_2^- is extremely low at these potentials, and that any excess would be consumed as soon as it is formed, MO_2 will dissolve readily, leading to infinitely low values of n_{MO_2}. Due to the limited precision of the model, this finally leads to negative values of n_{MO_2}. In order to overcome this divergence, an arbitrary constant is added in equation (VII.25). This addition leads to an equilibrium at high potentials, preventing the negative values. It also results in a constant addition of MO_2 at lower potentials. Thus it is set sufficiently low so that it does not have any effect on the voltammograms obtained; however, the faster the dissolution rate constant, the higher the value of the constant. Thus, there is an upper limit of the rate constant of (1s) that can be studied in the model. A possible way to overcome this limitation could be to dynamically set the constant depending on the conditions, which might lead to stability issues, or to use a function of the electrode potential in place of a constant.

Still, using this constant, several effects observed experimentally could be reproduced by the model. At the moment of the writing, these effects are only studied qualitatively. In particular, the brutal change of slope in presence of K^+ is reproduced in Figure VII.10. A diminution in the time and distance intervals does not affect the modelled voltammograms. Thus this change of slope is not attributed to any calculation artefact due to the approximations used, in particular the Taylor development, or to the limited precision of the model. As expected, it occurs when the concentration in O_2^- overcomes the saturation concentration. Thus, the current at which the change in slope occurs depends on both the solubility product K_{1s} but also the formation constant K_{1f}.

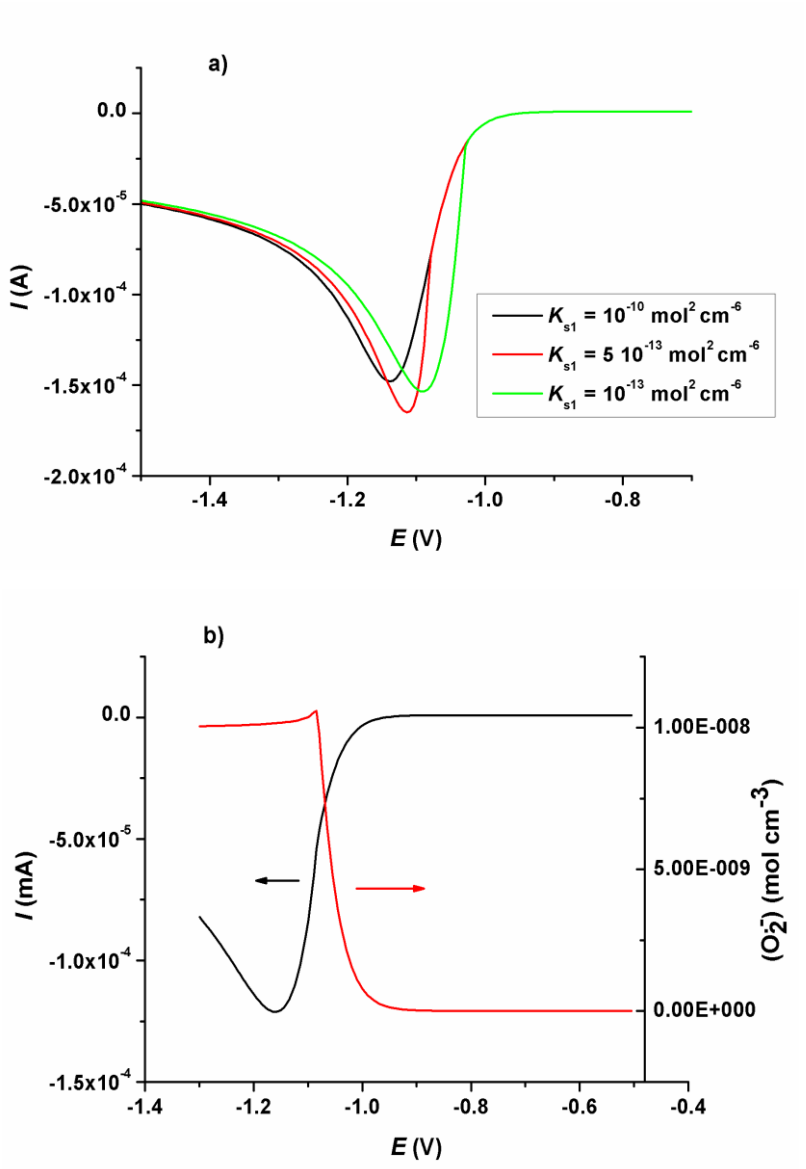

Figure VII.10. (a) Influence of the solubility product on the voltammograms simulated with (M^+) = 50 mM; $\Delta E^{o}_{1b-1,S}$ = 0.2 V ; k_{r1} = k_{o1} = 0.01 cm s^{-1}; k_{r1b} $C°$= k_{o1b} =0.01 cm s^{-1}; B_{MO_2}= 1 10^5 $mol^{-2/3}$; K_s = 10^{-10} mol^2 cm^{-6} (black) , K_s = 5 10^{-13} mol^2 cm^{-6} (red) or K_s = 10^{-13} mol^2 cm^{-6} (green) ; K_{gs} = 5 10^2 mol^2 cm^{-6}.

An estimation of these two constants is thus possible from the cyclic voltammetries:

- as long as the formation constant K_{f1} is not too large for the reaction rate of (1b) to limit the shift in potential, then the formation constant can be estimated by the shift in potential $\Delta E^{x\%}_{1b-1,S}$ measured at currents lower than the oversaturation current;
- the measure of the current at which the slope brutally changes gives an estimation of the sum of the solubility values of $O_2^{\cdot-}$ and $M^+ - O_2^{\cdot-}$;

- knowing K_{f1} and the sum of the solubility values of $O_2^{\cdot-}$ and $M^+ - O_2^{\cdot-}$, the actual solubility product K_{s1} can be estimated.

Using this method, the values estimated from a single concentration in K^+ in DMA and Acn are detailed in Table VII.2. The error-margin on these values is considerable; however, as a very first approximation, these values are consistent with the difference in pK_s calculated using transfer activity coefficients in chapter VI (Table VI.2). A solubility value of KO_2 can also be roughly estimated from the values obtained in DMA and Acn, using the relations between K_s in those solvents established in chapter VI. The solubility calculated is in the order of magnitude of the oxygen saturation concentration in DMSO. This is again consistent with the fact that precipitation of KO_2 was observed in DMSO, even though the steep change in slope was not observed.

Table VII.2. Estimated values for K_{f1} and K_{s1} for different solvents.

Solvent	$\Delta E_{1b-1,S}^{10\%}$ (mV)	K_{f1} (mol^{-1} L)	K_{s1} (mol^2 L^{-6})	$(O_2^{\cdot-})_{sat} + (M^+ - O_2^{\cdot-})_{sat}$ (K^+) = 50 mM (mM)
DMSO	20	20	$5\ 10^{-8}$	1
DMA	80	410	$5\ 10^{-10}$	0.2
Acn	150	6300	$3\ 10^{-11}$	0.2

Using this model, it is also possible to observe the effect of passivation (Figure VII.11). It is emphasized that passivation has been taken into account by a simple blocking of the surface due to the growth of non-conductive crystals, and that the corresponding parameters were not completely optimised: the amount of MO_2 precipitated on the surface was roughly estimated by the anodic charge on the backward scan (to positive potentials) on experimental voltammograms in presence of K^+ in Acn, and the corresponding value was used as the maximum amount of MO_2 that could be formed in the model before total covering of the surface. By definition of the model, this fixes the number of nucleation site N_s. K_{f1} can also be roughly estimated to provide a consistent shift in potential. Similarly, K_{s1} is fixed based on the current at which the oversaturation-related change of slope occurred on the experimental voltammetry. The only free parameter that was left corresponds to the kinetic of the precipitation K_{gs1}. The modelled voltammogram obtained is thus nearly completely determined by the experience and the basic principles of the model.

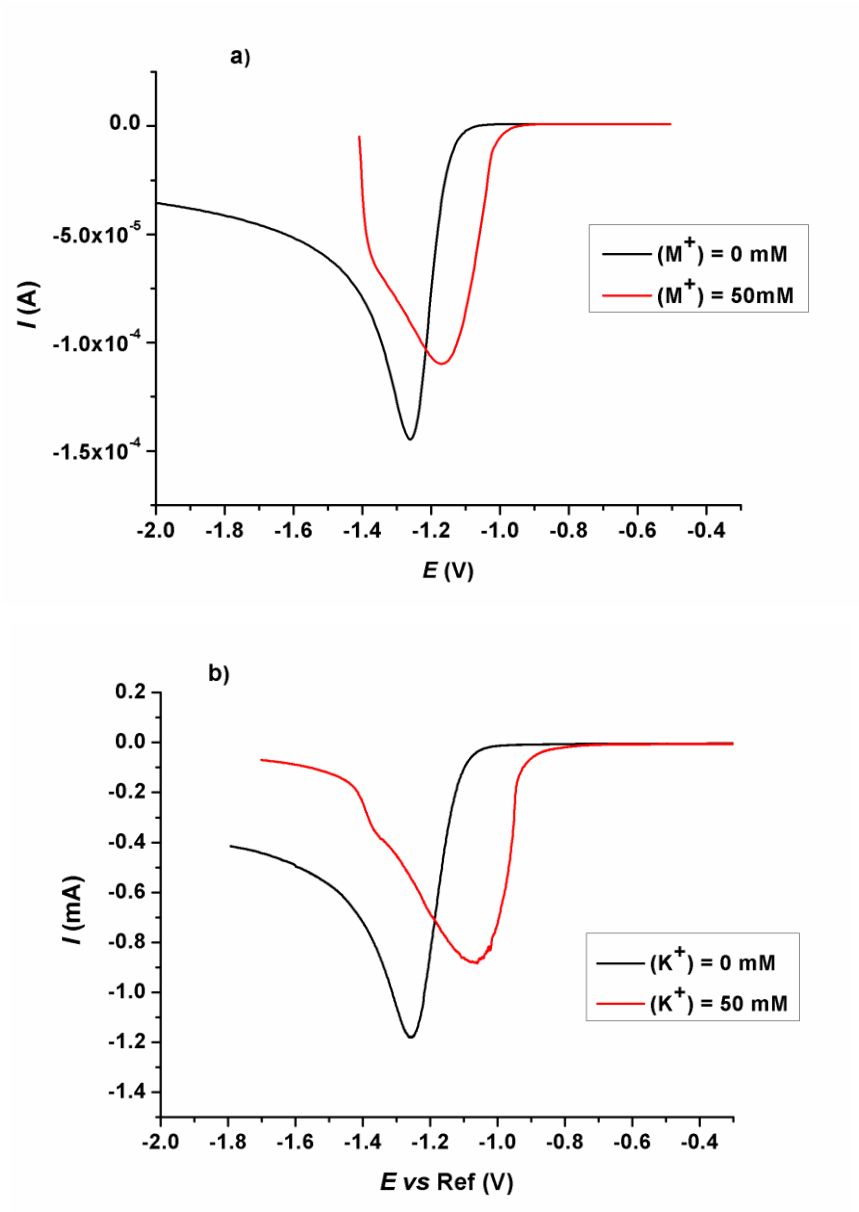

Figure VII.11. Correspondence between the simulation taking passivation into account (a) and experimental voltammograms (b) measured in oxygen-saturate Acn in presence of 150 mM $TBAPF_6$ (black) and 50 mM KPF_6 (red). Simulation parameters were: (M^+) = 0 mM (black) or (M^+) = 50 mM (red); $\Delta E^{o}_{1b-1,S}$ = 0.2 V ; $k_{r1} = k_{o1}$ = 0.01 cm s^{-1}; k_{r1b} $C^{o} = k_{o1b}$ =0.01 cm s^{-1}; B_{MO_2}= 3.3 10^5 $mol^{-2/3}$; K_s = 8 10^{-14} mol^2 cm^{-6} (black) , K_{gs} = 5 10^2 mol^2 cm^{-6}.

The qualitative correspondence between the experimental curves and the model is good. In particular, after the steep change of slope, the curve “bends” and forms an enlarged peak. The peak current obtained at that stage is smaller than the peak current obtained in the absence of M^+. The main difference between the model and the experience is observed near the full coverage of the surface by MO_2 solid products. In the model, the merging of the different crystals is not taken into account. This leads to a brutal passivation of the electrode at large coverage by solid products.

Theoretically, since MO_2 is set to be partially soluble, a complete passivation of the electrode should not occur. If it did, the concentration in $O_2^{\cdot-}$ near the electrode would decrease, leading to a faster dissolution of MO_2 and thus a recovery of the surface. The complete passivation is explained here by the steepness of the equations, which leads to negative active surface values, unless very short intervals in time and distance are used. Even under these conditions, the agreement between model and experience at large ORR overpotential values will remain poor and this is an intrinsic consequence of the choice of the model. This issue is related to a fundamental question that was partially answered: is it necessary to take lateral diffusion into account when considering the passivation of an electrode by the formation of crystals on its surface. If crystals are small enough, the hypothesis of a homogeneously-accessible electrode with negligible lateral mass-transport effects is a very good first approximation. This remains true as long as the surface coverage in solid (passivating) species is not too large, *i.e.* when merging of crystals does not become too favoured.

Conclusion

The kinetic model of the mechanism proposed to account for the ORR in presence of alkali metal cations has allowed the validation of several of the hypothesis previously made from the study of experimental voltammograms. In particular, the measure of $\Delta E_{1b-1,S}^{10\%}$ has shown to be a good approximation of the actual difference in standard potentials between the electrochemical steps (1b) and (1) (scheme VII.1). The importance of the kinetic of these electrochemical steps has also been emphasized and the possibility of the formation of triple ion-pairs has been considered to account for the results obtained in presence of Li^+ and Na^+ in poor cation-solvating solvents. This hypothesis might be extended to low-permittivity solvents were the formation of ion-pairs is favoured.

Based on relatively simple assumptions, the effect of solubility of the intermediates (MO_2) has been taken into account in the model. First simulations have shown the agreement between the model and the experiments, and a methodology has been proposed to evaluate the thermodynamic parameters of the mechanism.

It is worth noting that the principles developed for the first reduction process, in particular the solubility and passivation effects, can also be applied to the formation of M_2O_2 products by the second reduction process of the generalized mechanism (Scheme VII.1). Thus, the model will be extended in future work to validate the whole oxygen reduction mechanism in non-aqueous media, in the presence of alkali metal cations.

Bibliography :

1. Diard, J.-P.; Le Gorrec, B.; Montella, C., *Cinétique Electrochimique*, Hermann DL, **1996**.

2. Britz, D., *Digital Simulation in Electrochemistry*, Third ed., Springer, **2005**.

3. Savéant, J.-M., Effect of Ion Pairing on the Mechanism and Rate of Electron Transfer. Electrochemical Aspects. *The Journal of Physical Chemistry B* **2001**, *105*, 8995-9001.

General Conclusion

In the present work, the literature on non-aqueous metal-air (metal oxygen) batteries was critically reviewed (Chapter I), with special emphasis on the oxygen reduction reaction (ORR - Chapter II). Improving such systems, notably in terms of rechargeability and cyclability, relies on the thorough fundamental understanding of the double influences of (i) the alkali metal cations and (ii) the solvent properties (Chapter III) on the ORR mechanism. This thesis precisely focused on these fundamental aspects of the non-aqueous ORR, firstly in the presence of tetraalkylammonium cations (Chapter IV) and then of alkali metal cations (Chapter V and VI).

A unique mechanism, which accounts for the effect of alkali metal cations on the reduction of oxygen in non-aqueous solvents was proposed (Scheme C.1). One of the important basics of this mechanism is that the alkali metal cations M^+ are interacting with superoxide $O_2^{\cdot-}$ anions to form ion-pairs $M^+ - O_2^{\cdot-}$, which can ultimately form solid alkali metal superoxide MO_2. The larger the charge-density of the cations, the larger the formation constant K_{f1} of the ion-pairs $M^+ - O_2^{\cdot-}$, which translates in ORR voltammograms by a shift of the first oxygen reduction process towards higher electrode potential values. Furthermore, these ion-pairs can undergo a second electrochemical reduction to form secondary ion-pairs $M^+ - O_2^{2-}$, which, in turn, can precipitate as M_2O_2 on the surface of the electrode. Again, the potential of the second reduction process is shifted to higher electrode potentials when the cation's charge density increases. The reversibility of this second reduction step has been demonstrated in the presence of K^+ in DMSO, owing to the adequate stability of $K^+ - O_2^{2-}$ in that particular solvent.

$$MO_{2,s} + MO_{2,s} \overset{K_{disp}}{=} M_2O_{2,s} + O_2$$

$$K_{s1} \,||\, M^+$$

$$O_2 + e^- \overset{E^\circ_1}{=} O_2^{\cdot-} + e^- \overset{E^\circ_2}{=} O_2^{2-}$$

$$K_{f1} \,||\, M^+ \qquad K_{f2} \,||\, M^+$$

$$O_2 + M^+ + e^- = M^+\text{-}O_2^{\cdot-} + e^- = M^+\text{-}O_2^{2-}$$

$$K_{s2} \,||\, M^+$$

$$M_2O_{2,s}$$

Scheme C.1. Non-aqueous ORR mechanism in presence of alkali metal cations. This mechanism was validated for any alkali metal cation and many solvents of sufficiently high permittivity.

The solvent plays a pivotal role in the proposed mechanism. The larger the capability of the solvent to solvate both M^+ and $O_2^{\cdot-}$ species, the larger the solubility product K_{s1} and the smaller the formation constant K_{f1}. These effects cause a shift in potential of the first oxygen reduction upon addition of the alkali metal cations in ORR voltammograms. Besides, this shift in potential has been correlated to specific solvent parameters that were introduced (and detailed) in Chapter III.

Unlike admitted in some literature, it appears that the sole donor number (DN) is not the best descriptor of the solvent ability to orient the non-aqueous ORR towards a solution-based mechanism. Instead, the acceptor number (AN) of the solvent represents a good approximation of its capability to solvate $O_2^{\cdot-}$, while the gas-phase alkali metal cation basicity (MCB) represents a good marker of its capability to solvate M^+. Chapter VI demonstrated that a combination of these two parameters (AN and MCB) adequately described the effect of the solvent to orientate the ORR mechanism. Furthermore, it has been proposed that the extent and the reversibility of the second oxygen reduction also depends on the capability of the solvent to solvate M^+ and the secondary ion-pairs $M^+ - O_2^{2-}$. Using these correlations, it was possible to predict the behavior of other solvents, but also of solvent mixtures based on the concept of preferential solvation, and thus to rationalize the design of electrolytes for alkali metal oxygen batteries. This approach led to the development of a mixture of N,N-dimethylacetamide and ethylene diamine, which evidenced that the reversibility of the second reduction process in presence of K^+ was not limited to DMSO.

Finally, in Chapter VII, a kinetic model based on the proposed mechanism was developed. The effect of ion-pairs formation on the ORR voltammograms was studied: introducing ion-pairs in the ORR mechanism enabled to justify the experimental measurements proposed, but also to set their limitations. Based on a simple geometric description of the surface blocking due to the precipitation of partially soluble salts, the model also successfully reproduced several experimental features. In particular, the effect of the precipitation of KO_2 on the voltammograms was simulated. Finally, it allowed a rough estimation of several thermodynamic constants associated to the mechanism, which are consistent with tabulated values.

As an important result, this study allowed a better understanding of the ORR mechanism in presence of alkali metal cations in aprotic solvents. Furthermore, it enabled to establish the basis for a complete and precise determination of the thermodynamic and kinetic constants associated to the proposed mechanism, both on the experimental and theoretical sides. Last but not least, the approximations and techniques used to develop the present kinetic model have shown to be reliable and efficient.

Future work will be first devoted to complete this study. More experimental points, in particular ORR experiments in other solvents and solvent mixtures, are needed in order to further support the conclusions and refine the correlations presented in this thesis. A better theoretical understanding of the impact of the ions solvation and the ion-pairs formation on the ORR mechanism in the presence of alkali metal cations should also be achieved. In addition, a simulation of the full mechanism (including the second reduction and also the oxygen evolution reactions) would provide considerable support for many qualitative hypotheses, as well as lead to a quantitative description of the experiments performed using a rotating ring-disk electrode.

Physical characterization experiments are needed to further confirm several hypothesis of the proposed mechanism. The actual fine structure of the $M^+ - O_2^-$ ion-pairs has to be clarified and a characterization of the secondary ion-pairs $M^+ - O_2^{2-}$ is mandatory. Considering the low concentration of these products in the electrolytes as well as their reactivity, high-precision *in situ* spectroscopic techniques, in particular infrared and Raman spectroscopy, are necessary. To date, our attempts to use these techniques proved unsuccessful, but we have not explored all their capabilities, yet.

In the course of this work, several open questions were raised. Triple ion-pairs $M^+ - O_2^- - M^+$ were introduced as a possible mean to account for the ORR in the presence of high charge-density and poorly solvated cations. Their actual formation has to be assessed from the theoretical and experimental points of view (notably using the above-mentioned high-precision *in situ* spectroscopic techniques). Using glassy carbon microelectrodes would allow re-examining the kinetic constants associated to the electrochemical steps without Ohmic drop limitations and using high potential sweep rate characterizations.

Finally, from a more applied point of view, this work has led to an efficient prediction of the effect of the solvents, and thus enabled to design new electrolytes with desired properties much more efficiently. It has also led to the development of simple “model” electrochemical characterizations to improve their understanding. These characterizations will allow to evaluate the performances of new technical choices made by Hutchinson SA (but also of others) in the development of non-aqueous metal-air (metal oxygen) batteries.

Résumé

Afin de mieux comprendre et de dépasser les limites actuelles des systèmes métal-air non-aqueux, le mécanisme de réduction de l'oxygène (ORR) a été étudié en présence de cation alcalins dans divers solvants aprotiques. Sur la base de caractérisations électrochimiques sur électrode statique et d'électrodes tournantes disque-anneau, un mécanisme unique a été proposé afin de rendre compte de l'ORR en présence de cations alcalins. De plus, les différences observées d'un solvant à l'autre ont été expliquées en termes de capacité du solvant à solvater à la fois le cation alcalin en présence et l'anion superoxyde, mais aussi à sa capacité à séparer les paires d'ions. Un modèle cinétique basé sur ce mécanisme a montré un excellent accord avec les résultats expérimentaux.

Abstract

In order to better understand and overcome the current limitations of non-aqueous metal-air batteries, the oxygen reduction reaction (ORR) mechanism has been studied in presence of different alkali metal cations in several aprotic solvents. Based on electrochemical characterizations on static electrode and rotating ring-disk electrode, a unique mechanism has been proposed to account for ORR in presence of alkali metal cations. It has been further showed that the differences observed from one solvent to another could be linked to the solvent's ability to solvate both the alkali metal cation and the superoxide anion, as well as its capability to separate ion-pairs. A kinetic model based on this mechanism has shown very good agreement with experimental results.